

AD-764 644

LATTICE DYNAMICS OF CRYSTAL SURFACES

Richard F. Wallis

California University

Prepared for:

Office of Naval Research

August 1973

DISTRIBUTED BY:

**NTIS**

National Technical Information Service  
U. S. DEPARTMENT OF COMMERCE  
5285 Port Royal Road, Springfield Va. 22151

# LATTICE DYNAMICS OF CRYSTAL SURFACES\*

R. F. Wallis

University of California, Irvine

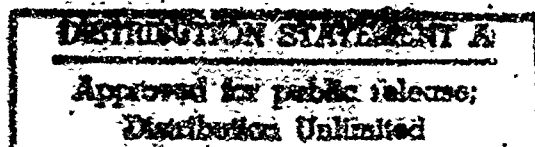
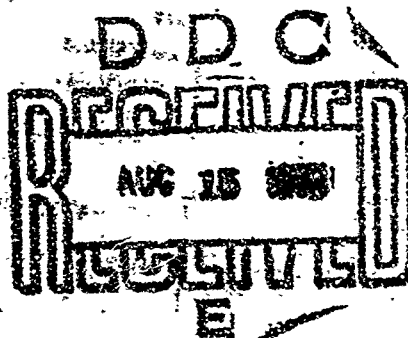
## CONTENTS

1. Introduction
2. Surface Modes of Vibration
  - A. Continuum Theory of Surface Vibrational Modes
    - (i) Isotropic Case
    - (ii) Anisotropic Case, Cubic Symmetry
      - a. Surface Waves on the (001) Surface
      - b. Pseudosurface Waves on (001) Surfaces
      - c. Surface Waves and Pseudosurface Waves on the (110) and (111) Surfaces
    - (iii) Non-Cubic Materials
    - (iv) Piezoelectric Materials
      - a. General Discussion
      - b. Bleustein-Gulyaev Surface Waves
  - B. Lattice Dynamical Theory of Surface Vibrational Modes
    - (i) Static Displacements Near a Surface
    - (ii) Equations of Motion for a Crystal with a Surface
    - (iii) Linear Monatomic Chain
    - (iv) Diatomic Linear Chain
    - (v) Two- and Three-Dimensional Anisotropic Lattices
      - a. Rosenstock-Nowell Models
      - b. Models with Rotationally Invariant Interactions

Technical Report No. 73-55

AD 764644

- (vi) Two- and Three-Dimensional Diatomic Lattices  
with Short-Range Interactions
- (vii) Three-Dimensional Diatomic Lattices with Long-  
Range Interactions
- (viii) Surface Waves in the Presence of Second Sound
- 3. Surface Specific Heat
  - A. Continuum Theory
  - B. Discrete Lattice Theory
  - C. Adsorbed Surface Layers
- 4. Attenuation and Amplification of Surface Waves
  - A. Theoretical Aspects of Surface Wave Attenuation
  - B. Experimental Aspects of Surface Wave Attenuation
  - C. Amplification of Surface Waves
- 5. Mean Square Displacements and Velocities of Surface Atoms
  - A. Introduction
  - B. Experimental Results
  - C. Theoretical Results
  - D. Mean Square Velocities of Surface Atoms
- 6. Inelastic Scattering from Crystal Surfaces
  - A. Introduction
  - B. Theoretical Development
  - C. Experimental Results
- 7. Thermal Diffuse Scattering
  - A. Introduction
  - B. Theoretical Development
  - C. Experimental Results



8. \*Surface Effects on Optical Properties

A. Infrared Absorption

(i) Theoretical Results

(ii) Experimental Results

B. Raman Scattering

C. Brillouin Scattering

9. Surface Thermal Expansion

References

\*Work supported in part by ONR Contract No. N00014-69-A-0200-9003.

## 1. INTRODUCTION

During the past few years there has been an upsurge of interest in the effect of free surfaces on the lattice dynamical properties of crystals. There are several reasons for this increased activity. From the point of view of fundamental knowledge, the development of experimental techniques such as low energy electron diffraction has made available experimental information concerning the dynamics of surface atoms. These experimental results have in turn stimulated theoretical investigations of the phenomena involved. From the point of view of applied research, the use of surface elastic waves in devices such as delay lines has led to much activity concerning the continuum theory of lattice dynamical surface waves, particularly in piezoelectric crystals. On the purely theoretical side, the investigation of surface effects on lattice dynamics has been aided considerably by the availability of high-speed computers and the development of many-body theoretic techniques.

In the present review, the theory of surface modes of vibration in crystal lattices will be developed from both the continuum and discrete lattice points of view. The dispersion of surface mode frequencies and the damping of surface modes by both anharmonicity and imperfections will be discussed. Changes in normal mode frequencies produced by free surfaces will modify thermodynamic properties such as specific heat. These effects on thermodynamic properties will be reviewed.

Particular attention will be given to effects associated with the interaction of particles and radiation with crystal surfaces.

In the case of low energy electron diffraction, the Debye-Waller factor provides information about the mean-square displacements of surface atoms. The inelastic scattering of electrons or neutral atoms from crystal surfaces can provide knowledge of the dispersion of surface mode frequencies. Mean-square velocities of surface atoms may be studied by means of the second order Doppler shift in the Mössbauer effect. The interaction of electromagnetic radiation with crystal surfaces may be manifested through either infrared absorption or the Raman effect. Both of these phenomena will be reviewed.

After the present review was started, the excellent treatise on the "Theory of Lattice Dynamics in the Harmonic Approximation" by Maradudin, Montroll, Weiss, and Ipatova appeared.<sup>(1)</sup> The reader is referred to the chapter on surface effects contained therein.

## 2. SURFACE MODES OF VIBRATION

A knowledge of the normal vibrational modes of the atoms in a crystal is essential for the calculation of the lattice-dynamical properties of the crystal. Thus, to study surface effects, it is important to know the effect of a free surface on the normal mode frequencies and eigenvectors. Generally speaking, the creation of a free surface tends to lower the normal mode frequencies and produce a class of modes called surface modes in which the displacement amplitudes are relatively large at the surface and decrease in essentially exponential fashion away from the surface. These effects may be viewed as arising in the following manner. Starting from a periodic crystal, one may create a pair of free surfaces by setting to zero the interactions coupling atoms on opposite sides of a plane lying between two adjacent lattice planes. This decrease in coupling constants produces a lowering in normal mode frequencies and an increase in the mean square displacements of surface atoms. In particular, surface mode frequencies are typically split off from the bottom of a band of bulk mode frequencies having the same wave vector components parallel to the surface. However, this does not mean that there may not be other bulk modes with lower frequencies than surface modes of the same wave vector.

Surface modes may be derived from either the acoustical or optical branches. We shall begin our discussion by considering the continuum theory of surface vibrational modes derived from the acoustical branch. For the case of an isotropic medium, we shall be led to the oldest example of surface vibrational modes, namely, Rayleigh waves. (2)

#### A. Continuum Theory of Surface Vibrational Modes.

Within the framework of linear elasticity theory, we may write Hooke's law in the form

$$\sigma_{pq} = c_{pqrs} \frac{\partial u_r}{\partial x_s} \quad (1)$$

where  $\sigma_{pq}$  is an element of the stress tensor,  $c_{pqrs}$  is an element of the elastic constant matrix,  $u_r$  is the  $r$ -th Cartesian component of displacement of the medium at the point whose position vector has the  $s$ -th Cartesian component  $x_s$ . The summation convention for repeated indices is assumed in Eq.(1). We shall take the 1 and 2 Cartesian components to be parallel to the free surface.

In order to discuss vibrations, we need the equations of motion which can be written in the form

$$\rho \frac{\partial^2 u_r}{\partial t^2} = \frac{\partial \sigma_{rs}}{\partial x_s}, \quad r = 1, 2, 3 \quad (2)$$

where  $\rho$  is the density of the medium. The definition of the problem is completed by specifying the boundary conditions at the free surface. If the free surface is specified by  $x_3 = 0$ , then the boundary conditions correspond to vanishing of the three components of stress across this surface:

$$\sigma_{r3} = 0 \quad \text{at} \quad x_3 = 0, \quad r = 1, 2, 3 \quad (3)$$

At this point it is helpful to specialize to a cubic crystal with principal axes parallel to the coordinate axes and adopt the Voigt (3) notation for the elastic constants. Combining Eqs.(1) and (2) we obtain the equations of motion.

$$\rho \frac{\partial^2 u}{\partial t^2} = \frac{\partial}{\partial x} \left[ c_{11} \frac{\partial u}{\partial x} + c_{12} \left( \frac{\partial v}{\partial y} + \frac{\partial w}{\partial z} \right) \right] + c_{44} \left[ \frac{\partial}{\partial y} \left( \frac{\partial u}{\partial y} + \frac{\partial v}{\partial x} \right) + \frac{\partial}{\partial z} \left( \frac{\partial u}{\partial z} + \frac{\partial w}{\partial x} \right) \right] \quad (4)$$

plus two other equations obtained by cyclically permuting (u,v,w) and (x,y,z). In Eq.(4),  $(u_1, u_2, u_3)$  have been replaced by (u,v,w) and  $(x_1, x_2, x_3)$  by (x,y,z), respectively. The boundary conditions take the form

$$\frac{\partial w}{\partial x} + \frac{\partial u}{\partial z} = 0, \quad \frac{\partial w}{\partial y} + \frac{\partial v}{\partial z} = 0$$

$$c_{12} \left( \frac{\partial u}{\partial x} + \frac{\partial v}{\partial y} \right) + c_{11} \frac{\partial w}{\partial z} = 0 \quad (5)$$

Surface wave solutions to Eqs.(4) and (5) are characterized by an exponential decrease in the displacement amplitudes in the positive z-direction. We accordingly seek solutions of the form

$$(u,v,w) = (U,V,W) \exp \{ \kappa [-qz + i(\ell x + m y - ct)] \} \quad (6)$$

where c is the phase velocity,  $\kappa$  is the magnitude of the two-dimensional wave vector describing the propagation parallel to the surface, q is a dimensionless attenuation constant, and  $\ell, m$  are the direction cosines of the propagation direction. Substitution of Eq.(6) into Eq.(4) yields the following secular equation which must be satisfied if the assumed solution is to be non-trivial:

$$\begin{vmatrix} g_1^2 \ell^2 + m^2 - p^2 - q^2 & \ell m (g_2 + 1) & \ell q (g_2 + 1) \\ \ell m (g_2 + 1) & \ell^2 + g_1^2 m^2 - p^2 - q^2 & m q (g_2 + 1) \\ \ell q (g_2 + 1) & m q (g_2 + 1) & p^2 + g_1^2 q^2 - 1 \end{vmatrix} = 0 \quad (7)$$

In Eq.(7),  $g_1 = c_{11}/c_{44}$ ,  $g_2 = c_{12}/c_{44}$ , and  $p^2 = \rho c^2/c_{44}$ . In

general, the solution of Eq.(7) gives three values of  $q^2$  for given values of the velocity  $c$  and direction cosines  $l, m$ . Denoting the three values of  $q$  with positive real parts by  $q_j$ ,  $j=1,2,3$ , we seek to satisfy the boundary conditions; Eq.(5), by the superposition<sup>(4)</sup>

$$(u, v, iw) = \sum_{j=1}^3 (\xi_j, \eta_j, \zeta_j) K_j \exp \{ \kappa [-q_j z + i(lx + my - ct)] \} \quad (8)$$

where

$$\begin{aligned} \xi_j &= (l^2 + g_1 m^2 - p^2 - q_j^2)(p^2 + g_1 q_j^2 - 1) - m^2 q_j^2 (g_2 + 1) \\ \eta_j &= 4m(g_2 + 1)[q_j^2 (g_2 + 1 - g_1) + 1 - p^2] \\ \zeta_j &= 4q_j (g_2 + 1)[m^2 (g_2 + 1 - g_1) - l^2 + p^2 + q_j^2] \end{aligned} \quad (9)$$

Substitution of Eq.(8) into Eq.(5) yields a set of linear homogeneous equations in the amplitudes  $K_j$  whose non-trivial solution requires that

$$|f_{ij}| = 0 \quad (10)$$

where

$$\begin{aligned} f_{1j} &= l\zeta_j - q_j \xi_j \\ f_{2j} &= m\zeta_j - q_j \eta_j \\ f_{3j} &= l\xi_j + m\eta_j + (c_{11}/c_{12})q_j \zeta_j \end{aligned} \quad (11)$$

The quantities  $q_j$  which appear in Eq.(10) are known functions of  $p^2$  from the solution of Eq.(7), the secular equation. Equation (10) can therefore be used to determine the surface wave velocity or frequency and will be called the frequency equation.

The nature of the surface waves in a given situation depends on the elastic constants of the material, the crystallographic plane to which the surface is parallel, and the direction of propagation of the wave. We now consider solutions of Eqs.(7) and (10) for some special cases.

(1). Isotropic Case.

An isotropic elastic medium is characterized by the Lamé constants  $\lambda, \mu$  which are related to the usual elastic constants  $c_{11}$ ,  $c_{12}$ , and  $c_{44}$  by

$$c_{11} = \lambda + 2\mu, \quad c_{12} = \lambda, \quad c_{44} = \mu. \quad (12)$$

Equations (12) imply a relationship among the elastic constants which is given by

$$c_{11} = c_{12} + 2c_{44} \quad (13)$$

For an isotropic material, the surface wave characteristics are independent of the direction of propagation. We therefore take  $l=1$ ,  $m=0$  in Eq.(7) and utilize Eqs.(12) and (13) to obtain the solutions

$$q_1 = \left(1 - \frac{p^2}{g}\right)^{\frac{1}{2}} \quad (14a)$$

$$q_2 = q_3 = \left(1 - p^2\right)^{\frac{1}{2}} \quad (14b)$$

where  $g = (\lambda + 2\mu)/\mu$ . We note that  $p$  is the ratio of the wave velocity  $c$  to the velocity  $c_t$  of transverse bulk waves, while  $p/g^{\frac{1}{2}}$  is the ratio of  $c$  to the velocity  $c_l$  of longitudinal bulk waves. In order to satisfy the boundary conditions, one must superpose solutions corresponding to  $q_1$  and  $q_2$ . The frequency equation, Eq.(10), can be reduced to the form

$$g(p^6 - 8p^4 + 24p^2 - 16) - 16(p^2 - 1) = 0. \quad (15)$$

Solutions of Eq.(15) corresponding to surface waves must have  $c < c_t, c_l$  so that  $q_1$  and  $q_2$  given by Eqs.(14) are real.

Physical values of the reduced surface wave velocity  $p$  obtained by solving Eq.(15) range from 0.96 for  $g = \infty$ , the incompressible case, to 0.69 for  $g = 1.333\dots$ , the smallest value of  $g$  consistent with crystal stability. The displacements associated with the surface wave can be expressed in the form

$$\begin{aligned} u &= K \left[ e^{-q_1 z} - (1 - \frac{1}{2} p^2) e^{-q_2 z} \right] e^{i\kappa(x-ct)} \\ v &= 0 \\ w &= iK \left[ 1 - (p^2/g) \right] \frac{1}{2} \left[ e^{-q_1 z} - (1 - \frac{1}{2} p^2) e^{-q_2 z} \right] e^{i\kappa(x-ct)} \end{aligned} \quad (16)$$

where  $K$  is a constant. We note from Eq.(16) that the particle displacements execute ellipses in the sagittal plane-i.e., the plane containing both the surface normal and the direction of propagation. We further note that two attenuation constants,  $q_1$  and  $q_2$ , are required to characterize the surface wave in isotropic materials. For the incompressible case,  $q_1 = 1.00$  and  $q_2 = 2.30$ . A diagram illustrating the displacements for  $g = 3$  is shown in Fig. 1.

#### (ii) Anisotropic Case, Cubic Symmetry

##### a. Surface waves on the (001) surface

For the case of the (001) surface of a cubic crystal, one must solve Eq.(10) for the reduced velocity  $p$  using the values of the elastic constant ratios  $\xi_1$  and  $\xi_2$  appropriate to the crystal

under consideration. For an arbitrary direction of propagation of the surface wave, it is difficult to obtain an equation analogous to Eq.(15) for the determination of  $p$ . However, Stoneley<sup>(4)</sup> was able to derive such equations for the two directions of high symmetry. In the [100] direction, he obtained the equation

$$(1-p^2)(g_1^2 - g_2^2 - g_1 p^2)^2 - g_1 p^4 (g_1 - p^2) = 0 \quad (17)$$

while in the [110] direction, he obtained the equation

$$(1-p^2)(g_1 g_3 - g_2^2 - g_1 p^2)^2 - g_1 p^4 (g_3 - p^2) = 0 \quad (18)$$

where  $g_3 = \frac{1}{2}(g_1 + g_2 + 2)$ . In other directions, it is necessary to solve Eqs.(7) and (10) simultaneously using a computer. The displacement patterns for surface waves propagating in the [100] and [110] directions are qualitatively similar to the isotropic case: i.e., the displacements are superpositions of two attenuated terms and trace out ellipses lying in the sagittal plane with a principal axis perpendicular to the surface. For other directions of propagation, the displacements are superpositions of three attenuated terms and trace out ellipses which in general are inclined at some non-zero angle to the sagittal plane.

It is found upon solving for the reduced velocity  $p$  and the attenuation constants  $q$ , that surface waves may exist having either real or complex attenuation constants depending on the elastic constants of the material. Surface waves characterized by real attenuation constants will be called ordinary Rayleigh waves, while those characterized by complex attenuation constants will be called generalized Rayleigh waves.

The distinction between materials having the two different types of surface waves can be illustrated graphically using a plot of the elastic constant ratios  $g_1$  vs  $g_2$ . The case of propagation in the [100] direction is shown in Fig. 2. The region of crystal stability is that to the right of the lines  $g_1 = g_2$  and  $g_1 + 2g_2 = 0$ . Points corresponding to a number of well-known cubic crystals are shown. Materials to the right of the line labeled "bound 1" possess ordinary Rayleigh waves, while those to the left of bound 1 possess generalized Rayleigh waves. The line of isotropy  $g_1 = g_2 = 2$  is shown in Fig. 2 and is seen to lie entirely in the ordinary Rayleigh wave region as expected. One may note that whether a surface wave is an ordinary or a generalized Rayleigh wave does not simply correspond to whether the anisotropy parameter  $2c_{44}/(c_{11} - c_{12})$  is less than or greater than unity, respectively. The line labeled "bound 3" in Fig. 2 will be discussed later.

Since cubic crystals in general are anisotropic, the velocity of surface waves will depend on their direction of propagation. The results of solving the frequency equation, Eq. (10), for the surface wave velocities of several materials is shown<sup>(5)</sup> in Fig. 3 where the reduced velocity  $p$  is plotted as a function of direction of propagation on the (001) surface. One sees that the velocity varies very slowly for the alkali halides KCl and NaCl, but shows a more pronounced variation, including a maximum, for Al, diamond, zinc blende, and Cu. It may be noted that these alkali halides exhibit ordinary Rayleigh waves, whereas the other materials exhibit generalized Rayleigh waves. Another point which may be made is that the alkali halide LiF, in contrast to KCl and NaCl, has gener-

alized Rayleigh waves.

The three attenuation constants  $q_1, q_2, q_3$  required to characterize a Rayleigh wave vary smoothly and rather uninterestingly with direction of propagation for the ordinary Rayleigh wave materials KCl and NaCl. For a generalized Rayleigh wave material such as Cu, however, the attenuation constants exhibit the rather interesting behavior shown<sup>(5)</sup> in Fig. 4. Here  $q_1$  and the real and imaginary parts of  $q_2$  and  $q_3$  are plotted as functions of direction of propagation. One notes that  $q_1$  goes to zero when the direction reaches the [110] direction. This means that the surface wave degenerates to a bulk wave at the [110] direction. Early numerical calculations<sup>(5)</sup> indicated that  $q_1$  reaches zero before the [110] direction is reached, but recently more precise calculations<sup>(6)</sup> have shown that it is only in the [110] direction itself that  $q_1$  is zero. Nevertheless, the generalized Rayleigh waves penetrate deeply into the material for propagation near the [110] direction, and for crystals of ordinary thickness 0.1-1.0 cm, surface waves will exist near [110] only for very short wave lengths.

From the foregoing one concludes that the curves in Fig. 3 for the generalized Rayleigh wave materials correspond to bulk (transverse) waves when the [110] direction is reached. However, surface waves do exist for these materials in the [110] direction, but the velocities are higher than the limiting velocities in the [110] direction shown in Fig. 3. The true surface wave velocities are solutions of Eq. (18). For Cu, the reduced velocity  $p$  of the surface wave is found to be 0.81 which may be compared to the limiting reduced velocity of 0.56 in the [110] direction.

We now ask which cubic materials have the surface wave velocity in the  $[110]$  direction higher than the limiting velocity in that direction for the surface wave branch. The answer is those materials whose elastic constant ratios fall to the left of bound 2 in Fig. 2. Bound 2 itself corresponds to the equality of these two velocities and is obtained by eliminating  $p^2$  from Eq. (18) and from the equation

$$p^2 - \frac{1}{2}(\epsilon_1 - \epsilon_2) = 0 \quad (19)$$

which specifies the limiting reduced velocity in the  $[110]$  direction. The result is

$$2(2 - \epsilon_1 + \epsilon_2)(\epsilon_1 \epsilon_2 + \epsilon_1 - \epsilon_2)^2 - \epsilon_1 (\epsilon_1 - \epsilon_2)^2 (\epsilon_2 + 1) = 0 \quad (20)$$

which is the equation for bound 2.

#### b. Pseudosurface waves on (001) surfaces.

The surface wave in the  $[110]$  direction on the (001) plane of Cu is the limiting case of so-called pseudosurface waves.<sup>(6,7)</sup> For directions near the  $[110]$  direction, these waves involve displacements of the type given by Eq. (8), but one of the attenuation constants  $q_j$  is pure imaginary rather than real or complex. This means that there is a component of the wave which does not attenuate in the direction away from the surface; hence, the name pseudosurface wave. The non-attenuated component causes a flow of energy away from the surface. This in turn requires that the wave vector components parallel to the surface have imaginary parts, so that the wave decays as it propagates along the surface. In many cases, the decay is so small that the pseudosurface wave is readily observable.

In Fig. 5, pseudosurface wave velocities calculated by Lin and Farasli<sup>(8)</sup> are shown for the (001) surface of copper. For angles

below  $20^\circ$ , the pseudosurface waves are nearly pure bulk waves, while at  $45^\circ$ , the wave is a pure surface wave. Also shown in Fig. 5 are the curves for the generalized Rayleigh surface waves and for the lower transverse bulk wave, as well as experimental points<sup>(7)</sup> for the surface and pseudosurface waves. The bulk wave curve approaches very closely to the surface wave curve for angles greater than  $30^\circ$  and finally merges with the surface wave curve at  $45^\circ$ . As we have seen, the surface wave degenerates into a bulk wave at  $45^\circ$ .

Pseudosurface waves are typically exhibited by materials having elastic constant ratios to the left of bound 2 in Fig. 2. A number of specific materials are discussed in detail in the recent review article by Farnell.<sup>(8)</sup> The situation for Cu is, however, fairly representative of that for other cubic materials exhibiting pseudosurface waves.

c. Surface waves and pseudosurface waves on the (110) and (111) surfaces

Rayleigh waves exist on the (110) and (111) surfaces of cubic crystals. Materials which exhibit ordinary Rayleigh waves on the (001) surface frequently exhibit generalized Rayleigh waves on the (110) surface and vice-versa. On the (111) surface, the surface waves are typically of the generalized Rayleigh type. Pseudosurface waves may exist on both (110) and (111) surfaces. For further information concerning surface waves on various surfaces of both cubic and non-cubic materials, the reader may consult the review by Farnell.<sup>(8)</sup>

### (iii). Non-Cubic Materials.

When one investigates materials of lower symmetry than cubic, the calculation becomes more formidable and a general, systematic treatment becomes desirable. Such a treatment has been given for the non-piezoelectric case by Ingebrigtsen and Tonning<sup>(9)</sup> who utilized a six-dimensional vector formalism.

Specific calculations have been carried out for a number of cases. Deresiewicz and Mindlin<sup>(10)</sup> showed that surface waves can propagate on the AT cut of quartz. Zeng et al.<sup>(11)</sup> have experimentally observed both surface and pseudosurface waves on various surfaces of quartz. Their data are in reasonable agreement with theoretical calculations.<sup>(12)</sup> Farnell<sup>(8)</sup> has summarized results of surface wave calculations for a variety of tetragonal, hexagonal, trigonal, and orthorhombic materials. Some of the features revealed by these calculations will now be discussed.

Surface waves propagating on the basal plane ( $(001)$  plane) of tetragonal crystals show marked similarities to surface waves propagating on the  $(001)$  plane of a cubic crystal. Some materials such as tin and zircon have ordinary Rayleigh waves with little variation of surface wave velocity with direction. Rutile, on the other hand, exhibits both generalized Rayleigh waves and pseudosurface waves, and has a marked variation of surface wave velocity with direction. The  $(110)$  plane also exhibits surface wave behavior analogous to that found for the  $(110)$  plane of cubic crystals. The  $(010)$  plane, however, has lower symmetry than the corresponding plane of a cubic crystal, and the surface wave

behavior more nearly resembles that of the (110) plane than the (001) plane.

The basal plane of hexagonal crystals is isotropic for the propagation of surface waves. For some materials, such as CdS, ZnO, and Cd, the surface waves are of the ordinary Rayleigh type, while for Zn the surface waves are of the generalized Rayleigh type. The basal plane of trigonal crystals is normal to a three-fold axis of symmetry and, as might be expected, exhibits surface wave behavior similar to that of the (111) plane of cubic crystals. For further results on non-cubic crystals, the article by Farnell may be consulted.

#### (iv). Piezoelectric Materials.

##### a. General discussion.

Many piezoelectric crystals have electromechanical coupling constants which are sufficiently small so that the piezoelectricity can be neglected when one is discussing surface elastic waves. For other materials, such as lithium niobate, this is no longer the case, and the surface wave problem must be reformulated to include the piezoelectric coupling. This has been done by Tseng and White<sup>(13)</sup> and by Kraut.<sup>(14)</sup> The three Cartesian components of displacement must be augmented as variables by the scalar potential  $\phi$  associated with the electric field produced by the strains. The stress is related to the strain and to the gradient of  $\phi$  by

$$\sigma_{rs} = c_{rspq} \frac{\partial u_p}{\partial x_q} + e_{prs} \frac{\partial \phi}{\partial x_p} \quad (21)$$

where the  $e_{prs}$  are the components of the piezoelectric coupling

tensor. The equations of motion are now obtained by substitution of Eq. (21) into Eq. (2) giving the result

$$\rho \frac{\partial^2 u_r}{\partial t^2} = \frac{\partial}{\partial x_s} \left( c_{rspq} \frac{\partial u_p}{\partial x_q} + e_{prs} \frac{\partial \varphi}{\partial x_p} \right) \quad (22)$$

The constitutive relation involving the electric displacement  $D$  and the dielectric tensor  $\epsilon_{pr}$

$$D_p = e_{prs} \frac{\partial u_r}{\partial x_s} - \epsilon_{pr} \frac{\partial \varphi}{\partial x_r} \quad (23)$$

together with the Maxwell equation

$$\nabla \cdot \underline{D} = 0 \quad (24)$$

yields the equation

$$\frac{\partial}{\partial x_p} \left( e_{prs} \frac{\partial u_r}{\partial x_s} - \epsilon_{pr} \frac{\partial \varphi}{\partial x_r} \right) = 0 \quad (25)$$

which is to be solved simultaneously with Eq. (22).

The boundary conditions for a surface defined by the plane  $x_3=0$  have the form

$$c_{3spq} \frac{\partial u_p}{\partial x_q} + e_{p3s} \frac{\partial \varphi}{\partial x_p} = 0, \quad s = 1, 2, 3, \quad (26)$$

corresponding to the vanishing of the three components of stress at  $x_3=0$ , and

$$-\epsilon_0 \frac{\partial \varphi}{\partial x_3} = e_{3rs} \frac{\partial u_r}{\partial x_s} - \epsilon_{3r} \frac{\partial \varphi}{\partial x_r} \quad (27)$$

corresponding to the continuity of the normal component of  $\vec{D}$  at  $x_3 = 0$ . In Eq. (27'),  $\phi$  is the electric potential outside the crystal. It must satisfy Laplace's equation and approach zero as  $x_3 \rightarrow -\infty$ .

For a general direction of propagation, one has 4x4 determinants in the secular equation and the frequency equation rather than 3x3 determinants as in the non-piezoelectric case. Surface wave solutions have been calculated<sup>(13)</sup> for a number of piezoelectric materials. In an approximate sense one can express the surface wave velocity in terms of elastic constants "stiffened" by the piezoelectric coupling. Another consequence of the piezoelectric coupling is the existence of a new type of surface wave, the Bleustein-Gulyaev wave.<sup>(15,16)</sup>

Specific calculations for the interesting material lithium niobate have been carried out by Cambell and Jones.<sup>(17)</sup> Their results show that omission of the piezoelectric coupling leads to surface wave velocities which are on the order of 15% too low. Tseng and White<sup>(13)</sup> have calculated surface wave velocities on the basal plane of CdS, CdSe, ZnO, and lead-titanate zirconate. The effect of various electromagnetic boundary conditions on surface wave propagation in piezoelectrics has been investigated by Ingebrigtsen.<sup>(18)</sup>

#### b. Bleustein-Gulyaev surface waves.

In the case of piezoelectric crystals a surface wave is possible which has no counterpart in ordinary, non-piezoelectric crystals. This wave was independently discovered by Bleustein<sup>(15)</sup> and Gulyaev.<sup>(16)</sup> It consists of a transverse wave having its mechanical displacement parallel to the surface.

An ordinary surface wave, on the other hand, has its mechanical displacement non-parallel to the surface. Consider a material such as CdS belonging to class  $C_{6v}$  and having its six-fold axis parallel to the  $x_3$  direction. If we consider a surface defined by  $x_2 = 0$  and restrict ourselves to displacements only in the 3-direction which are functions only of  $x_1$  and  $x_2$ , then Eqs. (22) and (25) reduce to

$$\rho \frac{\partial^2 u_3}{\partial t^2} = c_{44} \nabla^2 u_3 + e_{15} \nabla^2 \varphi \quad (28a)$$

$$0 = e_{15} \nabla^2 u_3 - \epsilon_{11} \nabla^2 \varphi \quad (28b)$$

where  $\nabla^2$  is the Laplacian in the variables  $x_1, x_2$  and the Voigt notation has been used for the elastic and piezoelectric constants.

The non-trivial boundary conditions at  $x_2=0$  can be written as

$$\overline{c}_{44} \frac{\partial u_3}{\partial x_2} + e_{15} \frac{\partial \varphi}{\partial x_2} = 0, \quad \varphi = \bar{\varphi}, \quad (29a)$$

$$- \epsilon_0 \frac{\partial \bar{\varphi}}{\partial x_2} = e_{15} \frac{\partial u_3}{\partial x_2} - \epsilon_{11} \frac{\partial \varphi}{\partial x_2} \quad (29b)$$

where  $\bar{\varphi} = \varphi - (e_{15}/\epsilon_{11}) u_3$  and  $\overline{c}_{44} = c_{44} + e_{15}^2/\epsilon_{11}$ .

Taking

$$u_3 = A \cos(kx_1 - \omega t) \exp(-qx_2), \quad x_2 \geq 0 \quad (30a)$$

$$\varphi = B \cos(kx_1 - \omega t) \exp(-kx_2), \quad x_2 \geq 0 \quad (30b)$$

$$\bar{\varphi} = C \cos(kx_1 - \omega t) \exp(kx_2), \quad x_2 \leq 0 \quad (30c)$$

and substituting into Eqs. (28), we find for a non-trivial solution that

$$\rho \omega^2 = \overline{c}_{44} (k^2 - q^2) \quad (31)$$

Substituting Eqs. (30) into Eqs. (29) we get the relation

$$q = \frac{e_{15}^2}{\epsilon_{11} \bar{c}_{44} (1 + \epsilon_{11})} k \quad (32)$$

Combining Eqs. (31) and (32), we obtain for the speed of the Bleustein-Gulyaev wave

$$v^2 = \frac{\bar{c}_{44}}{\rho} \left[ 1 - \frac{e_{15}^4}{\epsilon_{11}^2 \bar{c}_{44}^2 (1 + \epsilon_{11})^2} \right] \quad (33)$$

It can be seen that the speed is somewhat less than the transverse bulk wave speed calculated with the piezoelectrically stiffened elastic constant  $\bar{c}_{44}$ .

Bleustein<sup>(15)</sup> has also treated the case in which the surface is covered with a grounded thin perfectly conducting layer. Gulyaev<sup>(16)</sup> has considered the situation where free charge carriers are present in the crystal. Tseng<sup>(19)</sup> has shown that surface waves of the Bleustein-Gulyaev type can exist on certain surfaces of certain classes of cubic and orthorhombic crystals. Specific results are given for  $\text{Bi}_{12}\text{GeO}_{20}$  (cubic) and  $\text{Ba}_2\text{NaNb}_5\text{O}_{15}$  (orthorhombic).

## B. Lattice Dynamical Theory of Surface Vibrational Modes.

### (1). Static Displacements Near a Surface.

In the lattice dynamical theory, one assumes that the material under consideration is made up of discrete atoms or ions which vibrate about certain equilibrium positions. For an infinite crystal these equilibrium positions are associated with the sites of a crystal lattice periodic in three dimensions. The crystal can be

considered as made up of unit cells, each cell containing a certain number of atoms. The position vector  $\underline{r}(\ell\kappa)$  of the  $\kappa$ -th atom in the  $\ell$ -th unit cell may be expressed in the form  $\underline{r}(\ell\kappa) = \underline{R}^{(0)}(\ell\kappa) + \underline{u}(\ell\kappa)$  where  $\underline{R}^{(0)}(\ell\kappa)$  is the position vector of the equilibrium site and  $\underline{u}(\ell\kappa)$  is the displacement vector from equilibrium. In terms of the primitive translation vectors of the lattice  $\underline{a}_1, \underline{a}_2, \underline{a}_3$ , one can write

$$\underline{R}^{(0)}(\ell\kappa) = \ell_1 \underline{a}_1 + \ell_2 \underline{a}_2 + \ell_3 \underline{a}_3 + \underline{R}(\kappa) \quad (34)$$

where  $\ell_1, \ell_2, \ell_3$  are integers and  $\underline{R}(\kappa)$  is the position vector of the  $\kappa$ -th atom relative to the origin of the unit cell.

We shall consider semi-infinite crystals with a free surface parallel to some lattice plane. The crystal is periodic in the two dimensions parallel to the surface but not in the dimension which is normal to the surface. Two basis vectors  $\underline{a}_1$  and  $\underline{a}_2$  may be chosen parallel to the surface, while the third basis vector  $\underline{a}_3$  is chosen not parallel to the surface. These basis vectors may or may not be the primitive translation vectors of the infinite lattice. The equilibrium position vector  $\underline{R}(\ell\kappa)$  for an atom in the semi-infinite lattice can be expressed as

$$\underline{R}(\ell\kappa) = \underline{R}^{(0)}(\ell\kappa) + \underline{S}(\ell\kappa) \quad (35)$$

where the vector  $\underline{S}(\ell\kappa)$  takes into account the "relaxation" of the equilibrium atomic sites in the semi-infinite crystal away from the corresponding sites of the infinite crystal.

The static displacements  $\underline{S}(\ell\kappa)$  are specified by the equilibrium conditions

$$\underline{F}_a(\ell\kappa) = - \left. \frac{\partial \Phi}{\partial \underline{r}_a(\ell\kappa)} \right|_{\underline{r}(\ell\kappa) = \underline{R}(\ell\kappa)} = 0, \quad (36)$$

$$l_1, l_2 = 0, \pm 1, \pm 2, \dots$$

$$l_3 = 0, 1, 2, \dots$$

$$x = 1, 2, \dots, s; a = 1, 2, 3$$

where  $\Phi$  is the potential energy of the crystal as a function of the atomic positions and  $s$  is the number of atoms in a unit cell. If the static displacements are small, they may be determined by expanding the forces appearing on the left in Eq. (36) in power series about the configuration the atoms would have at equilibrium in the infinite lattice:

$$F_a(lx) = F_a^{(0)}(lx) - i \sum_{\alpha\beta} \Phi_{\alpha\beta}^{(0)}(lx; l'x') S_\beta(l'x') + \dots \quad (37)$$

$$\text{where } F_a^{(0)}(lx) = - \left. \frac{\partial \Phi}{\partial r_a(lx)} \right|_{S(lx) = 0} = 0, \quad (38)$$

$$\Phi_{\alpha\beta}^{(0)}(lx; l'x') = \left. \frac{\partial^2 \Phi}{\partial r_a(lx) \partial r_\beta(l'x')} \right|_{S(lx), S(l'x') = 0} = 0. \quad (39)$$

and higher terms in the series expansion are neglected. One should note that the forces  $F_a^{(0)}(lx)$  are not all zero because  $\Phi$  is the potential energy for the semi-infinite lattice; in fact, the  $F_a^{(0)}(lx)$  are non-zero for those atoms whose distance from the surface is less than the range of the interatomic forces. The  $\Phi_{\alpha\beta}^{(0)}(lx; l'x')$  are the harmonic coupling constants when the atoms are in the configuration appropriate to the infinite lattice. For some assumed set of interatomic interactions, the static displacements can be calculated from Eqs. (36) and (37) by solving a set of inhomogeneous algebraic equations.

Physically, the semi-infinite lattice may be regarded as arising from the infinite lattice by the removal of all atoms

beyond the bounding plane defining the free surface. Atoms near the surface are then acted upon by unbalanced forces,  $F_Q^{(0)}(x)$ , due to the removal of the interactions with atoms across the bounding plane and therefore relax to new equilibrium positions. Symmetry frequently requires that the static displacements be normal to the surface, but this is not always the case. <sup>(20)</sup>

A general discussion of the relaxation of atoms near a free surface has been given by Feuchtwang. <sup>(20)</sup> A number of calculations have been reported based on numerical solutions to Eq. (36) using models involving Lennard-Jones or Morse potential interactions between pairs of atoms. For example, various surfaces of face-centered cubic crystals with Lennard-Jones interactions have been studied by Shuttleworth, <sup>(21)</sup> Alder et al, <sup>(22)</sup> Schmidt and Jura, <sup>(23)</sup> Benson and Claxton, <sup>(24)</sup> and Allen and De Wette. <sup>(25)</sup> The results typically show an expansion outward of the crystal at the surface. The increase in the interlayer spacing is on the order of 2-3% at the surface and decreases rapidly toward the interior. Allen and de Wette <sup>(25)</sup> have shown that for an interatomic potential varying as  $1/r^p$ ,  $p > 3$ , then the increase in interlayer spacing varies at large distances  $d$  from the surface as  $1/d^{p-3}$ . Thus, for a 6-12 Lennard-Jones potential, the spacing varies as  $1/d^3$ , a result previously given by Alder et al. <sup>(22)</sup>

The (001) surface of a simple cubic lattice has been treated by Yun and Benson <sup>(26)</sup> using a Lennard-Jones potential. They find only a 0.5% increase in interlayer spacing at the surface. Vail <sup>(27)</sup>, on the other hand, used a Morse potential and

found a 2% increase. More extensive use of the Morse potential has been reported by Jackson<sup>(28)</sup> who studied the (100), (110), and (111) surfaces of a variety of face-centered and body-centered cubic metals. He found some surprisingly large relaxations of the surface layer e.g., 20% for the (110) surfaces of Ca and Sr, and 80 - 95% for the (111) surfaces of alkali metals. Whether such large deviations from the bulk interplanar spacings are physically reasonable remains to be seen.

Considerable work has been done on ionic crystals of the alkali-halide type by Benson and coworkers.<sup>(29)</sup> For the (100) surfaces, they find typically an alternating contraction and expansion of the surface layers. The surface layer contractions range from about seven percent for NaI to one-half percent for RbF.

Benson and coworkers allowed only the first five surface layers to relax, but permitted separate relaxation of the cations and anions within these layers. Tong and Maradudin<sup>(30)</sup> have followed a different tack by considering a NaCl crystal of 15 layers and allowing all layers to relax with respect to both intralayer and interlayer spacings. They did not, however, allow separate relaxation of cations and anions and required the intralayer relaxation to be the same in all layers. They found an intralayer contraction of about 1% relative to the infinite-crystal nearest-neighbor spacing and an interlayer expansion of about 1% relative to the new intralayer nearest-neighbor spacing. The interlayer expansion is somewhat smaller at the surface than in the interior.

Relatively few analytical results for the static displacements near a surface have been presented. Gazis and Wallis<sup>(31)</sup> have solved Eqs. (36) and (37) for a semi-infinite linear chain with nearest and next-nearest neighbor interactions. A similar calculation has been carried out for a body-centered cubic lattice with a (001) surface by Clark et al<sup>(32)</sup> using Lennard-Jones interactions between nearest and next-nearest neighbors. In both cases the static displacements were found to vary as  $\exp(-q l_3)$  for a surface at  $l_3 = 0$  where  $l_3$  is an integer  $\geq 0$  labelling the lattice planes,  $q$  has the form  $q = q_0 + i\pi\theta$ ,  $q_0$  is a real positive number on the order of unity, and  $\theta$  is 0 or 1 depending on the force constants. This exponential drop-off of the static displacements with distance from the surface is to be contrasted with the inverse power law dependence obtained by Alder et al<sup>(22)</sup> and by Allen and De Wette<sup>(25)</sup> for Lennard-Jones interactions between all atom pairs rather than just nearest and next-nearest neighbors.

#### (ii). Equations of Motion for a Crystal with a Surface.

The vibrations of the atoms in the crystal may be analyzed by expanding the potential energy in power series in the components of the displacements from the equilibrium sites of the semi-infinite lattice,

$$\begin{aligned} \Phi = \Phi_0 &+ \frac{1}{2} \sum_{\alpha\beta} \sum_{l'l''} \Phi_{\alpha\beta}(l, l', l'') u_{\alpha}(l) u_{\beta}(l') \\ &+ \frac{1}{6} \sum_{\alpha\beta\gamma} \sum_{l'l''l'''} \Phi_{\alpha\beta\gamma}(l, l', l'') u_{\alpha}(l) u_{\beta}(l') u_{\gamma}(l'') \\ &+ \dots \end{aligned} \quad (40)$$

where  $u(l) = \underline{r}(l) - \underline{R}(l)$ .

$$\Phi_{\alpha\beta}(l\kappa, l'\kappa') = \frac{\partial^2 \Phi}{\partial r_\alpha(l\kappa) \partial r_\beta(l'\kappa')} \Big|_{\{u(l\kappa)\} = 0} \quad (41a)$$

$$\Phi_{\alpha\beta\gamma}(l\kappa, l'\kappa', l''\kappa'') = \frac{\partial^3 \Phi}{\partial r_\alpha(l\kappa) \partial r_\beta(l'\kappa') \partial r_\gamma(l''\kappa'')} \Big|_{\{u(l\kappa)\} = 0} \quad (41b)$$

and  $\{u(l\kappa)\}$  stands for the entire set of displacements  $u(l\kappa)$ .

The coefficients  $\Phi_{\alpha\beta}(l\kappa, l'\kappa', l''\kappa'')$ , etc., are the harmonic coupling constants, the cubic anharmonic coupling constants, etc.

The coupling constants must satisfy certain invariance conditions. The periodicity of the lattice parallel to the surface (specified by  $l_3 = 0$ ) requires that the coupling coefficients be functions only of the differences  $l_1 - l'_1$ ,  $l_2 - l'_2$ ,  $l_1 - l''_1$ ,  $l_2 - l''_2$ , etc; however, they are in general functions of  $l_3$ ,  $l'_3$ ,  $l''_3$ , ... separately. Infinitesimal translational invariance requires that

$$\sum_{l'\kappa'} \Phi_{\alpha\beta}(l\kappa, l'\kappa') = 0, \quad \sum_{l'\kappa'} \sum_{l''\kappa''} \Phi_{\alpha\beta\gamma}(l\kappa, l'\kappa', l''\kappa'') = 0, \text{ etc.}, \quad (42)$$

while infinitesimal rotational invariance requires that

$$\sum_{l'\kappa'} \left\{ \Phi_{\alpha\beta}(l\kappa, l'\kappa') \left[ R_\gamma(l\kappa) - R_\gamma(l'\kappa') \right] \right. \\ \left. - \Phi_{\alpha\gamma}(l\kappa, l'\kappa') \left[ R_\beta(l\kappa) - R_\beta(l'\kappa') \right] \right\} = 0 \quad (43)$$

with corresponding equations for the anharmonic coupling coefficients. The constraints imposed on the coupling coefficients by rotational invariance are particularly important for surface problems. (33)

The normal modes of vibration for the semi-infinite crystal may be found by solving the harmonic equations of motion for the displacements  $u(l\kappa)$ . Using Eq. (40), these equations can be written as

$$M_{\kappa} \frac{\partial^2 u_{\alpha}(l\kappa)}{\partial t^2} = - \frac{\partial \phi}{\partial u_{\alpha}(l\kappa)} \\ = - \sum_{l'\kappa'\beta} \phi_{\alpha\beta}(l\kappa, l'\kappa') u_{\beta}(l'\kappa') \quad (44)$$

where we have used the symmetry property  $\phi_{\alpha\beta}(l\kappa, l'\kappa') =$

$\phi_{\beta\alpha}(l'\kappa', l\kappa)$ . The solution of Eq. (44) is complicated by two factors. First, there is no periodicity of the atomic sites in the direction normal to the surface; second, the coupling coefficients  $\phi_{\alpha\beta}(l\kappa, l'\kappa')$  are not necessarily the same as the corresponding coefficients for the infinite lattice.

A general discussion of the coupling constants in a semi-infinite crystal has been given by Feuchtwang.<sup>(20)</sup> One may expand the coupling coefficients in power series in the static displacements  $S(l\kappa)$ :

$$\phi_{\alpha\beta}(l\kappa, l'\kappa') = \phi_{\alpha\beta}^{(0)}(l\kappa, l'\kappa') + \sum_{l''\kappa''\gamma} \phi_{\alpha\beta\gamma}^{(1)}(l\kappa, l'\kappa', l''\kappa'') S_{\gamma}(l''\kappa'') \\ + \dots \quad (45)$$

It is clear from Eq. (45) that the changes in the coupling constants arise from anharmonic effects and that they will be large near the surface where the  $S(l\kappa)$  are large. The coupling coefficients with the superscript zero, it must be emphasized, are still not necessarily equal to the corresponding coefficients of the infinite lattice, because the atoms near the surface may be polarized even when they occupy the sites they would occupy in the infinite lattice.

Changes in surface coupling constants have been calculated by Clark et al<sup>(32)</sup> for the case of a (001) surface of iron using a model with Lennard-Jones interactions between nearest and next-nearest neighbors. They found relatively large decreases (20-30%) in certain of the coupling constants at the surface compared to the bulk values even though the static displacements at the surface are only about three percent of the bulk lattice spacing.

Turning now to the solution of the equations of motion, we exploit the translational periodicity parallel to the surface by seeking solutions to Eq.(44) of the form

$$u_{\alpha}(l, \kappa) = N_{\kappa}^{-1/2} v_{\alpha}(l_3 \kappa, k_p) e^{i(k_1 l_1 + k_2 l_2 - \omega t)} \quad (46)$$

where  $\omega$  is the circular frequency and  $k_p$  is a dimensionless two-dimensional wave vector parallel to the surface with components  $k_1$  and  $k_2$ . Substitution of Eq.(46) into Eq.(44) yields a set of linear difference equations in the amplitudes  $v_{\alpha}(l, \omega^2)$ ,

$$\omega^2 v_{\alpha}(l_3 \kappa, k_p) = \sum_{l'_3 \kappa', \beta} D_{\alpha\beta}(l_3 \kappa, l'_3 \kappa', k_p) v_{\beta}(l'_3 \kappa', k_p), \quad (47)$$

where

$$D_{\alpha\beta}(l_3 \kappa, l'_3 \kappa', k_p) = (N_{\kappa} N_{\kappa'})^{-1/2} \sum_{l'_1 l'_2} \delta_{\alpha\beta}(l, l', \kappa') e^{i[k_1(l'_1 - l_1) + k_2(l'_2 - l_2)]} \quad (48)$$

are the elements of the reduced dynamical matrix of the semi-infinite crystal.

The solution of the equations of motion specified by Eq.(44) is more complicated than for an infinite crystal for two reasons. First, a given atom does not interact with atoms beyond the bounding plane of the crystal so certain terms are missing from Eq.(44). Second, the coupling coefficients that are actually present may vary with the distance of the coupled atoms from the surface.

The normal mode frequencies of the crystal are specified by setting the determinant of the coefficients of the amplitudes in Eq.(47) equal to zero:

$$\left| D_{\alpha\beta}(L_3 x, L_3 x', k_p) - \omega^2 \delta_{L_3 L_3} \delta_{xx'} \delta_{\alpha\beta} \right| = 0. \quad (49)$$

For a semi-infinite crystal, the determinant in Eq.(49) is infinite in size. A finite determinant can be obtained, however, by introducing a second surface parallel to the first and specified by  $L_3 - L_3$ . One is now dealing with a plate having  $L_3$  atomic layers. The size of the determinant in Eq.(49) is then  $3sL_3 \times 3sL_3$  where  $s$  is the number of atoms in a unit cell. Results that seem reasonably representative of real crystals are obtained if  $L_3$  is as small as 20 or 30. For simple crystals one then must work with  $60 \times 60$  or  $90 \times 90$  determinants, which can easily be handled using modern high speed computers.

An alternative approach, particularly useful with short-range forces, is to regard each atom as having the same equations of motion. They must be augmented by boundary conditions, which are constraints that restore the effect of the surface on the equations of motion. The procedure is completely analogous to that employed with the continuum theory of surface elastic waves. The determinants which occur in the analogues of the secular equation and the frequency equation are generally on the order of  $3s \times 3s$  in size, which are relatively small and are easily handled on a computer.

Some general aspects of solutions to the equations of motion, Eq.(44), have been discussed by Feuchtwang.<sup>(20)</sup> For a semi-infinite crystal, such solutions may be "bulk" solutions where the displacements  $u_\alpha(L_k)$  do not approach zero as  $L_3 \rightarrow \infty$  and "surface" solutions where they approach zero as  $L_3 \rightarrow \infty$ . For a finite slab, the surface and bulk solutions differ according to whether the displacements

do or do not approach zero, respectively, at the center of the slab as the thickness becomes very large. In the following we shall consider the surface solutions for a variety of special cases.

(iii). Linear Monatomic Chain

A specific illustration of some of the points mentioned above is provided by the semi-infinite monatomic chain with nearest-neighbor interactions. The equations of motion for the displacement  $u_n$  of atom  $n$  are

$$M \ddot{u}_1 = \alpha'(u_2 - u_1) \quad (50a)$$

$$M \ddot{u}_2 = \alpha(u_3 - u_2) + \alpha'(u_1 - u_2) \quad (50b)$$

$$M \ddot{u}_n = \alpha(u_{n+1} + u_{n-1} - 2u_n), \quad n \geq 3 \quad (50c)$$

where  $\alpha$  and  $\alpha'$  are the coupling constants for bulk atoms and for surface atoms, respectively,  $M$  is the atomic mass, the double dot indicates a second time derivative, and the surface atom is specified by  $n = 0$ .

For an infinite chain, every atom has an equation of motion of the form of Eq. (50c). The normal modes of vibration can be written as travelling waves

$$u_n = U \exp[i(\varphi n - \omega t)] \quad (51)$$

where  $\varphi$  is a dimensionless wave number and  $\omega$  is the frequency specified by

$$\omega^2 = (4\alpha/M) \sin^2(\varphi/2) \quad (52)$$

The wave vector  $\varphi$  ranges from  $-\pi$  to  $+\pi$ , so that the squared frequencies range from 0 to  $4\alpha/M$ :

For the semi-infinite chain, we can obtain surface solutions under certain conditions. Let us write the displacements in the form

$$u_1 = U_1 \exp(i\omega t) \quad (53a)$$

$$u_n = U \exp(-qn + i\omega t), \quad n > 1. \quad (53b)$$

Substitution of Eq.(53b) into Eq.(50) yields the result

$$M\omega^2 = 2\alpha(1 - \cosh q) \quad (54)$$

An equation specifying the attenuation constant  $q$  is obtained by substituting Eqs.(53a) and (53b) into Eqs.(50a) and (50b), using Eq.(54), and setting the determinant of the coefficients of  $U_1$ ,  $U$  equal to zero. The result can be written as

$$q^3 = -c - (c^2 + c)^{1/2} \quad (55)$$

where  $c = (\alpha' - \alpha)/\alpha$ . For a surface mode, the real part of  $q$  must be positive. Such a solution to Eq.(55) exists for  $c > 1/3$  and has the form  $q = q_0 + i\eta$  where  $q_0$  is real and positive. The frequency is now specified by

$$\omega = [(2\alpha/M)(1 + \cosh q_0)]^{1/2} \quad (56)$$

and is larger than the maximum bulk mode frequency  $(4\alpha/M)^{1/2}$ . Thus, for  $c > 1/3$ , a surface mode frequency rises above the allowed band of frequencies of the infinite chain. It should be noted that no surface mode exists when the surface coupling constant  $\alpha'$  is unchanged from the bulk value  $\alpha$ .

If next-nearest neighbor interactions are included, the semi-infinite monatomic linear chain still does not possess a surface mode if the surface coupling constants are unchanged from the bulk values. (31)

One or two surface modes can be produced, however, by suitable changes in the surface coupling constants. (31)

Surface modes can also be produced by changing the mass of the atom at the free end of the chain. This situation corresponds to an adsorbed atom. For nearest-neighbor interactions only, one finds (34) that a surface mode exists provided

$$\frac{\alpha'}{c} > 4 \left( \frac{M'}{M} \right) / \left[ 2 \left( \frac{M'}{M} \right) + 1 \right] \quad (57)$$

where  $M'$  is the mass of the end atom.

If the surface coupling constant  $\alpha'$  has the bulk value  $\alpha$ , a surface mode exists if  $M' < M/2$ . This result has also been obtained by Matsuda (35) and by Asahi and Hori (36) using the transfer-matrix. The closely related scattering-matrix method has been used by Hori and Asahi (37) to treat the case of two isotopic impurity atoms at the free end of a monatomic chain with nearest-neighbor interactions. If the two impurity atoms have the same mass  $M'$ , two surface modes exist if  $M' < M(2-\sqrt{2})/4$ . This problem has also been treated by Masri and Armand (38) who discussed one-dimensional models for argon condensed on krypton and for carbon monoxide adsorbed on platinum. The results for the latter case agree well with those obtained using a three-dimensional model.

That perturbations in masses or coupling constants are required to produce a surface mode in the semi-infinite monatomic linear chain is understandable on the basis of Rayleigh's theorem. (1) Without such perturbations, the creation of the surface corresponds to setting one or more coupling constants to zero, and this by Rayleigh's theorem must depress the normal mode frequencies. For a one-dimensional system, a localized mode such as a surface mode

cannot have its frequency in an allowed band of frequencies of the infinite lattice. Since the allowed band extends down to zero frequency and since the surface mode cannot have a negative frequency, there is no gap into which a depressed frequency can move and thereby produce a surface mode.

#### (iv). Diatomic Linear Chain

The semi-infinite diatomic linear chain offers an interesting contrast to the semi-infinite monatomic linear chain in that a surface mode is possible<sup>(39)</sup> without changing the surface force constants, provided the atom at the free end is the lighter of the two atoms in the chain. If one assumes nearest-neighbor interactions, the equations of motion have the form

$$m \ddot{u}_1 = \alpha(u_2 - u_1) \quad (58a)$$

$$M \ddot{u}_{2j} = \alpha(u_{2j+1} + u_{2j-1} - 2u_{2j}), \quad j \geq 1 \quad (58b)$$

$$m \ddot{u}_{2j-1} = \alpha(u_{2j} + u_{2j-2} - 2u_{2j-1}), \quad j \geq 2 \quad (58c)$$

where the end atom is taken to have the smaller of the two masses  $m < M$ . A surface solution to Eqs.(58) exists<sup>(39)</sup> and can be written as

$$u_{2j-1} = U(-1)^{j-1} (m/M)^{j-1} \exp(i\omega t) \quad (59a)$$

$$u_{2j} = U(-1)^j (m/M)^j \exp(i\omega t) \quad (59b)$$

where the frequency  $\omega$  is specified by

$$\omega^2 = \frac{\alpha(m+M)}{mM} \quad (60)$$

The atomic displacements for the surface mode in a chain of 10 atoms are shown in Fig. 6.

The normal mode frequencies of the periodic diatomic chain lie in either the acoustical branch,  $0 \leq \omega^2 \leq 2\alpha/M$ , or the optical branch,  $2\alpha/m \leq \omega^2 \leq 2\alpha(m+M)/mM$ . No normal mode frequencies lie in

the gap between the bottom of the optical branch and the top of the acoustical branch. The semi-infinite lattice with a light atom at the free end, however, has its surface mode frequency within the "forbidden" gap. In terms of squared frequencies, this surface mode lies exactly at the center of the gap as shown in Fig. 7. The creation of free ends involves reducing a coupling constant to zero. In accordance with Rayleigh's theorem, this leads to a reduction in the normal mode frequencies. The surface mode in particular arises from an optical mode whose frequency drops from the bottom of the optical branch into the "forbidden" gap.

Surface modes in the semi-infinite diatomic chain with nearest and next-nearest neighbor interactions have been studied by Gazis and Wallis.<sup>(40)</sup> When a light atom is at the free end, the surface mode may be inhibited by making the next-nearest neighbor coupling constant sufficiently large. When a heavy atom is at the free end, however, a surface mode may be induced by proper choice of the next-nearest neighbor coupling constant.

The effect of changing the mass of the free-end atom in a semi-infinite diatomic chain with nearest-neighbor interactions has been studied by Hori and Asahi<sup>(37)</sup> using the scattering matrix method. Defining  $Q = (\alpha' - \alpha)/\alpha$  they find that a surface mode appears with frequency above the top of the optical branch if  $Q < -\frac{1}{2}$  for either  $m > M$  or  $m < M$ . For  $m < M$ , the surface mode with frequency in the forbidden gap merges into the optical branch and disappears for  $Q < -\frac{1}{2}$ , while for  $m > M$ , it comes into existence only for  $Q < -\frac{1}{2}$ .

#### (v). Two and Three-dimensional Monatomic Lattices

##### a. Rosenstock-Newell model

A relatively simple lattice-dynamical model which admits of exact analysis is that of Rosenstock and Newell<sup>(41)</sup> who

consider only nearest-neighbor interactions but with central and non-central components. For the two-dimensional simple square lattice with free boundaries, the equations of motion have the form

$$\begin{aligned}
 M \ddot{u}_{jk} = & \tau(u_{j,k-1} - u_{jk})(1 - \delta_{k,1}) + \sigma(u_{j-1,k} - u_{jk})(1 - \delta_{j,1}) \\
 & + \sigma(u_{j+1,k} - u_{jk})(1 - \delta_{j,N}) \\
 & + \tau(u_{j,k+1} - u_{jk})(1 - \delta_{k,N})
 \end{aligned} \quad (61)$$

for the x-component of displacement  $u$  with a similar set of equations for the y-component  $v$  in which  $u$  is replaced by  $v$ , the central force constant  $\sigma$  is replaced by the non-central force constant  $\tau$ , and  $\tau$  is replaced by  $\sigma$ . As in Eq. (50) the lattice sites are identified by integers  $j, k$  each ranging from 1 to  $N$  and the free boundaries are defined by  $j=1, N$  and  $k=1, N$ .

The exact solutions to the equations of motion have the form

$$\begin{aligned}
 u_{jk} &= U \cos(j - \frac{1}{2})\varphi_1 \cos(k - \frac{1}{2})\varphi_2 \exp(i\omega t) \\
 v_{jk} &= 0
 \end{aligned} \quad (62a)$$

and

$$\begin{aligned}
 u_{jk} &= 0 \\
 v_{jk} &= V \cos(j - \frac{1}{2})\varphi_2 \cos(k - \frac{1}{2})\varphi_1 \exp(i\omega t)
 \end{aligned} \quad (62b)$$

where  $\varphi_1 = n_1 \pi / N$ ,  $\varphi_2 = n_2 \pi / N$ , and  $n_1, n_2$  are integers in the range from 0 to  $N-1$ , inclusive. The normal mode frequencies are specified by

$$\omega^2 = (4\sigma/\mu) [\sin^2(\varphi_1/2) + (\tau/\sigma) \sin^2(\varphi_2/2)] \quad (63)$$

The normal modes of vibration are clearly all wave-like in character and have frequencies which lie in the range 0 to  $2[(\tau + \sigma)/\mu]^{\frac{1}{2}}$ . No surface modes, in particular, no Rayleigh waves, exist for the two-dimensional Rosenstock-Newell mode. A completely similar situation exists for the three-dimensional Rosenstock-Newell model.

The question arises as to why the Rosenstock-Newell model possesses no Rayleigh waves. The answer seems to be associated with the fact that this model is not rotationally invariant.<sup>(33)</sup> The lack of rotational invariance shows up when one applies Eq.(43) to the coupling constants involving a surface atom. Physically, one can see rather easily that a rigid rotation of the crystal about a surface atom will produce a net force acting on that atom as a result of the non-central forces. This is a clear violation of rotational invariance. Alternatively, one may view the lack of Rayleigh waves as due to the decoupling of the x, y, and z equations of motion.

Ludwig and Lengeler<sup>(42)</sup> have shown how to modify the Rosenstock-Newell model to make it rotationally invariant. They introduce additional non-central interactions involving the surface atoms which restore the rotational invariance. Thus, for the two-dimensional case with a free boundary defined by  $k=0$ , the coupling coefficients involving the atom (00) are taken to have the form

$$\phi(00, \pm 10) = - \begin{pmatrix} \sigma & \pm \delta \\ \mp \delta & \tau \end{pmatrix}, \quad \phi(00, 01) = - \begin{pmatrix} \tau & 0 \\ 0 & \sigma \end{pmatrix} \quad (64)$$

where the new coupling constant  $\delta$  must have the value  $\tau/2$  in order for Eq.(43) to be satisfied. It should be noted that the addition to the coupling constant matrix involving  $\delta$  is antisymmetric in contrast to the symmetric form of the bulk coupling constant matrix. We also observe that violating the condition of rotational invariance corresponds to the use of incorrect boundary conditions.

Although the Lengeler-Ludwig model makes possible the existence of Rayleigh waves, the simplicity of the Rosenstock-Newell model associated with the decoupling of the x-, y-, and z-components of displacement in the equations of motion is lost.

Surface modes may arise in the Rosenstock-Newell model without the Lengeler-Ludwig modification if isotopic impurities with sufficiently light mass are present on the surface. The two-dimensional monatomic case has been investigated by Masahi and Hori<sup>(36)</sup> who have considered the effect of replacement of either one or all of the host atoms in the surface row by an impurity atom or atoms. These authors present the conditions for the appearance of a surface mode above the bulk continuum in terms of the mass defect parameter  $Q = (M' - M)/M$  and the force constant ratio  $\gamma/\phi$ . This work has been extended by Fukushima.<sup>(43)</sup>

#### b. Models with Rotationally Invariant Interactions

The simplest way to insure rotational invariance is to choose individual interatomic interactions which are rotationally invariant. This can be accomplished by associating the forces acting on the displaced atoms with changes in the distance between atoms or the angle between atomic bonds or other quantities which remain invariant under a rigid body rotation. A simple application of this idea was made by Gazis, Herman, and Wallis<sup>(5)</sup> who treated the monatomic simple cubic lattice with nearest and next-nearest neighbor central forces plus angle-bending interactions involving pairs of nearest neighbors. For this case, the equations of motion of a bulk atom can be written as

$$\begin{aligned}
\Delta u_{l,m,n} = & -\alpha \left\{ \sum_{\delta=\pm 1} (u_{l+\delta,m,n} - u_{l,m,n}) \right\} \\
& + \beta \left\{ \sum_{c=\pm 1} \sum_{\delta=\pm 1} (u_{l+\delta,m+c,n} + u_{l+\delta,m,n+c} - 2u_{l,m,n}) \right\} \\
& + (\beta + \gamma) \left\{ \sum_{c=\pm 1} \sum_{\delta=\pm 1} \left[ \epsilon \delta (v_{l+\delta,m+c,n} + w_{l+\delta,m,n+c}) \right] \right\} \\
& + 4\gamma \left\{ \sum_{\delta=\pm 1} (u_{l,m+\delta,n} + u_{l,m,n+\delta} - 2u_{l,m,n}) \right\} \quad (65)
\end{aligned}$$

where  $\alpha$  and  $\beta$  are the central coupling constants,  $\gamma$  is the angle-bending coupling constant, and the other equations arise by cyclically permuting  $u, v, w$  and the increments  $\delta, c$  on the indices  $l, m, n$ .

The equations of motion must be augmented by boundary conditions in order to bring in the effect of the surface. For a (001) surface characterized by  $n=0$ , the boundary conditions have the form

$$\begin{aligned}
\sum_{\delta=\pm 1} & \left\{ \beta (u_{l+\delta,m,-1} - u_{l,m,\delta-\delta w_{l+\delta,m,-1}}) \right. \\
& \left. + \gamma [2(u_{l,m,-1} - u_{l,m,0}) - \delta (w_{l+\delta,m,0} + w_{l+\delta,m,-1})] \right\} = 0 \\
\sum_{\delta=\pm 1} & \left\{ \beta (v_{l,m+\delta,-1} - v_{l,m,\delta-\delta w_{l,m+\delta,-1}}) \right. \\
& \left. + \gamma [2(v_{l,m,-1} - v_{l,m,0}) - \delta (w_{l,m+\delta,0} + w_{l,m+\delta,-1})] \right\} = 0 \\
\sum_{\delta=\pm 1} & \left\{ \frac{1}{2} \alpha (w_{l,m,-1} - w_{l,m,0}) + \beta (w_{l+\delta,m,-1} + w_{l,m+\delta,-1} - 2w_{l,m,0}) \right. \\
& - \beta \delta (u_{l+\delta,m,-1} + v_{l,m+\delta,-1}) + 2\gamma (w_{l+\delta,m,0} + w_{l,m+\delta,0} - 2w_{l,m,0}) \\
& \left. + \gamma \delta (u_{l+\delta,m,0} - u_{l,m,\delta} - 1 + w_{l,m+\delta,0} - v_{l,m+\delta,-1}) \right\} \quad (66)
\end{aligned}$$

We shall solve Eqs. (63 and (66) in a manner analogous to that employed with the cubic continuum. If we assume a solution of the form

$$(u, v, w)_{l,m,n} = (U, V, W) \exp [-qn + i(\varphi_1 l + \varphi_2 m + \omega t)] \quad (67)$$

and substitute this expression into Eqs. (63), we get a set of linear equations in  $U, V, W$  whose determinant of coefficients must vanish:

$$|d_{ij}(\varphi_1, \varphi_2, \omega^2, q)| = 0 \quad (68)$$

For a given set of force constants and wave number components  $\varphi_1$  and  $\varphi_2$ , Eq. (68) constitutes a relationship between the frequency  $\omega$  and the attenuation constant  $q$ . Since it is a cubic equation in  $\cos q$ , one can solve for three values of  $q$  for given  $\omega$  and use these to form a solution which satisfies the boundary conditions. A surface wave results only if the real part of each  $q_j$  required in the solution is greater than zero.

We now seek to satisfy the boundary conditions by means of a solution of the form

$$(u, v, w)_{l,m,n} = \sum_{j=1}^3 (\xi_j, \eta_j, \zeta_j) K_j \exp [-q_j n + i(\varphi_1 l + \varphi_2 m + \omega t)] \quad (69)$$

where  $\xi_j, \eta_j, \zeta_j$  are the appropriate cofactors of  $|d_{ij}|$ . Substitution of Eq. (69) into Eqs. (66) leads to a set of linear equations in the amplitudes  $K_j$ . A non-trivial solution to these equations requires that a determinantal equation be satisfied,

$$|X_{ij}| = 0 \quad (70)$$

whose solution determines the frequency  $\omega$  or phase velocity  $c = \omega a / q$ , where  $a$  is the lattice constant.

The force constants  $\alpha, \beta, \gamma$  can be determined by making a best fit of calculated bulk phonon dispersion curves to experimental data from inelastic neutron scattering or by fitting the elastic constants. The latter procedure can be accomplished by expanding the displacement components in power series about those for the site  $l, m, n$ . For example,

$$u_{l+\delta, m+\epsilon, n} = u_{l, m, n} + \delta \frac{\partial u_{l, m, n}}{\partial x} + \epsilon \frac{\partial u_{l, m, n}}{\partial y} + \frac{1}{2} \delta^2 \left\{ \delta^2 \frac{\partial^2 u_{l, m, n}}{\partial x^2} + 2\delta\epsilon \frac{\partial^2 u_{l, m, n}}{\partial x \partial y} + \epsilon^2 \frac{\partial^2 u_{l, m, n}}{\partial y^2} \right\} + \dots \quad (71)$$

Substitution of these expansions into Eqs. (65) and (66) and retention of terms only through  $a^2$  yields partial differential equations which are completely analogous to the continuum equations of motion and continuum boundary conditions, respectively. Comparison of the coefficients of corresponding terms then provides the following identification of the elastic constants

$$\begin{aligned} c_{11} &= (\alpha + 4\beta)/a \\ c_{12} &= 2\beta/a \\ c_{44} &= (2\beta + 4\gamma)/a \end{aligned} \quad (72)$$

A calculation<sup>(5)</sup> has been carried out with the above model for surface waves propagating in the  $[100]$  direction on a  $(001)$  surface of KCl (considered monatomic). The results, given in Fig. 8, exhibit the dispersion of the Rayleigh waves expected in a lattice theory. Another interesting feature is the divergence of

one of the attenuation constants at a critical wave number  $q_c = 1.75$ . At  $q_c$  this attenuation constant switches from a real value to a complex value of the form  $q_c + i\pi$ .

Another case which has been treated with angle-bending interactions is the monatomic body-centered cubic lattice, <sup>(44)</sup> Phase velocities and attenuation constants were calculated for surface waves propagating in the [100] direction of the (001) surface of vanadium, which exhibits ordinary Rayleigh waves, and iron, which exhibits generalized Rayleigh waves. Dispersion of the phase velocities was established, but no divergence of an attenuation constant was found in either case.

Using the procedure described above, Kaplan <sup>(45)</sup> has studied the semi-infinite monatomic square lattice with nearest and next-nearest neighbor central forces for the situation where a homogeneous isotopic impurity layer is present on the surface edge. He found that the impurity layer has little effect on long-wavelength Rayleigh modes. This is to be expected because long-wavelength Rayleigh modes penetrate deeply into the crystal. At the Brillouin zone boundary, however, the Rayleigh modes are localized within an atomic layer or so of the surface, and they should be significantly affected by the impurity layer. This is just what Kaplan found. For a sufficiently heavy impurity-atom mass  $M'$ , there are two low-frequency surface modes, one of which is the Rayleigh mode. As the impurity mass decreases, in succession the extra low-frequency surface mode disappears, a high-frequency surface mode appears above the allowed band of frequencies, the Rayleigh mode disappears, and finally a second high frequency mode appears.

Surface modes of vibration in monatomic face-centered cubic lattices have been investigated recently by Allen, Alldredge, and DeWette<sup>(46)</sup> who assumed central interactions of the Lennard-Jones 6-12 type between all pairs of atoms in plates up to 21 atomic layers thick. The parameters characterizing the pair-wise interactions were taken to be the same at the surface as in the interior of the crystal. The model may be considered appropriate for a slab of a rare-gas solid.

Allen et al<sup>(46)</sup> first considered surface modes on a (111) surface with propagation in the  $\Gamma X$ ([110]) and  $\Gamma M$ ([112]) directions as well as in the  $MK$  direction along the edge of the Brillouin zone. By solving Eq.(49) on a computer, they found the expected dispersion of the Rayleigh modes. They also found additional surface modes of non-Rayleigh type whose frequencies lie in gaps in the spectrum of the bulk modes as shown in Fig. 9. The atomic displacements of the non-Rayleigh surface modes are primarily parallel to the surface, whereas those of Rayleigh modes are primarily perpendicular to the surface. In a second publication, Allen et al<sup>(47)</sup> report the existence of surface modes on a (100) surface which have the same frequencies as bulk modes with the same value of the two-dimensional wave vector parallel to the surface. We have already encountered surface modes of this type in the continuum theory of materials exhibiting generalized Rayleigh waves.

In a recent publication, Allen, Alldredge, and DeWette<sup>(48)</sup> have extended these calculations to the hexagonal close-packed crystals. Here again, they find surface modes in gaps in the bulk frequency spectrum.

These same authors have recently given<sup>(49)</sup> a general formulation of the surface vibrational mode problem. They discuss the circumstances under which the displacement ellipse of the particles lies in the sagittal plane (surfaces with "axial-inversion symmetry") and when surface modes can have frequencies lying within bulk mode subbands.

Detailed calculations have been reported by Allen et al.<sup>(50)</sup> for monatomic face-centered cubic crystals with (111), (100), and (110) surfaces. They find a number of surface mode branches for each surface-five for the (111) surface, at least nineteen for the (100) surface, and ten for the (110) surface. These results are probably dependent to some extent on the model employed - interactions between all pairs of atoms through a Lennard-Jones potential. Some of the surface modes found by Allen et al.<sup>(50)</sup> are primarily localized in the second layer from the surface or even a deeper layer, rather than in the surface layer itself. These various surface modes can be regarded as "peeling off" in succession from the bulk branches. The effects of surface force-constant changes were also considered.

Some calculations emphasizing the long wavelength region have been carried out by Alldredge, Allen, and DeWette<sup>(51)</sup> for the (100) surface of a face-centered cubic crystal. In addition to the usual Rayleigh waves and pseudosurface waves, they find an additional surface wave propagating in the [110] direction which is polarized shear horizontal. Alldredge<sup>(52)</sup> has shown, however, that the attenuation constant  $\alpha \sim k_p^2$  and hence vanishes in the long-wavelength limit, so this mode is not a Rayleigh-type surface wave.

An investigation of size and surface effects on the lattice dynamical properties of small particles has been reported by Dickey and Paskin<sup>(53)</sup> who used the Lennard-Jones potential and various crystal shapes. The frequency distributions for bulk, surface, and edge modes were calculated and were found to exhibit peaks occurring at successively lower frequencies in the order given.

The case of an isotopic impurity layer on the (111) surface of a face-centered cubic crystal has also been investigated by Allen et al.<sup>(46,47)</sup> As in the work of Kaplan<sup>(45)</sup> they found for a light impurity layer that high frequency surface modes may appear above the bulk continuum and that the Rayleigh mode may disappear at sufficiently large values of the wave vector. This work has been extended by Alldredge, Allen, and DeWette<sup>(54)</sup> to the (100) and (110) surfaces. For very light or very heavy adsorbed particles, there are three principal surface-mode branches associated with the adsorbed layer, but for non-extreme mass ratios, the separation of the principal surface-mode branches is not complete. They find that heavy adsorbed layers enhance the localization of Rayleigh waves and that light layers have the opposite effect.

Phonon frequency distributions for layered structures have been studied by Allen, Alldredge, and DeWette<sup>(55)</sup> who find that interface effects are small compared to surface effects. Some remarks are made concerning superconducting transition temperatures in thin films.

A treatment of an adsorbed layer on the (001) surface of a simple cubic crystal has been given by Dobrzynski and Mills<sup>(56)</sup> using the Rosenstock-Newell model. When the mass ratio of adsorbed and bulk atoms is less than unity, they find localized modes above the bulk continuum whereas if the ratio is greater than unity, they find localized modes below the bulk continuum. The latter are not Rayleigh waves, however, since the Rosenstock-Newell model does not exhibit Rayleigh waves.

Models which involve central forces only must satisfy Cauchy's relation,  $c_{12} = c_{44}$  (cubic crystal, for example). Many metals do not satisfy Cauchy's relation, so non-central forces are required for a proper description of their lattice-dynamical properties. Recently, Musser and Rieder<sup>(57)</sup> have studied surface waves propagating in the [001] direction on the (100) surface of a monatomic face-centered cubic crystal using nearest- and next-nearest neighbor central forces plus non-central forces between nearest neighbors. Rotational invariance was preserved using the procedure of Ludwig and Longaker.<sup>(42)</sup> Musser and Rieder found that the frequencies of long-wavelength Rayleigh waves were significantly affected if rotational invariance was ignored.

The effect of changing the value of the coupling constant for the central interaction between a surface atom and its nearest neighbors in the second layer has been studied by Musser and Rieder<sup>(57)</sup>

using a Green's function technique. If the surface coupling constant is smaller than the corresponding bulk value, a second low-frequency surface mode may appear for wave vectors near the Brillouin zone boundary. The Rayleigh mode frequency is also depressed. If the surface coupling constant is larger than the bulk value, a high-frequency surface mode may appear above the bulk continuum. These results are entirely consistent with Rayleigh's theorem.<sup>(1)</sup> Musser and Rieder also find surface modes with frequencies within a gap in the bulk continuum.

Several workers have studied localized modes associated with isolated atoms or molecules adsorbed on crystal surfaces using three-dimensional models. Grimley<sup>(58)</sup> considered an adatom on a (100) surface of a Rosenstock-Newell model of a simple-cubic lattice and obtained an expression for the localized mode frequencies using the Green's function technique of Montroll and Potts.<sup>(59)</sup> An adsorbed diatomic molecule and the interaction between a pair of adatoms were also treated. Specific application was made to hydrogen and to carbon monoxide adsorbed on platinum. The interaction between two adatoms has also been discussed recently by Cunningham, Dobrzynski, and Maradudin.<sup>(60)</sup>

A problem related to those just described - namely, that of an isotopic impurity atom located in or near a (100) surface of a simple-cubic lattice - has been investigated by Ashkin.<sup>(61)</sup>

The model employed consists of nearest and next-nearest neighbor central forces with the force constants chosen to give elastic isotropy in the long-wavelength limit. Utilizing the Montroll-Potts Green's function technique and by assuming that the local mode frequency is large compared to the maximum frequency  $\omega_M$  of the perfect lattice, Ashkin obtained the following expression for the square of the localized mode frequency

$$[\omega(\alpha, l)]^2 = \frac{a_1(\alpha, l)}{\lambda} + \frac{a_2(\alpha, l)}{a_1(\alpha, l)} + \frac{\lambda a_3(\alpha, l)}{[a_1(\alpha, l)]^2} + O(\lambda^2) \quad (73)$$

where  $\alpha$  denotes the polarization of the localized mode,  $l$  specifies the site of the impurity atom,  $\lambda = M'/M$  is the ratio of the impurity and host atom masses; and

$$a_1(\alpha, l) = D_{\alpha\alpha}(ll) \quad , \quad (74a)$$

$$a_2(\alpha, l) = \sum_{l' \neq l} \sum_{\beta \neq \alpha} D_{\alpha\beta}(ll') D_{\beta\alpha}(l'l) \quad , \quad (74b)$$

$$a_3(\alpha, l) = \sum_{l', l'' \neq l} \sum_{\beta, \gamma \neq \alpha} D_{\alpha\beta}(ll') D_{\beta\gamma}(l'l'') D_{\gamma\alpha}(l''l) \quad . \quad (74c)$$

In Eqs. (74),  $D_{\alpha\beta}(ll)$  is an element of the dynamical matrix for the crystal with a surface but without the impurity given by  $D_{\alpha\beta}(ll') = (Q/M) \phi_{\alpha\beta}(ll')$  where  $\phi_{\alpha\beta}(ll')$  is an element of the force constant matrix. Specific results are given by Ashkin for the model mentioned above. Qualitatively, the localized mode, which is triply degenerate if the impurity is in the bulk, is split by the surface into a singly degenerate mode polarized perpendicular

to the surface and a doubly degenerate mode polarized parallel to the surface. As might be expected, the localized mode frequency is decreased when the impurity is in the surface layer. Thus, for  $\lambda = 0.2$ , the perpendicular mode has a frequency 29 per cent lower and the parallel modes 9 per cent lower than the localized mode frequency when the impurity atom is in the bulk. For this case the bulk localized mode frequency is essentially achieved when the impurity atom is moved just one layer inward from the surface.

The work of Ashkin has been extended to body-centered cubic lattices by Dobrzynski<sup>(62)</sup> who used the model of Clark, Gazis, and Wallis<sup>(63)</sup> to consider both single adatoms and an adlayer on a (100) surface.

A theoretical investigation of vibrational edge modes has recently been carried out by Maradudin, Wallis, Mills, and Ballard<sup>(64)</sup> who treated an edge of a cubic elastic medium bounded by two (100) faces. For the case of elastic isotropy with the Lamé constants  $\lambda, \mu$  equal, they found a localized edge mode with speed  $0.9013 C_t$  compared to the Rayleigh wave speed of  $0.9194 C_t$ .

(vi). Two- and three-dimensional Diatomic Lattices with Short-range Interactions.

Ordinarily, diatomic crystals have ionic character, and the long-range Coulomb interaction between the ions must be taken into account in a lattice-dynamical mode. Some qualitative features, however, may be studied using a model with only short-

range interactions. A general formulation of the problem based on a Green's function method was given a number of years ago by Lifshitz and Rosenzweig<sup>(65)</sup> who noted the existence of both acoustical and optical surface modes. Wallis<sup>(66)</sup> later studied the Rosenstock-Newell model for finite two- and three-dimensional diatomic lattices of the rock-salt type using both a perturbative procedure and a Green's function procedure. It was found that a band of surface mode frequencies occurs in the gap between the acoustical and optical branches. These modes are closely related to the surface mode of the linear diatomic chain with nearest neighbor interactions. Furthermore, for the finite lattices considered, edge and corner modes were found in which the atomic displacements are localized near edges and corners, respectively. Typically, the frequencies of edge modes lie below those of the surface modes mentioned above and the frequencies of corner modes lie below those of the edge modes. This is physically reasonable in view of the decreasing number of interactions with neighbors possessed by an atom as it changes from a surface atom to an edge atom to a corner atom.

A surface mode calculation using a rotationally invariant model for a rock-salt type crystal was carried out by Wallis, Mills, and Maradudin<sup>(67)</sup> who found a surface branch in the gap between the acoustical and optical branches.

(vii). Three-dimensional Diatomic Lattices with Long-range Interactions.

Since diatomic crystals typically have ionic character, a realistic lattice-dynamical model must include the Coulomb interactions between the ions as well as interactions associated with the polarizability of the ions. The long-range character of the Coulomb interactions makes the calculation of the surface mode frequencies somewhat difficult because the effects of the surface are not localized within a few atomic layers of the surface. Furthermore, the possibility of retardation effects associated with the electromagnetic field introduces an aspect to the problem not encountered when only short-range interactions are considered.

We can formulate the surface mode problem with Coulomb interactions by simply noting that the coupling constant matrix  $\Phi_{\alpha\beta}(l\kappa, l'\kappa')$  now can be written as the sum of a Coulomb part and a short-range part:

$$\Phi_{\alpha\beta}(l\kappa, l'\kappa') = \Phi_{\alpha\beta}^C(l\kappa, l'\kappa') + \Phi_{\alpha\beta}^S(l\kappa, l'\kappa'). \quad (75)$$

The Coulomb part has the form

$$\Phi_{\alpha\beta}(l\kappa, l'\kappa') = \frac{\partial^2}{\partial r_{\alpha}(l\kappa) \partial r_{\beta}(l'\kappa')} \left( \frac{q_{\kappa} q_{\kappa'}}{|\underline{r}(l\kappa) - \underline{r}(l'\kappa')|} \right) \Big|_{\underline{u}(l\kappa) = 0} \quad (76)$$

where  $q_{\kappa}, q_{\kappa'}$  are the electrical charges on ions of type  $\kappa, \kappa'$ , respectively. The short-range part can be treated in terms of central forces and angle-bending forces as was done earlier. The calculation

of the surface mode frequencies then requires the solution of the secular equation, Eq. (49), using the coupling constants specified by Eq. (75). A major task involved is the evaluation of the lattice sums in the Coulomb contribution to the reduced dynamical matrix indicated in Eq. (48).

Upon solving the secular equation, one obtains acoustical surface modes which reduce to the Rayleigh waves in the long-wavelength limit. Of more interest in the present context, however, are optical surface modes which show significant effects due to the Coulomb interactions.

Fuchs and Kliewer<sup>(68)</sup> carried out a calculation for a slab of a NaCl-type crystal with a (001) surface for both rigid ions and polarizable ions. The short-range interactions were taken to be nearest-neighbor central forces. Fuchs and Kliewer neglected the changes in the short-range coupling constants and the relaxation of the ions near the surfaces. In the limit of long wavelengths ( $k_{\perp}$  small compared to the reciprocal of the lattice constant  $a$ ), the lattice sums can be replaced by integrals and the equations of motion become a set of integral equations which were solved by Fuchs and Kliewer. However, a simpler procedure, as pointed out by Kliewer and Fuchs<sup>(69)</sup>, is to treat the problem macroscopically in terms of Maxwell's equations and the appropriate boundary conditions. The effects of retardation can be included in a straightforward fashion.

Consider a slab of thickness  $L = 2d$  with surfaces normal to the  $z$ -direction at  $z = \pm d$ . The material is assumed to be optically isotropic with a dielectric constant  $\epsilon(\omega)$  taken to be that of the bulk medium. The electric and magnetic vectors are chosen to have the form of plane waves propagating along the surface with wave vector  $k$  and frequency  $\omega$ :

$$\underline{E} = \underline{E}(z) \exp [i(kx - \omega t)] , \quad (77a)$$

$$\underline{B} = \underline{B}(z) \exp [i(kx - \omega t)] . \quad (77b)$$

For this situation, Maxwell's equations decouple, the equations of interest involving  $E_x(z)$ ,  $E_z(z)$ , and  $B_y(z)$ . Upon eliminating  $B_y$ , one obtains the pair of equations

$$\frac{dE_z(z)}{dz} = -ikE_x(z) , \quad (78a)$$

$$ik \frac{dE_x(z)}{dz} = -[k^2 - \left(\frac{\omega^2}{c^2}\right)\epsilon(\omega)]E_z(z) . \quad (78b)$$

Inside the material, the solutions for a surface wave can be written as

$$E_x(z) = e^{\alpha z} \mp e^{-\alpha z} , \quad (79a)$$

$$E_z(z) = -i(k/\alpha)(e^{\alpha z} \pm e^{-\alpha z}) , \quad (79b)$$

where

$$\alpha^2 = k^2 - (\omega^2/c^2)\epsilon(\omega) . \quad (80)$$

Outside the material,  $\epsilon(\omega) = 1$  and the solutions can be taken to be

$$E_x(z) = A e^{-\alpha_0 |z|} , \quad (81a)$$

$$E_z(z) = i(k/\alpha_0) A e^{-\alpha_0 |z|} , \quad (81b)$$

where

$$\alpha_0^2 = k^2 - (\omega^2/c^2) . \quad (82)$$

The boundary conditions that  $E_x(z)$  and  $E_z(z)$  be continuous at  $z = \pm d$  yields

$$\epsilon(\omega) = \frac{\alpha}{\alpha_0} \left( \frac{e^{-\alpha d} \mp e^{\alpha d}}{e^{-\alpha d} \pm e^{\alpha d}} \right) \quad (83)$$

which is the dispersion relation for the surface optical phonons, hereafter called Fuchs-Kliener modes. It may be noted that for the isotropic case, the boundary conditions on  $\underline{B}$  require that  $E_y(z) = 0$ .

To complete the calculation,  $\epsilon(\omega)$  must be specified. For cubic crystals of the rocksalt or zincblende structure, we have

$$\epsilon(\omega) = \epsilon_{\infty} (\omega_L^2 - \omega^2) / (\omega_T^2 - \omega^2) \quad (84)$$

where  $\omega_T$  and  $\omega_L$  are the limiting long-wavelength frequencies of transverse and longitudinal optical phonons, respectively, and  $\epsilon_{\infty}$  is the dielectric constant at frequencies large compared to  $\omega_L$  but small compared to interband electronic transition frequencies.

The dispersion relations obtained by solving Eqs. (83) and (84) for several thicknesses of LiF are shown in Fig. 18. For a given thickness, there are two surface modes corresponding to the two surfaces. As  $L \rightarrow \infty$ , the two modes coalesce because the coupling between the front and back surfaces disappears. The modes start on the light line  $\omega = ck$  at  $\omega_T$ , rise rapidly, and then flatten out and approach a limiting frequency given by

$$\omega_{so}(\infty) = \omega_T [(\epsilon_0 + 1) / (\epsilon_{\infty} + 1)]^{1/2} \quad (85)$$

where  $\epsilon_0$  is the static dielectric constant. For a very thick slab,  $L \gg c/\omega_T$ , the dispersion relation for the Fuchs-Kliwer modes can be written as

$$c^2 k^2 / \omega^2 = \epsilon(\omega) / [\epsilon(\omega) + 1] \quad (86)$$

which may be solved together with Eq. (84) to give  $\omega_{so}^2(k) =$

$$(1/2\epsilon_0) [\epsilon_{\infty} + 1] c^2 k^2 + \epsilon_{\infty} \omega_L^2 - \{ [(\epsilon_{\infty} + 1) c^2 k^2 + \epsilon_{\infty} \omega_L^2]^2 - 4\epsilon_0 (\epsilon_{\infty} \omega_L^2 + \omega_T^2) c^2 k^2 \}^{1/2} \quad (87)$$

The electric vector of the surface optical modes in the optically isotropic case considered here executes elliptical motion in the sagittal plane. The ellipse approaches a circle as  $k \rightarrow \infty$ ; as  $k \rightarrow \omega_T/c$ , the surface wave becomes linearly polarized in the direction of propagation. Since the particle displacements  $u$  are proportional to the electric vector  $E$ , the displacements also exhibit the behavior just discussed. It should be noted that the Fuchs-

Kliewer modes are transverse in the sense that  $\nabla \cdot \mathbf{u} = 0$  and that at  $k = \omega_T/c$ , the modes are no longer localized at the surfaces.

The surface modes just described are non-radiative modes. The fields drop off exponentially outside the slab and do not interact directly with external radiation. Other surface modes exist, so-called radiative modes<sup>(69)</sup>, with incoming or outgoing waves outside the crystal. These modes are not true normal modes and are highly damped even when  $\epsilon(\omega)$  is real. The frequencies of the radiative modes lie above the light line  $\omega = ck$ , in contrast to the non-radiative modes which lie below this line.

An independent treatment of the optical modes of vibration of ionic crystals finite in one or more dimensions has been given by Engelman and Ruppin<sup>(70,71)</sup> in a series of papers. They generalize the results of Fuchs and Kliewer to crystals of diverse shapes using the same assumptions as Fuchs and Kliewer. In the case of a slab, their results agree with those of Fuchs and Kliewer. In the case of a sphere, the surface modes fall into two types. The so-called "electric modes," have no radial component of the magnetic vector and have frequencies specified by

$$j_1(k_1 R) [k_0 R h_2(k_0 R)]' = \epsilon_2 h_2(k_0 R) [k_1 j_1(k_1 R)]' \quad (88a)$$

where  $j_1$  and  $h_2$  are spherical Bessel and Hankel functions,  $k_0 = \epsilon_2 \omega/c$ ,  $k_1 = \epsilon_1 \omega/c$ ,  $\epsilon$  and  $\epsilon_2$  are the dielectric constants of the sphere and surrounding medium, and  $R$  is the radius. The "magnetic modes," on the other hand, have no radial component of the electric vector and have frequencies specified by

$$j_2(k_1 R) [k_0 R h_2(k_0 R)]' = h_2(k_0 R) [k_1 j_1(k_1 R)]' \quad (88b)$$

In the non-retarded limit, the surface mode frequencies of the electric type are

$$\omega_{so}^2(l) = \omega_T^2 \left\{ \frac{\epsilon_0 + \epsilon_\infty(l+1)/l}{\epsilon_0 + \epsilon_\infty(l+1)/l} \right\}, \quad l = 1, 2, 3, \dots, \quad (89)$$

where  $\epsilon_0$  and  $\epsilon_\infty$  are the static and high frequency dielectric constants of the sphere. The amplitudes of vibration vary with distance  $r$  from the center of the sphere as  $r^{l-1}$ . The mode  $l=1$  is therefore a uniform mode which has been studied by Fröhlich.<sup>(72)</sup>

Since there is a macroscopic electric field associated with surface optical phonons of the Fuchs-Kliever type, one may expect that these modes will interact with any free charge carriers present in the crystal. Indeed, it has been shown by Kheifets<sup>(73)</sup>, Supin<sup>(74)</sup>, by Chiu and Quinn<sup>(75)</sup>, and by Wallis and Brion<sup>(76)</sup> that the surface-optical phonons couple to the surface plasmons. For carriers in a simple parabolic energy band, one can utilize the procedure presented above except that the dielectric constant given by Eq. (84) is replaced by

$$\epsilon(\omega) = \epsilon_\infty \left\{ \frac{\omega_L^2 - \omega^2}{\omega_T^2 - \omega^2} - \frac{\omega_p^2}{\omega^2} \right\} \quad (90)$$

where  $\omega_p^2 = 4\pi n e^2 / \epsilon_\infty m$  is the plasma frequency,  $n$  is the carrier concentration and  $m$  their effective mass. In the non-retarded limit a relatively simple expression can be given for the coupled surface mode frequencies of a very thick slab,

$$\omega^2 = \frac{1}{2}(\omega_{so}^2 + \omega_{sp}^2) \pm \frac{1}{2}[(\omega_{so}^2 - \omega_{sp}^2)^2 + 4(\omega_{so}^2 - \omega_T^2)(\omega_{sp}^2 - \omega_T^2)]^{1/2}, \quad (91)$$

where  $\omega_{so}$  is given by Eq. (85) and  $\omega_{sp}$  given by

$$\omega_{sp}^2 = \omega_p^2 / (\epsilon_0 + 1/\epsilon_\infty) \quad (92)$$

is the surface plasmon frequency. Experimental verification of Eq. ( 91 ) has recently been reported by Reshina, Gerbshtein, and Mirlin<sup>(77)</sup> for  $n = \text{InSb}$ . Theoretical discussions of the effect of an external magnetic field on the coupled surface modes has been given by Ruppin<sup>(74)</sup>, by Brion, Wallia, Hartstein, and Burstein<sup>(78)</sup> and by Chiu and Quinn.<sup>(79)</sup>

There are a number of rather interesting physical phenomena associated with Fuchs-Kliwer surface modes. Mahan<sup>(80)</sup> has shown that the familiar problem of image charges can be discussed in terms of surface polaritons. If a source charge is located near the interface between two insulating dielectrics or a dielectric and a vacuum, the resulting potential field can be represented by a set of image charges. According to Mahan, surface polaritons make a notable contribution to the image charges; indeed, they give rise to the entire polarization field if the source charge is outside the dielectric.

A second phenomenon associated with surface polaritons is the Van der Waals interaction between solid bodies. It has been shown by Van Kampen, Nijboer, and Schram<sup>(81)</sup> (non-retarded case) and by Gerlach<sup>(82)</sup> (retarded case) that the Van der Waals interaction energy is simply the zero-point energy of the surface polaritons. That only the surface modes and not the bulk modes are involved is clear because only the surface modes have fields extending outside the media.

It will be recalled that Fuchs and Kliwer made two important approximations in their treatment - namely, they neglected the effect of the surface on the short-range interactions and they assumed the wavelength large compared to the lattice spacing. Lucas<sup>(83)</sup> has avoided the first of these approximations in an investigation of optical surface modes in thin slabs of an NaCl-type crystal with (001) surfaces. Nearest-neighbor central forces were assumed for the short-range interactions, and the absence of neighbors beyond the boundaries was taken into account in the equations of motion for the surface atoms. However, relaxation of the ions near the surfaces and retardation were neglected. The ions were assumed to be rigid, and the appropriate Coulomb sums were evaluated in plane-wise fashion.<sup>(84)</sup> Since each lattice plane contains equal numbers of positive and negative ions and is overall neutral, the interactions between planes decrease exponentially with separation, and the convergence of the interplanar interactions is therefore very rapid.

Lucas carried out specific calculations only for  $k_p = 0$  where  $k_p$  is the two-dimensional wave vector parallel to the surface. He found a transverse optical surface mode (displacements parallel to the surface) with a frequency very slightly below that of the transverse optical bulk mode for  $k = 0$ . This result is in contrast to that of Fuchs and Kliwer who found that the transverse optical surface mode is not localized at the surface for  $k_p = 0$ . This difference is attributable to the inclusion by Lucas of corrections to the short-range forces acting on surface ions due to their smaller number of neighbors. However, Lucas found no longitudinal

optical surface modes (displacements perpendicular to the surface) for  $k_p \rightarrow 0$  in agreement with Fuchs and Kliever.

A more refined calculation for the NaCl slab with (001) surfaces has been carried out by Tong and Maradudin<sup>(30)</sup> who assumed nearest-neighbor central forces and Coulomb forces between rigid ions. Proper account was taken of the number of short-range interactions of surface atoms, and the possibility of changes in the interplanar spacing near the surface was included in the formulation, but retardation was neglected. Calculations were made for wave vectors  $k_p$  covering the entire two-dimensional first Brillouin zone.

If we neglect the doubling of the surface modes due to the presence of two surfaces, then we can characterize the results of Tong and Maradudin as follows. For propagation in the [100] direction, there are four surface branches. One branch is acoustical in character and corresponds to Rayleigh waves. There are three optical surface branches. A high frequency branch lies between  $\omega_L$  and  $\omega_T$  and approaches a frequency somewhat below  $\omega_L$  as  $k_p \rightarrow 0$ . This branch would be significantly affected by retardation. A low frequency branch lies below the bulk optical mode frequencies for small  $k_p$ , approaches a frequency just below  $\omega_T$  as  $k_p \rightarrow 0$ , and is polarized in the sagittal plane. An intermediate frequency branch has the same frequency at  $k_p = 0$  as the low frequency branch, but rises into the region between  $\omega_L$  and  $\omega_T$ , and is polarized parallel to the surface. Tong and Maradudin calculated the deviation of the slab frequency distribution from the bulk distribution and found pronounced peaks corresponding to the surface branches.

The investigations of Fuchs and Kliewer and of Tong and Maradudin do not lead to an entirely consistent picture of the surface optical modes of an ionic crystal slab. The problem of reconciling these results has been undertaken by Jones and Fuchs<sup>(83)</sup> and by Chen, Allen, Alldredge, and De Wette<sup>(85,87)</sup>. The following picture emerges as shown in Fig. 11. The high frequency branch of Tong and Maradudin splits as  $k_p \rightarrow 0$  into two branches, one approaching  $\omega_L$  and the other  $\omega_T$ . These are the Fuchs-Kliewer modes. (Tong and Maradudin had not used a sufficiently small  $k_p$  to reveal the splitting.) Near  $k_p = 0$ , the Fuchs-Kliewer modes enter the bulk LO and TO continua and become "mixed" or pseudosurface waves. The low frequency branch enters the acoustical bulk continuum about midway to the Brillouin zone boundary and becomes a mixed mode branch. The intermediate branch does not couple to bulk modes and remains a pure surface branch out to the zone boundary.

Chen et al<sup>(85,87)</sup> have investigated several directions of propagation and have found a variety of surface modes in gaps in the bulk frequency spectrum. They have also utilized the shell model for an NaCl slab and find that the Fuchs-Kliewer modes are pseudosurface waves for all wave vectors. The other surface optical modes are still true surface modes near  $k_p = 0$ . The shell-model calculations have been extended<sup>(88)</sup> to RbF and RbCl, the rock-salt structure materials having the largest gaps between acoustical and optical branches. Well defined "microscopic" surface-mode branches<sup>(39)</sup> with frequencies lying within the gap were found for the (001) surfaces. Surface modes associated with the (001) surface of LiF have also been studied<sup>(89)</sup> using the shell model.

The problem of surface modes in a semi-infinite rocksalt crystal has been tackled by Achar and Barsch<sup>(90)</sup> using the scattering matrix method. However, their results appear to be in error<sup>(91)</sup>.

Another theoretical investigation of the ionic slab is that of Bryksin and Firsov<sup>(92)</sup> who found 24 surface modes in the long wavelength unretarded limit, of which 12 decay slowly away from the surface (like Fuchs-Kliwer modes) and 12 decay rapidly within a few lattice spacings of the surface. The relationship between these results and those of other workers has not been fully established.

#### (viii). Surface Waves in the Presence of Second Sound

Second sound - i.e., propagating temperature waves - has long been known in liquid helium and has recently been observed in solid helium<sup>(93)</sup> and in NaF<sup>(94)</sup>. An investigation of surface effects has been carried out by Ioffe<sup>(95)</sup> who considered the coupling of particle waves and temperature waves through the thermal expansion. Ioffe assumed a semi-infinite isotropic elastic continuum and obtained two surface waves, one corresponding to the Rayleigh waves and the other having a very slow velocity given by

$$v = C_0 (\alpha_T / s_L)^{1/2} (\alpha T)^{1/4} (\rho s_L^2 / CT)^{1/8} s_T \quad (93)$$

where  $\alpha$  is the thermal expansion coefficient,  $\rho$  is the density,  $T$  is the temperature,  $C$  is the specific heat,  $s_L$ ,  $s_T$ , and  $s_T$  are the speeds of bulk longitudinal, transverse, and second sound waves, and  $C_0$  is a constant on the order of unity. Ioffe's slow wave is not simply a surface second sound wave, but a coupled particle-temperature wave.

### 3. SURFACE SPECIFIC HEAT

Within the harmonic approximation, the specific heat of a crystal can be written as the sum of contributions from each of the  $s$  normal modes of vibration in the form

$$C_V = k_B \sum_s \left( \frac{1}{2} \beta \hbar \omega_s \right)^2 \operatorname{csch}^2 \left( \frac{1}{2} \beta \hbar \omega_s \right) \quad (94)$$

where  $\beta = (k_B T)^{-1}$  and  $\omega_s$  is the frequency of the  $s$ th normal mode. For a bulk crystal, the specific heat has the familiar Debye  $T^3$  form at low temperatures. When surfaces are present, the normal mode frequencies are modified from those for a perfectly periodic crystal, and the specific heat acquires a surface contribution whose form we now investigate.

#### A. Continuum Theory.

Early treatments of the surface specific heat are based on the Debye elastic continuum model of a crystal. The Debye theory utilizes a method of counting normal modes which, in its original form, yields the correct result in the limit of an infinite crystal, but an incorrect result for a finite crystal. Montroll<sup>(96)</sup> improved the Debye theory by correcting the counting procedure for the normal modes and found that the vibrational specific heat should have an additional term proportional to the surface area. In the low temperature limit, this correction term is proportional to  $T^2$  in contrast to the  $T^3$  dependence of the bulk term. However, Montroll used clamped boundaries rather than free boundaries.

The modifications of the normal modes by free surfaces have been taken into account in the isotropic elastic continuum theory by Brager and Sokolowiczky,<sup>(97)</sup> by Stratton,<sup>(98)</sup> and by

Dupuis, Mazo, and Onsager. ( 99 ) We shall utilize Stratton's approach in the discussion to follow.

In the continuum approximation the mean vibrational energy can be expressed as an integral over the normal mode frequencies

$$\langle E \rangle = \int_0^{\omega_m} g(\omega) \bar{E}(\omega) d\omega \quad ( 95 )$$

where  $g(\omega) d\omega$  is the number of normal mode frequencies in the range  $\omega$  to  $\omega + d\omega$  and  $\bar{E}(\omega)$  is the mean energy of a normal mode given by

$$\bar{E}(\omega) = \hbar\omega[n(\omega) + \frac{1}{2}] \quad ( 96 )$$

$$n(\omega) = [e^{\hbar\omega/k_B T} - 1]^{-1} \quad ( 97 )$$

The specific heat is then obtained from

$$C_V = \partial \langle E \rangle / \partial T \quad ( 98 )$$

Our basic problem is to calculate the frequency distribution function  $g(\omega)$ .

The enumeration of the normal modes is facilitated if we consider a slab of material bounded by parallel planes of area  $4L_x L_y$  and separated by a distance  $2L_z$ . The normal modes for the isotropic elastic slab were discussed by Lamb. (100) They may be classified as either symmetric or antisymmetric with respect to reflection in the mid-plane of the slab. A further classification can be achieved in terms of the values of the decay constants  $q_1, q_2$  of Sec. 2A(i). For  $q_1, q_2$  both real, we have Rayleigh waves; for  $q_1$  real and  $q_2$  imaginary, we have mixed waves; for  $q_1, q_2$  both imaginary, we have pure bulk waves with a longitudinal component. In addition to these three types of modes, there are pure transverse bulk waves.

The wave vector magnitude  $\kappa$ , the attenuation constants  $q_1, q_2$  and the frequency  $\omega = \kappa c$  are related by the equations

$$1 = [(1+2K)q_1^2 - Kq_2^2]/(1+K) \quad (99)$$

$$\omega^2 = \kappa^2 c_t^2 (q_1^2 - q_2^2)(1+2K)/(1+K) \quad (100)$$

where  $K = \mu/\lambda$  and  $\lambda, \mu$  are the Lamé constants. The wave vector components  $q_x = \kappa l$  and  $q_y = \kappa m$  are specified by periodic boundary conditions

$$q_x = n_x \pi / L_x, \quad n_x = 0, \pm 1, \pm 2, \dots \quad (101a)$$

$$q_y = n_y \pi / L_y, \quad n_y = 0, \pm 1, \pm 2, \dots \quad (101b)$$

The specification of the Rayleigh waves is completed by the boundary condition

$$\frac{\tanh \kappa q_2 L_z}{\tanh \kappa q_1 L_z} = \left[ \frac{4(1+K)(1+2K-\alpha^2 K)\alpha}{(1+2K+\alpha^2)^2} \right]^{\pm 1} = -[\xi_K(\alpha)]^{\pm 1} \quad (102)$$

where  $\alpha = q_2/q_1$  and the exponents  $+1, -1$  refer to the symmetric and antisymmetric modes, respectively. The number of Rayleigh modes with frequencies less than or equal to  $\omega$  is given, to an adequate approximation, by

$$G_R(\omega) = V \omega^2 Y_0^2 / 4\pi L_z c_t^2 \quad (103)$$

where  $V$  is the volume,  $Y_0^2 = (1+2K-\alpha_0^2 K)/(1+2K)(1-\alpha_0^2)$ , and  $\alpha_0$  is the solution of Eq. (102) for  $\kappa \rightarrow \infty$ .

The mixed modes have one attenuation constant replaced by a pure imaginary quantity  $q_2 = i\gamma_2$ . For large  $\kappa$ , the solution of

Eq. (102) is

$$q_2^i = (\pi n_z / 2L_z) + \delta_M \quad (104)$$

where  $\delta_M = \tan^{-1}[-ig_K(\alpha)]$ ,  $n_z = 0, 2, 4, 6, \dots$  for the symmetric modes and  $n_z = 1, 3, 5, 7, \dots$  for the antisymmetric modes. The number of mixed modes  $G_M(\omega)$  is given by

$$G_M(\omega) = \frac{V}{\pi^2} \left[ \frac{\omega^3}{6c_t^3} \left( \frac{1+K}{1+2K} \right)^{\frac{1}{2}} - \frac{\pi \omega^2}{L_z c_t^2} \left( \frac{1}{16} + \frac{1}{4} I \right) \right] \quad (105)$$

where

$$I = \frac{1}{\pi} \int_0^{\pi/2} \left( 1 + \frac{K}{1+2K} \tan^2 \varphi \right) \delta_M'(\tan \varphi) d\varphi \quad (106)$$

$\tan \varphi = u' = i\alpha$ , and  $\delta_M'(\tan \varphi) = \partial \delta_M / \partial \alpha'$ . The integral  $I$  can be evaluated by contour integration yielding

$$I = \frac{(1+K)}{(1+2K)} \left\{ \frac{(1+2K)^2}{(1+\alpha_0)[(1+2K)^2 + \alpha_0]} - \frac{1}{4} \right\} \quad (107)$$

The bulk modes have both attenuation constants replaced by imaginary quantities,  $q_1^i = iq_1$  and  $q_2^i = iq_2$ . For large  $\kappa$ , the solution of Eq. (102) can be written as

$$q_2^i = (\pi n_z / L_z) + \delta_B \quad (108)$$

where  $\delta_B = \tan^{-1}[g_K(\alpha) \tan(\kappa q_1^i L_z)]$  and the  $n_z$  are non-negative integers. For the number of bulk modes  $G_B(\omega)$ , we have

$$G_B(\omega) = \frac{V}{\pi^2} \left\{ \frac{\omega^3}{6c_t^3} \left[ \left( \frac{K}{1+2K} \right)^{3/2} - \left( \frac{1+K}{1+2K} \right)^{\frac{1}{2}} + 1 \right] - \frac{\pi \omega^2}{16L_z c_t^2} \left( \frac{K}{1+2K} \right) \right\} \quad (109)$$

Finally, the values of  $q_2'$  for the pure transverse bulk waves are specified by

$$q_2' = \pi n_z / 2L_z, \quad n = 0, 1, 2, 3, 4, 5, \dots \quad (110)$$

The number of transverse modes with frequencies less than or equal to  $\omega$  is

$$G_T(\omega) = \frac{V}{\pi^2} \left( \frac{\omega^3}{6c_t^3} + \frac{\pi \omega^2}{16L_z c_t^2} \right) \quad (111)$$

The total number of modes with frequencies less than or equal to  $\omega$  is given by

$$G(\omega) = G_R(\omega) + G_M(\omega) + G_B(\omega) + G_T(\omega) \quad (112)$$

The part of  $G(\omega)$  involving  $\omega^3$  gives the bulk contribution to the specific heat, while the part involving  $\omega^2$  gives the surface contribution. The total number of modes is  $3N$  where  $N$  is the number of atoms in the crystal. If  $\omega_m$  is the maximum frequency of the crystal, then

$$3N = G(\omega_m) \quad (113)$$

Utilizing the above expressions for the contributions to  $G(\omega)$ , we obtain from Eq. (113) an expression for  $\omega_m$  in the form

$$\omega_m = \omega_{mB} + \Delta\omega_{mS} \quad (114)$$

where  $\omega_{mB}$  is the maximum frequency of the bulk crystal given by

$c_t [18\pi^2 N/V]^{1/3} / \{2 + [K/(1+2K)]^{3/2}\}^{1/3}$  and  $\Delta\omega_{mS}$  is the change in  $\omega_m$  produced by the surface,

$$\Delta\omega_{mS} = - \frac{\pi \{Y_0^2 - 1 - [K/4(1+2K)]\}}{2(18\pi^2)^{1/3} \{2 + [K/(1+2K)]^{3/2}\}^{2/3}} \cdot \frac{\Delta\omega_{mB}}{n^{1/3} V} \quad (115)$$

where  $A$  is the area of the crystal and  $n = N/V$ .

The differential frequency distribution  $g(\omega)$  is related to  $G(\omega)$  by  $g(\omega) = dG(\omega)/d\omega$ . The internal energy, neglecting the zero-point contribution, can be written from Eq. (95) as

$$\langle E \rangle = \int_0^{\omega_m} \frac{dG}{d\omega} \frac{\hbar\omega}{e^{\hbar\omega/k_B T} - 1} d\omega \quad (116)$$

From Eq. (94), the specific heat becomes

$$C_V = k_B \int_0^{\omega_m} \frac{dG}{d\omega} \left( \frac{\hbar\omega}{k_B T} \right)^2 \frac{e^{\hbar\omega/k_B T}}{(e^{\hbar\omega/k_B T} - 1)^2} d\omega \quad (117)$$

Breaking up both  $\omega_m$  and  $dG/d\omega$  into their bulk and surface parts, we can write the surface contribution to the specific heat,  $C_{VS}$ , in the form

$$C_{VS} = k_B F(K) n^{2/3} [D(x) - E(x)] \quad (118)$$

where

$$F(K) = \frac{3}{2} \left( \frac{3}{2} \pi \right)^{1/3} \frac{\{Y_0^2 - 1 - [K/(1+2K)]\}}{[2 + \{K/(1+2K)\}^{3/2}]^{2/3}} \quad (119a)$$

$$D(x) = \frac{2}{x^2} \int_0^x \frac{u^3 e^u}{(e^u - 1)^2} du \quad (119b)$$

$$E(x) = \frac{x^2 e^x}{(e^x - 1)^2} \quad (119c)$$

and  $x = \hbar\omega_m/k_B T$ .

In the low temperature limit, one finds with the aid of the explicit expressions for  $Y_0$  and  $I$  that

$$C_{VS} = 3\pi\zeta(3) \frac{k^3}{h^2} \frac{2c_t^4 - 3c_t^2 c_l^2 + 3c_l^4}{c_t^2 c_l^2 (c_l^2 - c_t^2)} AT^2 \quad (120)$$

where  $c_l$  is the speed of longitudinal bulk waves specified by  $c_l^2 = (\lambda + 2\mu)/\rho_0$  and  $\zeta(3)$  is the Riemann zeta function of argument 3. Equation (120) was first obtained by Dupuis, Maza, and Onsager<sup>(89)</sup> who used a contour integral representation for  $C_V$ .

The surface specific heat is seen to be proportional to the surface area and to the square of the absolute temperature at low temperatures. For fine powders at sufficiently low temperatures, the surface specific heat may become comparable to the bulk  $T^3$  contribution.

#### B. Discrete Lattice Theory.

The first lattice dynamical theory of the surface specific heat was developed by Patterson<sup>(101)</sup> who utilized the Rosenstock-Newell<sup>(41)</sup> model involving nearest-neighbor central and non-central interactions in a simple cubic lattice. At low temperatures his result reduced to a quantity proportional to  $AT^2$ . However, the lack of rotational invariance of the Rosenstock-Newell model makes the result lack quantitative significance.

A more recent lattice-dynamical calculation is that of Maradudin and Wallis<sup>(102)</sup> who treated the surface as a perturbation and employed a Green's function method. The perturbation involves setting to zero the force constants coupling atoms on opposite sides of the plane defining the surface. In principle, it might also involve changes in force constants at or near the surface but not crossing the defining plane. The latter changes are neglected in the treatment to follow.

Equation (94) for the specific heat may be re-expressed as a power series in  $\exp(-\beta\hbar\omega_s)$

$$C_V = k_B \sum_{n=1}^{\infty} n \sum_s (\beta\hbar\omega_s)^2 \exp(-n\beta\hbar\omega_s). \quad (121)$$

The sum over the normal modes can be replaced by a contour integral, so that

$$C_V = \frac{k_B (\beta\hbar)^2}{\pi i} \sum_{n=1}^{\infty} n \int_C z^3 e^{-n\beta\hbar z} F(z^2) dz \quad (122)$$

where

$$F(z^2) = \sum_s [1/(z^2 - \omega_s^2)] \quad (123)$$

and the contour encloses the positive real axis and thus encloses the poles at  $\pm\omega_s$  of  $F(z^2)$ .

The frequencies  $\omega_s$  are those of the crystal with a pair of free surfaces. We shall also need the frequencies  $\omega_{0s}$  of the perfect periodic crystal and the function  $F_0(z^2)$  obtained by replacing  $\omega_s$  by  $\omega_{0s}$  in Eq. (123). The surface contribution to the specific heat can then be expressed as

$$C_{VS} = \frac{k_B (\beta\hbar)^2}{\pi i} \sum_{n=1}^{\infty} n \int_C z^3 e^{-n\beta\hbar z} [F(z^2) - F_0(z^2)] dz. \quad (124)$$

By expanding in inverse powers of  $z$ , one finds that  $F(z^2) - F_0(z^2)$  is of order  $z^{-4}$ , so that the contour can be taken along the imaginary axis and closed by an infinite semicircle lying in the right-hand side of the complex plane. Since the contribution from the semicircle vanishes, the surface specific heat can be written as

$$C_{VS} = -[2k_B(\beta\hbar)^2/\pi] \sum_{n=1}^{\infty} n J(n\beta\hbar) \quad (125)$$

where  $y = -iz$ ,

$$J(n\beta\hbar) = \int_0^{\infty} y^3 \sin(n\beta\hbar y) \Omega(y^2) dy, \quad (126)$$

$$\text{and } \Omega(y^2) = \mathcal{F}_0(-y^2) - \mathcal{F}(-y^2) \quad (127)$$

In the low temperature limit, we are interested in the asymptotic behavior of  $J(n\beta\hbar)$  as  $n\beta\hbar \rightarrow \infty$ . Now it can be shown<sup>(102)</sup> that  $\Omega(y^2)$  has as its only singularity a logarithmic dependence on  $|y|$  as  $y \rightarrow 0$ ,

$$\Omega(y^2) \sim -\Omega_0 \ln|y| + o(\ln|y|), \quad (128)$$

so that the dominant term in the asymptotic behavior of  $J(n\beta\hbar)$  as  $n\beta\hbar \rightarrow \infty$  is given by<sup>(102)</sup>

$$J(n\beta\hbar) \sim -3\pi\Omega_0/(n\beta\hbar)^4 + o(n^{-4}). \quad (129)$$

The low temperature limit of the surface specific heat then becomes

$$C_{VS} \sim 6\pi\Omega_0(3)k_B(k_B T/\hbar)^2 + o(T^2). \quad (130)$$

The problem now is to calculate  $\Omega(y^2)$  and this requires consideration of the lattice dynamics.

Let the force constant matrices for the perfect crystal and for the crystal with the free surface be  $\mathcal{F}_0$  and  $\mathcal{F}$ , respectively. The equations determining the normal modes for these two cases can be written as

$$\underline{L} \underline{u} = 0 \quad (131)$$

and

$$(\underline{L} - \delta \underline{L}) \underline{u} = 0 \quad (132)$$

where

$$\underline{L} = \omega^2 \underline{M} - \underline{\xi}_0 \quad (133a)$$

$$\delta \underline{L} = \underline{\xi} - \underline{\xi}_0 \quad (133b)$$

$\underline{M}$  is the (diagonal) mass matrix, and  $\underline{u}$  is the complete displacement vector of the atoms.  $\delta \underline{L}$  is the perturbation matrix associated with the free surface.

We now introduce the Green's function matrices  $\underline{G}$  and  $\underline{U}$  for the perfect and perturbed crystals, respectively, by

$$\underline{G} = \underline{L}^{-1} \quad (134)$$

$$\text{and } \underline{U} = (\underline{L} - \delta \underline{L})^{-1} \quad (135)$$

One sees from Eqs. (134) and (135) that  $\underline{U}$  is a solution of

$$\begin{aligned} \underline{U} &= \underline{G} + \underline{G} \delta \underline{L} \underline{U} \\ &= \underline{G} + \underline{G} \underline{T} \underline{G} \end{aligned} \quad (136)$$

where the matrix  $\underline{T}$  satisfies

$$\underline{T} = \delta \underline{L} + \delta \underline{L} \underline{G} \underline{T} \quad (137)$$

It will turn out that  $\Omega(y^2)$  can be expressed in terms of  $\underline{T}$  and that  $\underline{T}$  can be calculated exactly for certain cases of interest.

At this point, we find it convenient to express the elements of  $\underline{U}$  in terms of the eigenvector components  $B_s(\underline{k}\alpha)$  and eigenvalues  $\omega_s^2$  of the dynamical matrix,

$$U_{\alpha\beta}(\underline{k}\alpha; \underline{k}'\alpha'; \omega^2) = \frac{1}{(M_{\alpha} M_{\alpha'})^{\frac{1}{2}}} \sum_s \frac{B_s(\underline{k}\alpha) B_s(\underline{k}'\alpha')}{\omega_s^2 - \omega^2} \quad (138)$$

where the  $B_s(\ell\kappa a)$  satisfy the normalization condition

$$\sum_{\ell\kappa a} B_s(\ell\kappa a) B_{s'}(\ell\kappa a) = \delta_{ss'} \quad (139)$$

Utilizing Eqs. (123) and (138), we see that  $F(\omega^2)$  can be written as

$$F(\omega^2) = \sum_{\ell\kappa a} M_{\kappa} U_{aa}(\ell\kappa; \ell\kappa; \omega^2) \quad (140)$$

A similar expression holds for  $F_0(\omega^2)$  in terms of  $G$  - namely,

$$F_0(\omega^2) = \sum_{\ell\kappa a} M_{\kappa} G_{aa}(\ell\kappa; \ell\kappa; \omega^2) \quad (141)$$

so that

$$\begin{aligned} \Omega(\gamma^2) &= - \sum_{\ell\kappa a} M_{\kappa} [U_{aa}(\ell\kappa; \ell\kappa; \omega^2) - G_{aa}(\ell\kappa; \ell\kappa; \omega^2)] \\ &= - \text{Tr } \underline{M} \underline{G} \underline{T} \underline{G} \end{aligned} \quad (142)$$

The eigenvectors of the perfect crystal  $B_{\underline{k}j}^{(0)}(\ell\kappa a)$  can be taken in the form

$$B_{\underline{k}j}^{(0)}(\ell\kappa a) = \frac{1}{\sqrt{N}} a(\underline{\kappa} | \underline{k}j) e^{i \underline{k} \cdot \underline{x}(\ell)} \quad (143)$$

where the mode index  $s$  now stands for the wave vector  $\underline{k}$  and branch index  $j$ . The elements of  $\underline{G}$  can then be written as

$$\begin{aligned} G_{\alpha\beta}(\ell\kappa; \ell'\kappa'; \omega^2) &= \frac{1}{N(M_{\kappa} M_{\kappa'})^{\frac{1}{2}}} \sum_{\underline{k}j} \frac{a_{\alpha}(\underline{\kappa} | \underline{k}j) a_{\beta}(\underline{\kappa}' | \underline{k}j)}{\omega^2 - \omega^2(\underline{k}j)} \times \\ &\times e^{i \underline{k} \cdot [\underline{x}(\ell) - \underline{x}(\ell')]} \end{aligned} \quad (144)$$

The matrix  $\underline{T}$  is conveniently calculated by means of a double Fourier transform defined by

$$T_{\alpha\beta}(\underline{k}; \underline{k}'; \omega^2) = \frac{(M_{\alpha} M_{\beta})^{\frac{1}{2}}}{N} \sum_{\underline{k}_1 \underline{j}_1} \sum_{\underline{k}_2 \underline{j}_2} e_{\alpha}(\underline{k} | \underline{k}_1 \underline{j}_1) e_{\beta}(\underline{k}' | \underline{k}_2 \underline{j}_2) \times \\ \times e^{i \underline{k}_1 \cdot \underline{x}(\underline{k}) + i \underline{k}_2 \cdot \underline{x}(\underline{k}')} t(\underline{k}_1 \underline{j}_1; \underline{k}_2 \underline{j}_2; \omega^2). \quad (145)$$

Substitution of Eq. (145) into Eq. (137) yields the integral equation satisfied by  $t(\underline{k} \underline{j}; \underline{k}' \underline{j}'; \omega^2)$

$$t(\underline{k} \underline{j}; \underline{k}' \underline{j}'; \omega^2) = V(\underline{k} \underline{j}; \underline{k}' \underline{j}'; \omega^2) + \sum_{\underline{k}_1 \underline{j}_1} \frac{V(\underline{k} \underline{j}; -\underline{k}_1 \underline{j}_1; \omega^2)}{\omega^2 - \omega^2(\underline{k}_1 \underline{j}_1)} t(\underline{k}_1 \underline{j}_1; \underline{k}' \underline{j}'; \omega^2) \quad (146)$$

where

$$V(\underline{k} \underline{j}; \underline{k}' \underline{j}'; \omega^2) = \frac{1}{N} \sum_{\underline{k} \alpha \beta} \sum_{\underline{k}' \alpha' \beta'} e_{\alpha}^*(\underline{k} | \underline{k} \underline{j}) e_{\beta'}(\underline{k}' | \underline{k}' \underline{j}') \frac{\delta L_{\alpha\beta}(\underline{k}; \underline{k}')}{(M_{\alpha} M_{\beta'})^{\frac{1}{2}}} \times \\ \times e^{-i \underline{k} \cdot \underline{x}(\underline{k}) - i \underline{k}' \cdot \underline{x}(\underline{k}')} \quad (147)$$

In terms of  $t(\underline{k} \underline{j}; \underline{k}' \underline{j}'; \omega^2)$ , the function  $\Omega(y^2)$  can be expressed as

$$\Omega(y^2) = - \sum_{\underline{k} \underline{j}} \frac{t(\underline{k} \underline{j}; -\underline{k} \underline{j}; -y^2)}{[y^2 + \omega^2(\underline{k} \underline{j})]^2} \quad (148)$$

The key to obtaining  $\Omega(y^2)$  is the solution of the integral equation (146). In general, this is a difficult task, but it can be accomplished for special cases. We now discuss one such case - namely, a simple cubic lattice with nearest and next-nearest neighbor central forces. The potential energy for this model can be written as

$$\Phi = \frac{1}{4} \sum_{ll'} \sum_{\alpha\beta} \varphi_{\alpha\beta}(r_{ll'}) [u_{\alpha}(l) - u_{\alpha}(l')] [u_{\beta}(l) - u_{\beta}(l')] \quad (149)$$

where the prime on the first sum means the term for  $l = l'$  is omitted and the coupling constants  $\varphi_{\alpha\beta}(r_{ll'})$  may be taken in the form

$$\varphi_{\alpha\beta}(r_{ll'}) = \frac{x_{\alpha}(ll') x_{\beta}(ll')}{(r_{ll'})^2} \varphi''(r_{ll'}) \quad (150)$$

With central forces Cauchy's relation  $c_{12} = c_{44}$  must be satisfied by the elastic constants. We also impose the isotropy condition  $c_{11} = c_{12} + 2c_{44}$  which leads to the restriction

$$\varphi''(a_0) = \varphi''(2^{1/2} a_0) \quad (151)$$

where  $a_0$  is the lattice constant. In the long wavelength limit (which is all we need for the low temperature specific heat), the eigenvalues  $\omega^2(kj)$  are

$$\omega^2(k1) = (3c_{44}/\rho) k^2 \quad (152a)$$

$$\omega^2(k2) = \omega^2(k3) = (c_{44}/\rho) k^2 \quad (152b)$$

The eigenvector  $e(k1)$  is given by

$$e(k1) = \left( \frac{k_x}{k}, \frac{k_y}{k}, \frac{k_z}{k} \right) \quad (153)$$

The other two eigenvectors can always be eliminated with the aid of the closure relation

$$\sum_j e_{\alpha}^*(kj) e_{\beta}(kj) = \delta_{\alpha\beta} \quad (154)$$

For the model just discussed, we introduce a pair of (001) free surfaces by setting to zero all interactions coupling atoms on opposite sides of the plane  $z = \frac{1}{2}a_0$ . A total of five "bonds" are thus cut which link a given atom in the plane  $z = 1$  with atoms in the plane  $z = 0$ . The perturbation  $\delta L$  is specified by

$$\delta L_{\alpha\beta}(\ell\ell') = \varphi_{\alpha\beta}(r_{\ell\ell'}) \left[ \delta_{\ell_z,0} \delta_{\ell'_z,1} + \delta_{\ell_z,1} \delta_{\ell'_z,0} \right], \ell \neq \ell' \quad (155)$$

$$\delta L_{\alpha\beta}(\ell\ell) = - \sum_{\ell'} \delta L_{\alpha\beta}(\ell\ell')$$

The kernel  $V(\underline{k}j; \underline{k}'j'; \omega^2)$  then becomes

$$V(\underline{k}j; \underline{k}'j'; \omega^2) = \delta(k_x + k'_x) \delta(k_y + k'_y) \sum_{\ell} v_{\ell}^{-}(\underline{k}j) v_{\ell}^{-}(\underline{k}'j') \quad (156)$$

where  $\bar{\ell} = \ell - \ell'$ ,

$$v_{\ell}^{-}(\underline{k}j) = \delta_{\ell_z, -1} \frac{2[\varphi''(r_{\ell}^{-})]^{\frac{1}{2}}}{(1M)^{\frac{1}{2}} \cdot r_{\ell}^{-}} [\underline{x}(\bar{\ell}) \cdot \underline{e}(\underline{k}j)] \times$$

$$\times e^{(i/2)\underline{k} \cdot \underline{x}(\bar{\ell})} \sin \frac{1}{2} \underline{k} \cdot \underline{x}(\bar{\ell}), \quad (157)$$

and the volume of the crystal is  $(La_0)^3$ . It should be emphasized that  $\bar{\ell}$  takes on only the five values corresponding to the bonds broken in forming the surface.

From Eq. (156) one sees that the kernel is separable. Equation (146) can then be solved by standard methods to yield the result

$$i(\underline{k}j; \underline{k}'j'; \omega^2) = \delta(k_x + k'_x) \delta(k_y + k'_y) \sum_{\ell\ell'} v_{\ell}^{-}(\underline{k}j) \times$$

$$\times \left[ \frac{1 - N(\underline{k}_x \underline{k}_y; \omega^2)}{2\ell} \right]^{-1} v_{\ell'}^{-}(\underline{k}'j') \quad (158)$$

where  $\underline{I}$  is the  $5 \times 5$  unit matrix and  $\underline{M}(\underline{k}_x \underline{k}_y; \omega^2)$  is a  $5 \times 5$  matrix whose elements are

$$M_{\ell\ell'}(\underline{k}_x \underline{k}_y; \omega^2) = \sum_{\underline{k} \neq \underline{j}} \frac{v_{\ell}(-\underline{k}\underline{j}) v_{\ell'}(\underline{k}\underline{j})}{\omega^2 - \omega^2(\underline{k}\underline{j})} \quad (159)$$

It is convenient to introduce a new  $5 \times 5$  matrix  $\underline{m}(\underline{k}_x \underline{k}_y; \omega^2)$  by

$$\underline{M}(\underline{k}_x \underline{k}_y; \omega^2) = \underline{E}^{-1}(\underline{k}_x \underline{k}_y) [\underline{I} - \underline{m}(\underline{k}_x \underline{k}_y; \omega^2)]^{-1} \underline{E}(\underline{k}_x \underline{k}_y) \quad (160)$$

where

$$E_{\ell\ell'}(\underline{k}_x \underline{k}_y) = \delta_{\ell\ell'} e^{(1/2) a_0 (\underline{k}_x \underline{\ell}_x + \underline{k}_y \underline{\ell}_y)} \quad (161)$$

Using Eqs. (157), (158), and (160), one obtains for  $\Omega(y^2)$  the expression

$$\Omega(y^2) = \sum_{\ell\ell'} \sum_{\underline{k}\underline{j}} \frac{w_{\ell}(\underline{k}\underline{j}) w_{\ell'}(\underline{k}\underline{j})}{[y^2 + \omega^2(\underline{k}\underline{j})]^2} [\underline{I} - \underline{m}(\underline{k}_x \underline{k}_y; -y^2)]_{\ell\ell'}^{-1} \quad (162)$$

where

$$w_{\ell}(\underline{k}\underline{j}) = \frac{2}{(1\lambda)^2} \frac{q''(r_{\underline{k}})}{r_{\underline{k}}} [\underline{x}(\underline{\ell}) \cdot \underline{e}(\underline{k}\underline{j})] \sin \frac{1}{2} \underline{k} \cdot \underline{x}(\underline{\ell}) \quad (163)$$

The singular behavior of  $\Omega(y^2)$  as  $y \rightarrow 0$  arises from a divergence in the sum over  $\underline{k}$  in Eq. (162) associated with small  $\underline{k}$  values. In fact, it is the matrix  $[\underline{I} - \underline{m}(\underline{k}_x \underline{k}_y; \omega^2)]^{-1}$  which is singular as  $\underline{k} \rightarrow 0$ . We can therefore restrict our attention to small  $\underline{k}$  values, replace the sum over  $\underline{k}$  by an integral. The result for  $\Omega(y^2)$  is

$$\Omega(y^2) = \frac{A}{8\pi^2} \sum_{\ell\ell'} \int_{-\frac{\pi}{2a_0}}^{\frac{\pi}{2a_0}} d\underline{k}_x \int_{-\frac{\pi}{2a_0}}^{\frac{\pi}{2a_0}} d\underline{k}_y \underline{m}_{\ell\ell'}^{(2)}(\underline{k}_x \underline{k}_y; -y^2) \times \\ \times [\underline{I} - \underline{m}^{(1)}(\underline{k}_x \underline{k}_y; -y^2)]_{\ell\ell'}^{-1} \quad (164)$$

where  $A$  is the area created by cutting the bonds,

$$m_{\ell\ell'}^{(p)}(k_x k_y; -y^2) = \frac{a_1 c_2^2}{2\pi \ell \ell'} \sum_j \int_{-\frac{\pi}{a_0}}^{\frac{\pi}{a_0}} dk_z \frac{[\tilde{\ell} \cdot \tilde{e}(kj)][\tilde{\ell}' \cdot \tilde{e}(kj)]}{[y^2 + c_j^2 k^2]^p} (\tilde{\ell} \cdot \tilde{\ell}')(k \cdot \tilde{\ell}'), \quad (165)$$

$$\text{and } c_1^2 = 3c_2^2 = 3c_3^2 = 3\gamma^2 (2^{\frac{1}{2}} a_0)/a_0 \rho.$$

The evaluation of the elements of  $m^{(1)}$  and  $m^{(2)}$  using Eq. (165) is straightforward but tedious and is given in detail in Ref. (102).

The result for the limit of  $\Omega(y^2)$  as  $y \rightarrow 0$  is

$$\Omega(y^2) = - \frac{A}{8\pi c_t^2} (10/3) \ln|y| + o(\ln|y|). \quad (166)$$

Using Eqs. (130) and (166) we obtain for the surface specific heat at low temperatures

$$C_{VS} = 3\pi (k_B^3/h^2) \zeta(3) (10/3c_2^2) A T^2 \quad (167)$$

which corresponds to the results of Dupuis et al.<sup>(99)</sup> and of Stratton<sup>(98)</sup> when  $c_\ell^2 = 3c_t^2$ .

At this point it might be well to discuss experimental attempts to observe the surface specific heat. Lien and Phillips<sup>(103)</sup> measured the specific heat of MgO powder in the range 1.5 to 4°K and found a contribution of the form  $C = 0.163T^2$  mJoules/mole/deg. The discrepancy may be attributed to uncertainties in the surface area, the Debye temperature, and the true elastic constants of the small particles. Morrison and Patterson<sup>(104)</sup> carried out measurements on NaCl powder in the range 10°K to room temperature. The excess specific heat over the bulk value between 10°K and 20°K is about

1.5 times the theoretical surface specific heat of Dupuis et al<sup>(98)</sup>. Similar results have recently been obtained by Barkman, Anderson, and Brackett<sup>(109)</sup> for NaCl powder. However, the coefficient multiplying  $T^2$  in the surface specific heat was found to be about 40 per cent less than the value of Morrison and Patterson and is therefore in better agreement with the theoretical result.

De Sorbo and Nichols<sup>(106)</sup> measured the specific heat of lampblack, but the excess specific heat over that of bulk graphite seems to be due more to changes in the elastic constants<sup>(107)</sup> than to surface effects.

The theoretical discussion so far presented has been restricted to isotropic materials. Some recent work is applicable to non-isotropic crystals. A computer calculation of the surface specific heat for a (100) surface of a face-centered cubic lattice with Lennard-Jones (6,12) interactions between all pairs of atoms has been carried out by Allen and De Wette<sup>(25)</sup> using Eq. (94). The results are applicable to crystals of noble-gas atoms and were obtained over a broad range of temperature. At low temperatures, the expected  $T^2$  dependence was found; at higher temperatures, the surface specific heat was found to pass through an inflection point. Indeed, the surface specific heat must pass through a maximum and approach zero as the temperature increases since the high temperature specific heat has the value  $k_B$  per normal mode, independent of the presence of a surface.

This behavior has been found by Allen and De Wette<sup>(108)</sup> who extended the calculations just discussed to the (110) and (111) surfaces of noble gas crystals in addition to the (100) surface.

The surface specific heat was found to peak in the vicinity of  $10^{\circ}\text{K}$  for Ne and at slightly higher temperatures for Ar, Kr, and Xe. Allen and De Wette also calculated the surface free energy which varies linearly with temperature at high  $T$  and approaches the zero-point value as  $T \rightarrow 0$ .

Similar behavior has been found recently by Chen, Alldredge, De Wette, and Allen<sup>(109)</sup> who have calculated surface thermodynamic functions for NaCl slabs using the rigid ion model involving Coulomb interactions and nearest-neighbor Born-Mayer interactions. The results for the surface specific heat are in quite good agreement with experiment.<sup>(105)</sup> The calculated surface specific heat exhibits a maximum at  $45^{\circ}\text{K}$  which is close to the experimental value of  $40^{\circ}\text{K}$ .

The Rosenstock-Newell model<sup>(41)</sup> has been employed by Dobrzynski and Leman<sup>(110)</sup> to calculate the surface specific heat by means of a phase shift method. The result in the low temperature limit has the form

$$C_{\text{vs}} = (3/4\pi c_{\text{t}}^2) [1 + 2(c_{44}/c_{11})^2] \zeta(3) (k_{\text{B}}^3/h^2) AT^2 \quad (168)$$

which is qualitatively similar to the result of Depuis et al.<sup>(99)</sup>

Cunningham<sup>(111)</sup> has calculated the specific heat for an anisotropic (110) surface of a simple cubic lattice using two different nearest-neighbor force constant models. One model assumes a decoupling of the motions parallel and perpendicular to the surface; the other is the Rosenstock-Newell model. The Green's function method<sup>(102)</sup> was used to calculate the surface specific

heat which was found to be about 10 percent lower in the isotropic limit than the correct value. This discrepancy may be due to the lack of rotational invariance of the models.

The surface entropy  $\Delta S$  of face-centered, body-centered and diamond-type cubic crystals has been investigated by Dobrzynski and Friedel<sup>(112)</sup> utilizing a nearest-neighbor central-force model. The (100), (110), and (111) surfaces were studied, and for each lattice it was found that

$$\Delta S(100) > \Delta S(110) > \Delta S(111)$$

#### C. Adsorbed Surface Layers.

Some investigations have recently been reported concerning the surface specific heat of crystals having adsorbed atoms on the surface. Dobrzynski and Mills<sup>(56)</sup> have used a Green's function method similar to that described above to study the Rosenstock-Newell model of a simple cubic lattice with a layer of adsorbed atoms on a (100) surface. The central and non-central force constants were assumed to be equal, and the same value of this constant was used in the bulk and at the surface.

Taking the masses of the surface and bulk atoms to be  $M_s$  and  $M_b$ , respectively, Dobrzynski and Mills found that the mass deviation at the surface gave a contribution to the specific heat at low temperatures of the form

$$\Delta C_{VS} \sim N_S (144 \sqrt{3/5}) \pi^2 \alpha k_B (T/\theta_D)^3 \quad (169)$$

where  $N_S$  is the number of surface atoms (mass  $M_S$ ),  $\alpha = (M_S - M)/M$ , and  $\theta_D$  is the bulk Debye temperature. Since this contribution is smaller on the order of  $T/\theta_D$  than the ordinary surface specific heat, it will be very hard to observe experimentally.

Additional calculations of surface thermodynamic functions for adsorbed particles have been made by Allen, Alldredge, and De Wette<sup>(113)</sup> for the (100), (110), and (111) surfaces of a face-centered cubic lattice with Lennard-Jones interactions. The changes in the thermodynamic functions due to the change in mass of the adsorbed particles were calculated numerically as functions of temperature.

The effect of a step on the surface specific heat, entropy, and free energy has been worked out by Masri, Allan, and Dobrzyński<sup>(114)</sup> for a [100] step on a (001) surface of a simple cubic crystal using the Rosenstock-Newell Model. The step is found to increase the surface specific heat and entropy, but decrease the free energy.

#### 4. ATTENUATION AND AMPLIFICATION OF SURFACE WAVES

Only recently have either the experimental or theoretical aspects of the attenuation of surface waves received detailed attention. We first survey the theoretical situation and then briefly discuss the available experimental results.

##### A. Theoretical Aspects of Surface Wave Attenuation

Various mechanisms can contribute to the damping of surface waves. These include the anharmonic interaction between phonons, the interaction of the surface phonon with impurities and imperfections in the crystal, and the interaction of surface phonons with conduction electrons in metals or semiconductors.

Since long wavelength surface waves penetrate deeply into the material, it may be expected that the damping constant for such surface waves can be related to the damping constants for bulk waves. Press and Healy<sup>(115)</sup> have considered the isotropic case where the Rayleigh wave velocity  $c_R$  is specified by

$$\left(2 - \frac{c_R^2}{c_t^2}\right)^2 - 16 \left(1 - \frac{c_R^2}{c_l^2}\right) \left(1 - \frac{c_R^2}{c_t^2}\right) = 0 \quad (170)$$

where  $c_l$  and  $c_t$  are the velocities of compressional and shear bulk waves, respectively. Dissipation can be incorporated by letting each velocity become complex:

$$\begin{aligned} c_l &\rightarrow v_l = c_l(1 + i\delta_l)^{\frac{1}{2}} \\ c_t &\rightarrow v_t = c_t(1 + i\delta_t)^{\frac{1}{2}} \\ c_R &\rightarrow v_R = c_R(1 + i\delta_R)^{\frac{1}{2}} \end{aligned} \quad (171)$$

If one takes the total differential of Eq. (170) and solves for the increment  $\delta_R$  in terms of  $\delta_t$  and  $\delta_l$ , one finds

$$\delta_R = \frac{\left[ 4 \left( 1 - \frac{c_R^2}{c_l^2} \right) - \left( 2 - \frac{c_R^2}{c_t^2} \right)^3 \right] \delta_t + \left[ 4 \left( 1 - \frac{c_R^2}{c_t^2} \right) \left( \frac{c_t^2}{c_l^2} \right) \right] \delta_l}{4 \left( 1 - \frac{c_R^2}{c_t^2} \right) \frac{c_t^2}{c_l^2} + 4 \left( 1 - \frac{c_R^2}{c_l^2} \right) - \left( 2 - \frac{c_R^2}{c_t^2} \right)^3} \quad (172)$$

The damping constant is proportional to the imaginary part of the wave vector. Writing

$$k = \frac{\omega}{v} = \frac{\omega}{c} - i\alpha \quad (173)$$

and using Eqs. (171), we obtain for  $\alpha$

$$\alpha = \frac{\omega \delta}{2c} \quad (174)$$

The damping constant for the Rayleigh waves  $\alpha_R$  can now be written in terms of the damping constants  $\alpha_l$  and  $\alpha_t$  for compressional and shear waves, respectively, as

$$\alpha_R = \frac{\left[ 4 \left( 1 - \frac{c_R^2}{c_l^2} \right) - \left( 2 - \frac{c_R^2}{c_t^2} \right)^3 \right] \left( \frac{c_t}{c_R} \right) \alpha_t + \left[ 4 \left( 1 - \frac{c_R^2}{c_t^2} \right) \left( \frac{c_t^2}{c_l^2} \right) \right] \left( \frac{c_l}{c_R} \right) \alpha_l}{4 \left( 1 - \frac{c_R^2}{c_t^2} \right) \frac{c_t^2}{c_l^2} + 4 \left( 1 - \frac{c_R^2}{c_l^2} \right) - \left( 2 - \frac{c_R^2}{c_t^2} \right)^3} \quad (175)$$

The theoretical prediction contained in Eq. (175) was found by Press and Healy to be in good agreement with experimental data for plexiglass sheets.

The procedure of adapting the theory for bulk wave attenuation to surface waves has been pushed further by Mc Bride<sup>(116)</sup> who applied the results of Maris<sup>(117)</sup> for bulk wave attenuation by cubic anharmonicity to the surface wave problem. Even at liquid helium temperatures, the wavelength of typical thermal phonons is much less than the wavelength of the ultrasonic surface phonon, so the principal scattering of the ultrasonic surface phonon is by bulk phonons and not by thermal surface phonons. In particular, the dominant process is

$$\Sigma + T \rightarrow T$$

where  $\Sigma$  stands for the ultrasonic surface phonon and  $T$  stands for a thermal transverse bulk phonon. At low temperatures where  $\omega\tau \gg 1$  ( $\tau$  is the lifetime of the  $T$  phonons), Mc Bride finds

$$\alpha \sim T^4 \tau^{-1} \quad (176)$$

where  $T$  is the absolute temperature. This result is at variance with results of other workers to be discussed later.

A somewhat different macroscopic approach has been followed by Maris<sup>(118)</sup> who related the attenuation of ultrasonic surface waves to the bulk viscosity, heat conduction, and thermal expansion of the crystal in the limit that the mean free path of the thermal phonons is much less than the wave length of the surface wave. The procedure should therefore be applicable at high temperatures. A similar treatment has been reported by King and Sheard<sup>(119)</sup> who give a specific expression for the surface wave damping constant. The displacement vector  $u$  which satisfies the free surface boundary conditions can be written in the form (cf. Eq. (8))

$$\underline{u} = \sum_{J=1}^3 \underline{B}_J \underline{K}_J \exp[i(\underline{k}_J \cdot \underline{x} - \omega t)] \quad (177)$$

where  $\underline{B}_J$  and  $\underline{k}_J$  have Cartesian components whose analogues in Eq. (8) are  $\xi_J$ ,  $\eta_J$ ,  $-i\zeta_J$  and  $x_1$ ,  $x_2$ ,  $ix_3$ , respectively. The viscosity tensor components  $\eta_{ijkl}$  enter the Rayleigh dissipation function

$$\dot{\varphi} = \frac{1}{2} \sum_{ijkl} \eta_{ijkl} \dot{e}_{ij} \dot{e}_{kl} \quad (178)$$

where  $e_{ij}$  is an element of the strain tensor

$$e_{ij} = \frac{1}{2} \left( \frac{\partial u_i}{\partial x_j} + \frac{\partial u_j}{\partial x_i} \right) \quad (179)$$

For a general elastic medium, the damping constant  $\alpha$  takes the form

$$\alpha = 8.7 \omega^2 \eta_{\text{eff}} / 2\pi c^3 \quad \text{dB/cm} \quad (180)$$

where

$$\eta_{\text{eff}} = \frac{\sum_{ijkl} \eta_{ijkl} K_J B_{iJ} \alpha_J^{J*} K_J^* B_{kJ}^* \alpha_J^J / (q_J + q_J^*)}{\sum_{iJ} K_J B_{iJ} K_J^* B_{iJ}^* / (q_J + q_J^*)} \quad (181)$$

$\underline{k}_J \cdot \underline{x} = x(\alpha_1 x_1 + \alpha_2 x_2 + \alpha_3^J x_3) = x \sum_i \alpha_i^J x_i$ , and  $\alpha_3^J = iq_J$ . For an isotropic medium, there are only two independent, non-zero elements of the viscosity tensor and the expression for the damping constant reduces to a form equivalent to that of Press and Healy.

A continuum treatment applicable to anisotropic crystals at low temperatures ( $\omega\tau \gg 1$ ) has been presented recently by King and Sheard.<sup>(120)</sup> Proper account is taken of the free surface boundary

conditions. The displacement vector  $u$  which satisfies these boundary conditions can be written in the form given by Eq. (177). Since the damping constant is calculated quantum mechanically using perturbation theory, it is convenient to quantize the displacement field by writing

$$u = \sum_J \sum_{\underline{k}} \left( \frac{\hbar}{2\rho S c_s E} \right)^{\frac{1}{2}} \left[ B_J K_J b_{\underline{k}} \exp i \underline{k}_J \cdot \underline{r} + B_J^* K_J^* b_{\underline{k}}^+ \exp(-i \underline{k}_J \cdot \underline{r}) \right] \quad (182)$$

where  $b_{\underline{k}}$  and  $b_{\underline{k}}^+$  are the annihilation and creation operators for the mode  $\underline{k}$ ,  $c_s$  is the velocity of the surface wave,  $S$  is the surface area, and  $E$  is a normalization constant which can be calculated from the kinetic energy (half the total energy) and is given by

$$E = \sum_{J, J'; 1} B_{1J}^* B_{1J'} K_J^* K_{J'} / (q_J^* + q_{J'}). \quad (183)$$

King and Sheard neglect the effect of the surface on the bulk modes. The corresponding quantization condition for bulk modes of wave vector  $\underline{k}$  and polarization  $p$  can then be written as

$$u = \sum_{\underline{k}, p} \left( \frac{\hbar}{2\rho V \omega_{\underline{k}p}} \right)^{\frac{1}{2}} e_{\underline{k}p} \left( a_{\underline{k}p} e^{i \underline{k} \cdot \underline{r}} + a_{\underline{k}p}^+ e^{-i \underline{k} \cdot \underline{r}} \right) \quad (184)$$

where  $e_{\underline{k}p}$  is the polarization vector and  $a_{\underline{k}p}$ ,  $a_{\underline{k}p}^+$  are the annihilation and creation operators.

The cubic anharmonic interaction in the continuum approximation has the form

$$H_3 = (1/3!) \int \sum_{ijk\ell mn} A_{ijk\ell mn} \frac{\partial u_i}{\partial x_j} \frac{\partial u_k}{\partial x_\ell} \frac{\partial u_m}{\partial x_n} d\mathbf{r} \quad (185)$$

where the coefficients  $A_{ijk\ell mn}$  are related to the second and third order elastic constants. Considering only interactions between a surface phonon and a bulk phonon to produce another bulk phonon,

$$\mathbf{k} + (\mathbf{k}_1, p_1) \rightleftharpoons (\mathbf{k}_2, p_2)$$

King and Sheard obtain for the matrix element of  $H_3$  for this process

$$\begin{aligned} M(\mathbf{k}, \mathbf{k}_1, p_1, \mathbf{k}_2, p_2) = & S \left( \frac{\hbar}{2\rho V} \right) \left( \frac{\hbar}{2\rho S c_s E} \right)^{\frac{1}{2}} \times \left( \frac{k_1 k_2}{c_1 c_2} \right)^{\frac{1}{2}} \times \\ & \times \sum_j [F_j / (1 + q_j + k_{1z} - k_{2z})] \delta(k_x + k_{1x}, k_{2x}) \delta(k_y + k_{1y}, k_{2y}) \times \\ & \times [n_k n_1 (n_2 + 1)]^{\frac{1}{2}} \end{aligned} \quad (186)$$

where  $c_1, c_2$  are the bulk mode velocities,  $n_k, n_1$ , and  $n_2$  are the mode occupation numbers, and

$$F_j = (1/3!) \sum_{ijk\ell mn} \sum_P A_{ijk\ell mn} B_{ijK_j}^j e_{1k}^k e_{1\ell}^{\ell} e_{2m}^m e_{2n}^n \quad (187)$$

where  $P$  denotes the six permutations of the pairs  $(ij)$ ,  $(k_\ell)$ ,  $(mn)$ .

Using perturbation theory, the transition rate and thence the

relaxation time  $\tau_s$  for surface phonons can be calculated. The

result is

$$\frac{1}{\tau_S} = \sum_{p_1 p_2} \iint \frac{\hbar \kappa^2 k_1 k_2}{64\pi^3 \rho c_S^2 \kappa c_1 c_2} (\bar{n}_1 - \bar{n}_2) \left| \sum_J \frac{F_J}{1 + q_J + k_{1z} - k_{2z}} \right|^2 \times$$

$$\times \delta(\omega_S + \omega_1 - \omega_2) \int_{-1}^1 dk_{2z} \quad (188)$$

where  $\bar{n}_1$  and  $\bar{n}_2$  are the mean occupation numbers of the bulk phonons, and  $\omega_S$ ,  $\omega_1$ ,  $\omega_2$  are the frequencies of surface and bulk phonons, respectively. It should be noted that the dominant processes attenuating surface waves are energy conserving (cf. Mc Bride<sup>(116)</sup>), so no relaxation time for the thermal bulk phonons appears in Eq.(188).

The integrals in Eq.(188) may be simplified if one introduces the new variable  $K = k_2 - k_1$  and uses polar coordinates  $k_1$   $\theta$ ,  $\phi$  for  $\underline{k}_1$  with  $K$  as axis. Only small  $K$  are important, so both bulk phonons can be taken in the same branch,  $k_1 k_2 \approx k_1^2$ ,  $v_1 v_2 \approx v_1^2$ . Evaluating the integral over  $k_2$  in Eq.(188), one gets

$$\frac{1}{\tau_S} = \frac{\hbar \omega_S}{64\pi^3 \rho c_S^2 \kappa} \left( \frac{kT}{\hbar} \right)^4 \sum_{p_1} \int D_4 \frac{1}{c_1} \left| \sum_J \frac{F_J}{1 + q_J - \lambda} \right|^2 \delta(\Delta) \sin \theta d\theta d\phi d\lambda \quad (189)$$

where

$$\Delta = 1 - \frac{c_1 K}{c_S \kappa} \cos \theta + \frac{K}{c_S \kappa} \sin \theta \frac{\partial c_1}{\partial \theta}, \quad (190)$$

$$D_4 = \int_0^{x_m} \frac{x^4 e^x}{(e^x - 1)^2} dx, \quad (191)$$

$x_m = \hbar c_1 k_1 / k_B T$ , and  $\lambda = K / \kappa$ . In the low temperature limit,

$D_4 = 4\pi^4/15$ , so one has

$$\frac{1}{\tau_S} = \omega_S T^4 \quad (192)$$

The evaluation of the remaining integrals in Eq. (189) is difficult and has been carried out in approximate fashion by King and Sheard for surface waves propagating in the X direction on the Y and Z surfaces of quartz. The results for the Y surface differ by less than a factor of two from the experimental data of Salzmann et al.<sup>(121)</sup>

A lattice dynamical calculation of surface wave damping for an isotropic cubic crystal has been carried out by Maradudin and Mills<sup>(122)</sup> using a Green's function method. A model with nearest and next-nearest neighbor central harmonic interactions and nearest neighbor cubic anharmonic interactions was employed. Using standard techniques of many-body theory, Maradudin and Mills relate the damping constant  $\Gamma_s(\omega)$  (proportional to the reciprocal of the lifetime) for the s-th normal mode to the proper self energy  $P_s(\omega)$  through the equation

$$\Delta_s(\omega) + i\Gamma_s(\omega) = -\frac{k_B T}{\hbar} \lim_{\epsilon \rightarrow 0} P(\omega - i\epsilon) \quad (193)$$

where  $\Delta_s(\omega)$  is the frequency shift due to the anharmonicity and  $\omega$  is to be taken equal to the normal mode frequency  $\omega_s$ .

In terms of the Green's function  $U_{\alpha\beta}(\mathbf{r}, \mathbf{r}'; \omega^2)$  introduced in our discussion of surface specific heat,  $P_s(\omega)$  can be expressed in lowest order of perturbation theory as

$$P_s(\omega_s) = (\hbar/4\pi N) \sum_{\mathbf{l}_1 \mathbf{l}_2 \mathbf{l}_3} \sum_{\alpha_1 \alpha_2 \alpha_3} \sum_{\mathbf{m}_1 \mathbf{m}_2 \mathbf{m}_3} \sum_{\beta_1 \beta_2 \beta_3} \delta_{\alpha_1 \alpha_2 \alpha_3} (\mathbf{l}_1 \mathbf{l}_2 \mathbf{l}_3) \times \\ \times \delta_{\beta_1 \beta_2 \beta_3} (\mathbf{m}_1 \mathbf{m}_2 \mathbf{m}_3) B_s(\mathbf{l}_1 \alpha_1) B_s(\mathbf{m}_1 \beta_1) \times \\ \times \sum_{\mathbf{n}} U_{\alpha_2 \beta_2}(\mathbf{l}_2 \mathbf{m}_2; -\omega_n^2) \Gamma_{\alpha_3 \beta_3}[\mathbf{l}_3 \mathbf{m}_3; (\omega_s - \omega_n)^2] \quad (194)$$

where the indices  $n, n'$  have been dropped,  $M$  is the mass of an atom,  $\phi_{\alpha_1 \alpha_2 \alpha_3}(\ell_1 \ell_2 \ell_3)$  is the cubic anharmonic coefficient appearing in the cubic anharmonic Hamiltonian

$$H_3 = (1/6) \sum_{\ell_1 \ell_2 \ell_3} \sum_{\alpha_1 \alpha_2 \alpha_3} \phi_{\alpha_1 \alpha_2 \alpha_3}(\ell_1 \ell_2 \ell_3) u_{\alpha_1}(\ell_1) u_{\alpha_2}(\ell_2) u_{\alpha_3}(\ell_3), \quad (195)$$

and  $\omega_\ell = 2\pi k_B T / \hbar$  with  $\ell$  an integer. At this point Maradudin and Mill. expand in terms of the eigenfrequencies  $\omega(\underline{k}j)$  and eigenvectors  $B_{\underline{k}j}^{(0)}(\underline{\ell})$  for the perfect periodic crystal

$$u_{\alpha\beta}(\underline{\ell}\underline{\ell}'; \omega^2) = (1/\hbar) \sum_{\underline{k}_1 j_1} \sum_{\underline{k}_2 j_2} B_{\underline{k}_1 j_1}^{(0)}(\underline{\ell}) B_{\underline{k}_2 j_2}^{(0)}(\underline{\ell}') \times \\ \times u(\underline{k}_1 j_1, \underline{k}_2 j_2; \omega^2), \quad (196a)$$

$$B_{\underline{k}}^{(0)}(\underline{\ell}) = \sum_{\underline{j}} B_{\underline{k}j}^{(0)}(\underline{\ell}) C_{\underline{k}}(\underline{j}), \quad (196b)$$

where  $B_{\underline{k}j}^{(0)}(\underline{\ell})$  is given by Eq. (143). The proper self-energy now becomes

$$P_{\underline{k}}(i\omega) = \frac{72}{\hbar^2 \omega_n} \sum_{\underline{k}_1 \underline{k}_2 \underline{k}_3} \sum_{j_1 j_2 j_3} \sum_{\underline{k}_1' \underline{k}_2' \underline{k}_3'} \sum_{j_1' j_2' j_3'} C_{\underline{k}}(\underline{k}_1 j_1) C_{\underline{k}}(\underline{k}_1' j_1') \\ \times W(\underline{k}_1 j_1, \underline{k}_2 j_2, \underline{k}_3 j_3) W(\underline{k}_1' j_1', \underline{k}_2' j_2', \underline{k}_3' j_3') \\ \times \sum_{\omega} u(\underline{k}_2 j_2, \underline{k}_2' j_2'; -\omega_n^2) u(\underline{k}_3 j_3, \underline{k}_3' j_3'; -(\omega_\ell - \omega_n)^2) \quad (197)$$

where

$$W(k_1j_1, k_2j_2, k_3j_3) = [w(k_1j_1)w(k_2j_2)w(k_3j_3)]^{\frac{1}{2}} \times \\ \times V(k_1j_1, k_2j_2, k_3j_3) \quad (198)$$

and

$$V(k_1j_1, k_2j_2, k_3j_3) = \frac{1}{6} \left( \frac{\hbar}{2M} \right)^{3/2} [w(k_1j_1)w(k_2j_2)w(k_3j_3)]^{-\frac{1}{2}} \times \\ \times \sum_{l_1l_2l_3} \sum_{\alpha_1\alpha_2\alpha_3} \theta_{\alpha_1\alpha_2\alpha_3} (l_1l_2l_3)_{k_1j_1}^{B(0)} (l_1\alpha_1)_{k_2j_2}^{B(0)} (l_2\alpha_2)_{k_3j_3}^{B(0)} (l_3\alpha_3). \quad (199)$$

The sum over  $n$  in Eq. (198) can be evaluated if use is made of the spectral representation for  $u(kj, k'j'; \omega^2)$ ,

$$u(kj, k'j'; \omega^2) = \int_{-\infty}^{\infty} \frac{\bar{u}(kj, k'j'; \nu)}{\nu - \omega} d\nu. \quad (200)$$

Using the theory of contour integration, one finds

$$\sum_{n=-\infty}^{\infty} \left( \frac{1}{\nu_1 - i\omega_n} \right) \left( \frac{1}{\nu_2 - i(\omega_n - \omega)} \right) = \frac{\hbar}{E_B T} [\theta(\nu_1) + \theta(\nu_2)] / (\nu_1 + \nu_2 - i\omega). \quad (201)$$

where  $\theta(\nu) = \frac{1}{2} \coth(\hbar\nu/2k_B T)$ . The damping constant  $\Gamma_S(\omega)$  now follows from Eqs. (193), (198) and (202) and can be written as

$$\Gamma_S(\omega) = \frac{72\pi}{\hbar^2 \omega_S} \sum_{k_1k_2k_3} \sum_{j_1j_2j_3} \sum_{k'_1k'_2k'_3} \sum_{j'_1j'_2j'_3} C_2(k_1j_1) C_S(k_2j_2) \\ W(k_1j_1, k_2j_2, k_3j_3) W(k'_1j'_1, k'_2j'_2, k'_3j'_3) \times \quad (202)$$

$$\times \int_{-\infty}^{\infty} d\nu_1 \int_{-\infty}^{\infty} d\nu_2 \bar{u}(k_2j_2, k'_2j'_2; \nu_1) \bar{u}(k_3j_3, k'_3j'_3; \nu_2) [\theta(\nu_1) + \theta(\nu_2)] \delta(\omega_S - \nu_1 - \nu_2)$$

Turning now to the case where the mode  $s$  is the Rayleigh surface mode, we consider the quantity  $\bar{u}(\underline{k}j, \underline{k}'j'; \nu)$  in the presence of a surface. Since the wavelength of ultrasonic surface phonons is long compared to the wavelength of thermal surface phonons and the penetration distance is proportional to the wavelength, the interaction of the ultrasonic surface phonon with thermal bulk phonons is the main mechanism for damping. If the effect of the surface on the thermal bulk phonons is neglected, Maradudin and Mills show that the spectral density  $\bar{u}(\underline{k}j, \underline{k}'j'; \omega)$  is well approximated by that for the perfect crystal without the surface,  $\bar{u}_0(\underline{k}j, \underline{k}'j'; \nu)$ , given by

$$\bar{u}_0(\underline{k}j, \underline{k}'j'; \omega) = \Delta(\underline{k} + \underline{k}') \delta_{jj'} [\delta(\omega + \omega(\underline{k}j)) - \delta(\omega - \omega(\underline{k}j))] / 2\omega(\underline{k}j). \quad (203)$$

The next ingredient required is  $C_s(\underline{k}j)C_s(\underline{k}'j')$  for the Rayleigh wave. Now from the definition of the Green's function  $U_{\alpha\beta}(\underline{L}\underline{L}'; \omega^2)$ , we see that

$$\frac{B_s(\underline{L}\alpha)B_s(\underline{L}'\beta)}{2\omega_s} = M \operatorname{Res}_{\omega_s} \{U_{\alpha\beta}(\underline{L}\underline{L}'; \omega^2)\} \quad (204)$$

where  $\operatorname{Res}_{\omega_s} \{U_{\alpha\beta}(\underline{L}\underline{L}'; \omega^2)\}$  stands for the residue of  $U_{\alpha\beta}(\underline{L}\underline{L}'; \omega^2)$  at the simple pole  $\omega = \omega_s$ . From Eqs. (139) and (196) we see that

$$\frac{C_s(\underline{k}j)C_s(\underline{k}'j')}{2\omega_s} = \operatorname{Res}_{\omega_s} \{u(\underline{k}j, \underline{k}'j'; \omega^2)\} \quad (205)$$

The double Fourier-transformed Green's function  $u(\underline{k}j, \underline{k}'j'; \omega^2)$  can be written as

$$u(\underline{k}j, \underline{k}'j'; \omega^2) = u_0(\underline{k}j, \underline{k}'j'; \omega^2) + \Delta u(\underline{k}j, \underline{k}'j'; \omega^2) \quad (206)$$

where  $u_0(\underline{k}j, \underline{k}'j'; \omega^2)$  refers to the perfect crystal and is given by

$$u_0(\underline{k}j, \underline{k}'j'; \omega^2) = \frac{\Delta(\underline{k} + \underline{k}') \delta_{jj'}}{\omega^2 - \omega^2(\underline{k}j)} \quad (207)$$

while  $\Delta u(\underline{k}j, \underline{k}'j'; \omega^2)$  is the increment in  $u(\underline{k}j, \underline{k}'j'; \omega^2)$  produced by the surface and is given by

$$\Delta u(\underline{k}j, \underline{k}'j'; \omega^2) = \frac{t(\underline{k}j, \underline{k}'j'; \omega^2)}{[\omega^2 - \omega^2(\underline{k}j)][\omega^2 - \omega^2(\underline{k}'j')]} \quad (208)$$

with  $t(\underline{k}j, \underline{k}'j'; \omega^2)$  specified by Eq.(158). Since  $u_0$  has no pole at the Rayleigh wave frequency, only  $\Delta u$  contributes to the residue in Eq.(205). Maradudin and Mills evaluated  $\Delta u$  for the nearest and next-nearest neighbor central force model of a simple cubic lattice employed in the surface specific heat calculation. (102)

The final ingredient required by Eq.(208) is the anharmonic coefficient  $V(\underline{k}j, \underline{k}_1j_1, \underline{k}_2j_2)$ . Maradudin and Mills argue that the nearest-neighbor interactions are dominant in the anharmonic terms if the interaction potential  $\phi(r)$  drops off rapidly with increasing  $r$ . The cubic anharmonic coefficient in general involves  $\phi'''(r)$ ,  $\phi''(r)$ , and  $\phi'(r)$ . The third derivative  $\phi'''(r)$  generally is the most important, and only this contribution is retained by Maradudin and Mills. Furthermore, for deeply penetrating Rayleigh waves, the effect of the surface on the anharmonic coefficients gives a negligible contribution to the damping constant.

The Rayleigh wave damping constant can now be evaluated for the nearest and next-nearest neighbor central force model with

isotropy in the long wavelength limit. The details are cumbersome and can be found in Ref. (122). The result in the low temperature limit is

$$\Gamma_R(\omega_R) = \frac{0.397}{(2\pi)^3} \zeta(4) \left[ 0.0521 + 0.337 \left( \frac{c_t}{c_R} \right)^6 \right] [\phi''''(r_0)]^2 \times$$

$$\times \frac{\omega_R (k_B T)^4}{3^2 c_R^2 c_t^7 \hbar^3} \quad (209)$$

where  $r_0$  is the nearest neighbor distance and the Rayleigh wave speed is given by  $c_R = 0.919c_t$ . The result contained in Eq. (209) has the same  $\omega T^4$  dependence found by Landau and Rumar<sup>(123)</sup> for the damping of bulk waves. Maradudin and Mills have used their model to calculate the ratio of the damping constants for Rayleigh waves and transverse bulk waves and find that the Rayleigh wave damping is much larger than the bulk wave damping. This result is at least in part, however, a consequence of the approximations made in their treatment.

Besides anharmonicity, Rayleigh waves can be damped through their interaction with impurities or other imperfections. Steg and Klemens<sup>(124)</sup> have calculated the Rayleigh wave damping constant for impurity scattering using the isotropic continuum model. The surface wave displacements were taken to have the usual form given by Eqs. (14), (15), and (16), but the bulk wave displacements were not chosen so as to fully satisfy the free boundary conditions. The result for the inverse scattering time when the impurity is a mass defect at a distance  $z$  from the surface can be written as

$$\frac{1}{\tau_R} = \frac{n(\Delta m)^2}{8\rho^2 B^2 c_R^4} \omega^5 [A_1(\kappa z) + A_2(\kappa z) + A_3(\kappa z)] \quad (210)$$

where  $n$  is the concentration of defects per unit surface area,  $\Delta m$  is the additional mass of the defect, and  $A_1, A_2, A_3$ , and  $B$  are dimensionless parameters. The terms  $A_1, A_2$ , and  $A_3$  describe the scattering of the Rayleigh wave into other Rayleigh waves, into longitudinal bulk waves, and into transverse bulk waves, respectively, while  $B$  is a slowly varying function of Poisson's ratio.

Steg and Klemens investigated the ratio of scattering into other Rayleigh waves to the scattering into bulk waves. They found that this ratio is significantly greater than unity for wavelengths greater than the distance  $z$  of the impurity from the surface, but becomes very small when the wavelength is much less than  $z$ . Equation (210) predicts a very strong  $\omega^5$  dependence on frequency for  $z=0$  (defect on the surface). This suggests that the successful propagation of very high frequency surface waves ( $\omega \geq 10\text{GHz}$ ) may require very smooth surfaces.

#### B. Experimental Aspects of Surface Wave Attenuation

An excellent review of experimental techniques used in the study of surface elastic waves has recently been published by Dransfeld and Salzmann.<sup>(125)</sup> A somewhat older survey is contained in Viktorov's book.<sup>(126)</sup> We shall give only a brief discussion.

A number of methods have been employed for the generation of Rayleigh waves. A mechanical method utilizes a wedge or prism placed on the surface to be studied. A transducer placed on an oblique surface of the wedge launches longitudinal elastic waves of speed

$C_w$  into the wedge. At the interface between the wedge and the solid of interest, the longitudinal waves are partially converted into surface waves of speed  $C$  which then propagate along the surface of the solid. If  $\theta$  is the angle between the oblique surface of the wedge and the surface of the solid, then  $\sin\theta = C_w/C$ . The prism must therefore be made of a material with a small longitudinal wave speed,  $C_w < C$ , such as a plastic.

Another procedure applicable to piezoelectric materials involves a series of linear electrodes deposited with a spacing  $d$  on the surface.<sup>(127)</sup> If the electrodes are all connected together, one has a single-phase array; if alternate electrodes are connected together, one has an alternate-phase array. Application of a rf electric field to the electrodes generates surface waves through the electro-mechanical coupling of the piezoelectric. The wavelength of the Rayleigh waves generated is equal to the electrode spacing  $d$ . Non-piezoelectric materials can be handled by depositing a layer of piezoelectric material on part of the surface to be studied and then depositing the electrodes on the piezoelectric layer.

The single-phase or alternate-phase electrode schemes can also be employed to detect surface waves. Recently, optical techniques using lasers have been developed<sup>(128)</sup> for detecting surface waves.

Relatively few experimental results are available on the damping of surface waves. Salzmann, Plieninger, and Dransfeld<sup>(121)</sup> have studied Rayleigh wave damping as a function of frequency and temperature for several surfaces of quartz. At low temperatures (below 40°K), the damping was found to exhibit the  $\omega T^4$  dependence calculated by Maradudin and Mills.<sup>(122)</sup> At high temperatures (above 60°K) where  $\omega T \ll 1$ , the damping is independent of  $T$  and

varies as  $\omega^2$ . The  $\omega^2$  dependence can be understood in terms of the viscosity coefficient theory of Maris<sup>(118)</sup> and of King and Sheard<sup>(119)</sup>. The actual experimental data lie somewhat above the values predicted by these theories, but improved experiments by Budreau and Carr<sup>(129)</sup> have removed this discrepancy as well as the discrepancy with the frequency-independent results of Daniel and De Klerk.<sup>(130)</sup>

### C. Amplification of Surface Waves

Recent interest in surface wave devices has focused attention on the amplification of surface waves, particularly in piezoelectric materials. For such materials it is possible to couple drifting current carriers to the surface wave and thus transfer energy from the carriers to the surface wave.

In practice, one can avoid screening effects in the piezoelectric by having the carriers in a thin slab of semiconductor placed adjacent to the piezoelectric. This case has been discussed theoretically by Gulyaev and Pustovoi<sup>(131)</sup>. The attenuation or amplification of the surface wave is determined by the imaginary part of the wave vector  $k$ ,

$$\frac{\text{Im}k}{k} = -\zeta^2 \cdot \frac{\epsilon_1 \epsilon_2 \text{Im}\xi}{|(\epsilon_1 + \epsilon_2)\xi - \epsilon_1|^2} \cdot \frac{F(\omega, k)}{kh}, \quad (211a)$$

where

$$\xi = \Lambda(\Lambda + k)r_D^2, \quad (211b)$$

$$\Lambda^2 = \frac{1+k^2 r_D^2}{r_D^2} + i \frac{v\omega}{v_T^2} \left(1 - \frac{v_d}{c_s}\right), \quad (211c)$$

$F(\omega, k) \sim 1$ ,  $h$  is the thickness of the slab,  $\zeta$  is the coupling constant,  $r_D$  is the Debye radius,  $\nu$  is the carrier collision frequency,  $\omega$  is the frequency,  $\epsilon_1$  and  $\epsilon_2$  are the dielectric constants of semiconductor and piezoelectric,  $v_T$  and  $v_d$  are the thermal and drift velocities of the carriers (assumed non-degenerate; if degenerate,  $v_T \sim v_F/\sqrt{3}$  where  $v_F$  is the Fermi velocity), and  $c_S$  is the velocity of the surface wave. From Eqs. (211), we see that amplification occurs if  $v_d > c_S$ .

A theoretical discussion of amplification of Rayleigh waves by an electron beam passing near the surface has been given by Gulyaev and Zil'berman<sup>(132)</sup> Viktorov<sup>(133)</sup> and Kaliski<sup>(134)</sup> have discussed the particular case of CdS. The effect of a magnetic field has been treated by Bers and Burke<sup>(135)</sup>

The experimental observation of surface wave amplification was first reported by White and Voltmer<sup>(136)</sup> and by Vas'kova and Viktorov<sup>(137)</sup> for CdS. The procedure involving a semiconductor slab adjacent to the piezoelectric has been utilized recently by Collins, Lakin, Quate, and Shaw<sup>(138)</sup> to study amplification of surface waves on  $\text{LiNbO}_3$ . The amplification of Bloustein-Gulyaev waves propagating in the  $[110]$  direction on the  $(110)$  surface and of Rayleigh waves propagating in the  $[110]$  direction on the  $(001)$  surface has just been reported by Ludvik and Quate<sup>(139)</sup>

## 5. MEAN SQUARE DISPLACEMENTS AND VELOCITIES OF SURFACE ATOMS

### A. Introduction

The mean square displacements of surface atoms can be studied experimentally using low-energy electron diffraction (LEED) or the Mössbauer effect. Since only a few radioactive nuclei such as  $^{57}\text{Fe}$  and  $^{119}\text{Sn}$  are suitable for Mössbauer investigations, we shall devote our primary attention to LEED.

Let us consider the diffraction of low-energy electrons from a crystal. As the temperature of the crystal increases, the increasing vibrational amplitudes of the atoms cause the diffraction spots to broaden in width and decrease in peak intensity. The decrease in intensity of a Bragg peak is described by the Debye-Waller factor,  $\exp[-2M(\underline{Q})]$ , where

$$M(\underline{Q}) = \frac{1}{2} \langle [\underline{Q} \cdot \underline{u}(\underline{x})]^2 \rangle, \quad (212)$$

$\underline{u}(\underline{x})$  is the displacement of atom  $\underline{x}$ , and  $\underline{Q}$  is a wave vector to be specified. In the kinematic or single scattering approximation the intensity of scattered electrons from a crystal with one atom per unit cell can be expressed as<sup>(140)</sup>

$$I = I_0 \sigma_0 f_0^2 \sum_{\underline{l}} \sum_{\underline{l}'} \alpha(\underline{l}) \alpha(\underline{l}') e^{i \underline{Q} \cdot [\underline{R}(\underline{l}) - \underline{R}(\underline{l}')] } \times e^{-\frac{1}{2} \langle [\underline{Q} \cdot (\underline{u}(\underline{l}) - \underline{u}(\underline{l}'))]^2 \rangle} \quad (213)$$

where  $I_0$  is the incident intensity,  $\sigma_0$  is the Thomson factor,  $f_0$  is the atomic scattering factor,  $\alpha(\underline{t})$  is a transmission factor, and  $\underline{Q} = \underline{K}' - \underline{K}$  with  $\underline{K}$  and  $\underline{K}'$  the wave vectors of the incident and scattered electron. The angular brackets in Eqs. ( 212 ) and ( 213 ) denote a thermal average. The factor involving the thermal average in Eq. ( 213 ) can be rewritten as

$$\begin{aligned} & \frac{-M(\underline{t})}{\sigma_0} \frac{-M(\underline{t}')}{\sigma_0} \langle [\underline{Q} \cdot \underline{u}(\underline{t})][\underline{Q} \cdot \underline{u}(\underline{t}')] \rangle \\ & \approx \frac{-M(\underline{t})}{\sigma_0} \frac{-M(\underline{t}')}{\sigma_0} \{ 1 + \langle [\underline{Q} \cdot \underline{u}(\underline{t})][\underline{Q} \cdot \underline{u}(\underline{t}')] \rangle + \dots \} \end{aligned} \quad (214)$$

so that

$$I = I_1 + I_2 + \dots \quad (215)$$

where

$$I_1 = I_0 \sigma_0 f_0^2 \left| \sum_{\underline{t}} \alpha(\underline{t}) e^{i \underline{Q} \cdot \underline{R}(\underline{t})} \frac{-M(\underline{t})}{\sigma_0} \right|^2, \quad (216)$$

$$\begin{aligned} I_2 = I_0 \sigma_0 f_0^2 \sum_{\underline{t}} \sum_{\underline{t}'} \alpha(\underline{t}) \alpha(\underline{t}') e^{i \underline{Q} \cdot [\underline{R}(\underline{t}) - \underline{R}(\underline{t}')] } \\ \times \frac{-M(\underline{t})}{\sigma_0} \frac{-M(\underline{t}')}{\sigma_0} \langle [\underline{Q} \cdot \underline{u}(\underline{t})][\underline{Q} \cdot \underline{u}(\underline{t}')] \rangle. \end{aligned} \quad (217)$$

The quantity  $I_1$  is the Laue scattering and  $I_2$  is the first-order thermal diffuse scattering.

From Eq. ( 216 ) we see that the mean square displacement of an atom in the crystal can be extracted from the logarithm of the peak intensity of a Laue scattering spot. If very low energy electrons (typically less than 50 volts) are used, the scattering is mainly from the surface layer, and the mean square displacement then refers to a surface atom. It is convenient to discuss the mean square displacement in terms of an effective Debye temperature  $\Theta$  which is defined by the relation

$$\langle u^2 \rangle = (3\hbar^2 T / m k_B \Theta^2) \phi(\Theta/T) \quad ( 218 )$$

where

$$\phi(x) = D_1(x) + \frac{1}{2}x \quad ( 219 )$$

and  $D_1(x)$  is the Debye function,

$$D_1(x) = \frac{1}{x} \int_0^x \frac{t \, dt}{e^t - 1} \quad ( 220 )$$

At high temperatures,  $\phi(\Theta/T) \rightarrow 1$ , and  $\langle u^2 \rangle$  is proportional to the temperature  $T$ .

The discussion just given has been based on the kinematic or single scattering approximation. Since very low energy electrons are strongly scattered by the crystal, one must consider the effects of multiple scattering. This has been done by Duke and Laramore<sup>(141)</sup> who show that the lattice vibrations enter the theory in the form of a Debye-Waller type factor multiplying the electron-ion core scattering amplitude. The multiple scattering leads to products of

Debye-Waller type factors, so the peak intensity may decay more rapidly with increasing temperature than would occur for single scattering. The extraction of the mean square displacements of surface atoms from LEED data is a complicated problem when multiple scattering is significant.

An attempt to assess the importance of multiple scattering effects on the extraction of surface Debye temperatures from LEED data has very recently been initiated by Jepsen, Marcus, and Jona.<sup>(142)</sup> They consider the (111) surface of silver and calculate the LEED spectra for a given value of  $\theta$  from dynamical theory and then evaluate the results using kinematic theory to re-extract the value of  $\theta$ . The procedure yields values close to the surface Debye temperature for electron energies around 40 - 50 eV and values close to the bulk Debye temperature for energies above 140 eV. Below 40 eV, the values of  $\theta$  turn upward and become larger than the surface Debye temperature by 10 to 15 percent.

We now discuss a number of experimental results which have been analyzed using kinematic theory. The surface Debye temperatures so obtained must be treated with some reservation until the role of multiple scattering effects is fully clarified.

## B. Experimental Results

Experimental observations of surface atom mean square displacements were first made by Zamsha and Kalashnikov<sup>(143)</sup> on silver. Subsequent work was carried out by Menzel-Kopp and Menzel<sup>(144)</sup> on copper surfaces and by MacRae and Germer<sup>(145)</sup> on nickel surfaces. These early investigations demonstrated that surface atoms typically have larger mean square displacements than bulk atoms. The effective Debye temperature for surface atoms is therefore smaller than that for bulk atoms.

The availability of commercial LEED apparatus during the last decade has stimulated considerable work on surface Debye-Waller factors. Of particular interest is the investigation of various surfaces of nickel by MacRae<sup>(146)</sup> which revealed that the mean square displacement of a surface atom in a cubic crystal is anisotropic even though symmetry requires that the bulk atom mean square displacement be isotropic. MacRae's data are shown in Fig. 12 for the (110) surface. The effective Debye temperatures were found to be 220°K for the [110] direction (perpendicular to the surface) and 330°K and 220°K in the [110] and [001] directions, respectively (both parallel to the surface). All three surface Debye temperatures are less than the bulk value of 390°K.

Additional experimental results are available for other f.c.c. metals at room temperature and above. Jones, McKinney, and Webb<sup>(147)</sup> studied the (111) surface of silver and found approximate isotropy of the surface mean square displacements. This may be compared with the early results of Zamsha and Kalashnikov<sup>(143)</sup> for the (001) surface who found a strong anisotropy with the tangential mean

square displacement larger than the normal component. Additional investigations<sup>(148)</sup> of silver have been reported by Corotte, Ducros, and Macall for the (111) surface and by Rovida, Torrini, and Zanazzi for the (001) and (111) surfaces. The latter workers found a parallel mean square displacement at the (111) surface which is nearly equal to the perpendicular mean square displacement. Normal components of surface mean square displacements have been measured for various surfaces of platinum by Lyon and Somorjai<sup>(149)</sup> and for palladium and lead by Goodman, Farrell and Somorjai.<sup>(150)</sup> Some additional work on nickel has been reported by Andersson and Kasemo.<sup>(151)</sup> Copper has been investigated by Woodruff and Seah<sup>(152)</sup> and by Reid<sup>(153)</sup> and iridium by Goodman.<sup>(154)</sup> Both Woodruff and Seah and Reid discuss difficulties in obtaining surface mean square displacements from LEED data. A summary of surface Debye temperatures for fcc metals is given in Table 1.

Table 1. Surface Debye temperatures (normal component of displacement) for fcc metals.

<u>Metal</u>	<u>Surface</u>	<u><math>\theta_S(^{\circ}\text{K})</math></u>	<u><math>\theta_D(^{\circ}\text{K})</math></u>	<u>Reference</u>
Ni	(110)	220	390	146
Ni	(001)	280	415	151
Ag	(111)	155	225	147.
Ag	(111)	145	225	148
Cu	(111)	244	334	152
Cu	(001)	230	334	153
Pb	(111)	44	90	150
Pb	(110)	25	90	154
Pt	(001)	118	234	149
Pt	(110)	107	234	149
Pt	(111)	111	234	149
Pd	(001)	181	274	150
Pd	(111)	145	274	150
Ir	(001)	216	285	154

Somewhat less experimental data is available on bcc metals. Aldag and Stern<sup>(155)</sup> and Baudoing<sup>(156)</sup> have studied the (110) surface of tungsten, while Estrup<sup>(157)</sup> has studied the (001) surface. The (001) surface has been investigated for niobium by Tabor and Wilson<sup>(158)</sup> and for chromium and molybdenum by Tabor, Wilson, and Bastow.<sup>(159)</sup> The foregoing work is restricted to room temperature and above. Kaplan and Somorjai<sup>(160)</sup> have made the first investigation of surface Debye-Waller factors at low temperatures. The case considered was the (110) surface of chromium at temperatures down to 100°K. More detailed discussion of this work will be given later. A summary of surface Debye temperatures for bcc metals is given in Table 2.

Table 2. Surface Debye temperatures (normal component of displacement) for bcc metals.

<u>Metal</u>	<u>Surface</u>	<u><math>\theta_S(^{\circ}\text{K})</math></u>	<u><math>\theta_B(^{\circ}\text{K})</math></u>	<u>Reference</u>
W	(110)	200	280	155, 156
W	(001)	183	280	157
Nb	(001)	106	291	158
Cr	(001)	175	440	159
Cr	(110)	333	450	160
Mo	(001)	239	380	159

Relatively little experimental work on surface Debye-Waller factors has been carried out for insulating crystals. However, an interesting investigation has recently been reported on solid xenon by Ignatjevs et al.<sup>(161)</sup> who found that the low energy electron scattering from this material is essentially kinematic. The experimental values of the surface Debye-Waller factor agree quite well

with theoretical values calculated for fcc crystals by Wallis et al.<sup>(162)</sup> and by Allen and Dewette<sup>(25)</sup>. Semiconductors have been investigated by Nesterenko, Borodkin, and Snitko<sup>(163)</sup> who found surface-to-bulk mean square displacement ratios (normal components) of 1.5 for GaAs (110) and 2.2 for silicon (111)-7.

The semimetal graphite has been investigated by Alhinet, Biberian, and Bienfait<sup>(164)</sup> who obtained a surface Debye temperature of 690°K for the (00.1) surface. This is to be compared with the bulk value of 800°K. A model calculation gave a value for  $\theta_s$  of 720-730°K.

An alternative way of obtaining information about the mean square displacements of surface atoms is through measurements of the recoilless fraction in the Mössbauer effect. The recoilless fraction is proportional to the Debye-Waller factor and is consequently temperature dependent. Ordinarily, the radioactive nucleus is an impurity, but for a few materials such as iron and tin, one can get information about the host crystal atoms. Results have been reported for <sup>57</sup>Fe on various surfaces. Allen<sup>(165)</sup> found a larger mean square displacement for <sup>57</sup>Fe at the (100) and (111) surfaces of silicon than in the bulk. Qualitatively similar results were obtained by Burton and Godwin<sup>(166)</sup> for <sup>57</sup>Fe on polycrystalline tungsten. The latter workers, however, found the opposite effect for <sup>57</sup>Fe on the (100) surface of silver. This result is in interesting contrast to the LEED results of Zamsha and Kalashnikov<sup>(143)</sup> and Jones et al.<sup>(147)</sup> for pure silver surfaces.

Anisotropy in the mean square displacements has been observed by Flinn, Ruby, and Kehl<sup>(167)</sup> who found the normal component to be larger than the parallel component for <sup>57</sup>Fe on alumina. Burton and Godwin,<sup>(166)</sup> on the other hand, found the parallel component to be larger than the normal component for <sup>57</sup>Fe on polycrystalline

tungsten. A possible explanation is that the  $^{57}\text{Fe}$  atoms lie above the surface layer rather than in it, but further experimental and theoretical work is required to clarify this situation. It is clear that a major problem in using the Mössbauer effect to study surfaces is the lack of precise information as to the location of the radioactive nucleus relative to the surface layer.

### C. Theoretical Results

Qualitatively, one can visualize several effects arising from a free surface. The mean square displacement of an atom is determined by the interatomic forces acting upon it. A surface atom is acted upon by fewer neighbors than an interior atom, so this in itself will generally cause the mean square displacement to be larger for the surface atom. <sup>(168)</sup> Furthermore, the interatomic forces may have different coupling constants at the surface than in the bulk. The environment of a surface atom has different symmetry than that of an interior atom, and this may lead to an anisotropy of the mean square displacements at the surface even in cubic crystals.

To calculate the mean square displacements we assume initially that the displacement components satisfy harmonic equations of motion

$$m_x \ddot{u}_\alpha(\underline{l}x) = - \sum_{\underline{l}'x'\beta} \phi_{\alpha\beta}(\underline{l}x; \underline{l}'x') u_\beta(\underline{l}'x') \quad (221)$$

where  $u_\alpha(\underline{l}x)$  is the  $\alpha$ -th Cartesian component of displacement of the  $x$ -th atom in the  $\underline{l}$ -th unit cell,  $m_x$  is the mass of the  $x$ -th kind of atom and the  $\phi_{\alpha\beta}(\underline{l}x; \underline{l}'x')$  are the harmonic coupling coefficients.

Making the transformation

$$v_\alpha(\underline{l}x) = m_x^{-1/2} u_\alpha(\underline{l}x), \quad (222)$$

we find

$$\ddot{v}_\alpha(\underline{l}x) = - \sum_{\underline{l}'x'\beta} D_{\alpha\beta}(\underline{l}x; \underline{l}'x') v_\beta(\underline{l}'x') \quad (223)$$

where the  $D_{\alpha\beta}(\underline{x};\underline{x}')$  are the elements of the dynamical matrix defined by

$$D_{\alpha\beta}(\underline{x};\underline{x}') = (m_x m_{x'})^{-1/2} \phi_{\alpha\beta}(\underline{x};\underline{x}') . \quad (224)$$

The presence of the free surface is reflected in the values of appropriate elements of either the coupling-constant matrix or the dynamical matrix.

The dynamical matrix can be diagonalized by means of the normal coordinate transformation

$$v_\alpha(\underline{x}) = \sum_p e_{p\alpha}(\underline{x}) Q_p \quad (225)$$

where  $e_{p\alpha}(\underline{x})$  is  $\underline{x}\alpha$ -th component of the eigenvector of the dynamical matrix for the  $p$ -th normal mode and  $Q_p$  is the normal coordinate for that mode. Then

$$\langle u_\alpha^2(\underline{x}) \rangle = (1/m_x) \sum_p |e_{p\alpha}(\underline{x})|^2 \langle |Q_p|^2 \rangle \quad (226)$$

where we have used the fact that

$$\langle Q_p^* Q_p \rangle = \langle |Q_p|^2 \rangle \delta_{pp} . \quad (227)$$

Now from the quantum statistical mechanics of a harmonic oscillator,

$$\langle |Q_p|^2 \rangle = \bar{\epsilon}(\omega_p) / \omega_p^2 \quad (228)$$

where  $\omega_p$  is the frequency of normal mode  $p$  and  $\bar{\epsilon}(\omega_p)$  is the mean energy of the mode given by

$$\bar{\epsilon}(\omega_p) = \frac{1}{2} \hbar \omega_p \coth(\hbar \omega_p / 2k_B T) . \quad (229)$$

The mean square displacement component can now be written as

$$\langle u_\alpha^2(\underline{x}) \rangle = (1/m_x) \sum_p |e_{p\alpha}(\underline{x})|^2 \bar{\epsilon}(\omega_p) / \omega_p^2 . \quad (230)$$

Alternatively, using a well-known theorem of matrices<sup>(140)</sup> and Eq. (229) we can rewrite Eq. (230) directly in terms of the dynamical

matrix

$$\langle u_{\alpha}^2(\underline{l}_x) \rangle = (\hbar/2m_x) [D^{-1} \coth(\hbar D^{\frac{1}{2}}/2k_B T)]_{\underline{l}_x \alpha, \underline{l}_x \alpha} \quad (231)$$

At high and low temperatures, we have the limiting results

$$\langle u_{\alpha}^2(\underline{l}_x) \rangle \approx (k_B T/m_x) [D^{-1}]_{\underline{l}_x \alpha, \underline{l}_x \alpha}, \quad T > \Theta_D \quad (232a)$$

$$\langle u_{\alpha}^2(\underline{l}_x) \rangle \approx (\hbar/2m_x) [D^{-1}]_{\underline{l}_x \alpha, \underline{l}_x \alpha}, \quad T = 0^\circ K \quad (232b)$$

For a monatomic crystal, the mean square displacement is independent of the atomic mass at high temperatures and varies as  $m^{-1/2}$  at low temperatures.

In actual calculations, it is convenient to introduce periodic boundary conditions in the two directions (say, the 1 and 2 directions) parallel to the surface and an associated two-dimensional wave vector  $\underline{q} = (q_1, q_2)$ . The eigenvectors then have the form

$$e_{j\alpha}(\underline{l}_x) = \frac{1}{\sqrt{N_s}} e^{i(q_1 l_1 + q_2 l_2)} e_{j\alpha}(\underline{l}_3 x; q_1, q_2) \quad (233)$$

where  $N_s$  is the number of unit cells in a surface layer and  $j$  identifies the normal modes for given  $q_1, q_2$ . A reduced dynamical matrix can be defined whose elements are specified by

$$[D(q_1, q_2)]_{\underline{l}_3 x \alpha, \underline{l}_3' x' \beta} = \sum_{\underline{l}_1, \underline{l}_2} D_{\alpha\beta}(\underline{l}_x; \underline{l}_x') e^{i[q_1(\underline{l}_1 - \underline{l}_1') + q_2(\underline{l}_2 - \underline{l}_2')]} \quad (234)$$

The alternative expressions for  $\langle u_{\alpha}^2(\underline{l}_x) \rangle$  can now be rewritten as

$$\langle u_{\alpha}^2(\underline{l}_x) \rangle = (1/m_x N_s) \sum_{\underline{q}} \sum_j |e_{j\alpha}(\underline{l}_3 x; \underline{q})|^2 \times \bar{\epsilon}[\omega(\underline{q})]/\omega^2(\underline{q}) \quad (235)$$

and

$$\langle u_{\alpha}^2(\underline{l}_x) \rangle = (\hbar/2m_x N_s) \sum_{\underline{q}} [D^{-1}(\underline{q}) \coth(\hbar D^{\frac{1}{2}}(\underline{q})/2k_B T)]_{\underline{l}_3 x \alpha, \underline{l}_3 x \alpha} \quad (236)$$

If  $L$  is the number of layers in the crystal, the size of the reduced dynamical matrix is  $3rL \times 3rL$  where  $r$  is the number of atoms per unit cell, whereas the original dynamical matrix is  $3rLN_s \times 3rLN_s$ . For a crystal 20 atomic layers on each edge, the reduced dynamical matrix is smaller by a factor of 400 than the unreduced dynamical matrix. One can save considerable computer time by working with the reduced matrix.

We now discuss specific calculations. An early theoretical discussion of surface mean square displacements was given by Kalashnikov<sup>(169)</sup> who used the Debye isotropic continuum model. He found an anisotropy of the surface mean square displacements in qualitative agreement with the experimental results of Zamsha and Kalashnikov<sup>(143)</sup> on silver. Recently, Dennis and Huber<sup>(170)</sup> have given theoretical expressions based on the continuum model.

The first lattice-dynamical calculation was reported by Rich<sup>(171)</sup> who used a nearest-neighbor model to study the (001) surface of a simple cubic lattice and found a 10-30% larger mean square displacement for a surface atom than for an interior atom over a temperature. The anisotropy of the mean square displacement at the surface was not revealed by Rich's calculation because of the special character of his model. Additional calculations based on a nearest-neighbor model have been carried out by Corciovei and coworkers<sup>(172)</sup> by Cely,<sup>(173)</sup> and by Kothari and Singal.<sup>(174)</sup> The latter authors considered finite microcrystallites and calculated the mean square displacements for atoms on surfaces, edges, and corners. As one might surmise, the mean square displacements increase successively from surface to edge to corner. A related problem - the mean square displacements of atoms on steps on surfaces -

has been attacked by Masri, Allan, and Dobrzynski<sup>(114)</sup> for a [100] step on a (001) surface of a simple cubic crystal using the Rosenstock-Newell model. They find that the ratio of mean square displacements for an atom on the step edge and an atom on the flat surface is  $\sim 1.3$  at temperatures comparable to the Debye temperature.

Maradudin and Melngailis<sup>(175)</sup> have studied the (001) surface of a simple cubic lattice with nearest and next-nearest neighbor central forces which is isotropic in the long wavelength limit. Their procedure is based on the Green's function formalism of Section 3 in which the surface is created as a perturbation on an otherwise perfect periodic crystal. The mean square displacement component of an atom at lattice site  $\underline{l}$  (only one atom per unit cell is assumed) is given by

$$\langle u_{\alpha}^2(\underline{l}) \rangle = -(k_B T / Nm) \sum_{\underline{k}j} \sum_{\underline{k}'j'} e_{\alpha}(\underline{k}j) e_{\alpha}(\underline{k}'j') \times \\ \times e^{i(\underline{k}+\underline{k}') \cdot \underline{x}(\underline{l})} \sum_{n=-\infty}^{\infty} u(\underline{k}j, \underline{k}'j'; -\omega_n^2) \quad (237)$$

where  $u(\underline{k}j, \underline{k}'j'; -\omega_n^2)$  is given by Eq. (206) and  $\omega_n = (2\pi n k_B T / h)$  with  $n$  an integer. In the high temperature limit, Eq. (237) reduces to

$$\langle u_{\alpha}^2(\underline{l}) \rangle = (k_B T / Nm) \sum_{\underline{k}j} \sum_{\underline{k}'j'} e_{\alpha}(\underline{k}j) e_{\alpha}(\underline{k}'j') \times \\ \times e^{i(\underline{k}+\underline{k}') \cdot \underline{x}(\underline{l})} \left\{ \frac{\Delta(\underline{k}+\underline{k}') \delta_{jj'}}{\omega^2(\underline{k}j)} - \frac{t(\underline{k}j, \underline{k}'j'; 0)}{\omega^2(\underline{k}j) \omega^2(\underline{k}'j')} \right\} \quad (238)$$

where  $t(\underline{k}j, \underline{k}'j'; 0)$  is given by Eq. (158) with  $\omega^2 = 0$ . Using Eq. (238), Maradudin and Melngailis have evaluated the mean square

displacements for their model numerically on a computer. In addition to the features found by Rich,<sup>(171)</sup> their results indicate that at the surface the Debye-Waller factor is anisotropic with the component of mean square displacement perpendicular to the surface significantly larger than the parallel component. The mean square displacements approach the bulk value very closely at five or so atomic layers from the surface.

Calculations based on the high temperature limit of Eqs. (235) and (236) have been carried out by Clark, Herman, and Wallis<sup>(176)</sup> for a nearest-neighbor central-force model of a face centered cubic lattice. The (001), (110), and (111) surfaces were studied. It was found that the normal component of mean square displacement is about double the bulk value for all three surfaces. The (110) surface reveals an anisotropy in the tangential components not found in the other surfaces. This anisotropy together with the rapid fall off of the mean square displacement with increasing distance from the surface are illustrated in Fig. 13. The results for this surface are summarized in Table 3 and compared with the experimental results of MacRae<sup>(146)</sup> for nickel.

Table 3. Theoretical and experimental mean square displacement components (relative units) for atoms at a (110) surface and in the bulk of a fcc crystal.

	[110]	[110]	[001]	Bulk
Theoretical	0.80	0.64	0.86	0.40
Experimental	1.41	0.63	1.41	0.45

The agreement between theory and experiment is qualitatively satisfactory, but quantitatively leaves something to be desired. Since

the nearest-neighbor model gives a reasonable fit to the phonon dispersion curves, the discrepancy probably lies elsewhere. One possibility is multiple scattering effects. Another is that the force constants at the surface are different from those in the bulk. This possibility has been investigated by Wallis, Clark, and Herman<sup>(177)</sup> who found that agreement of theory with MacRae's data can be significantly improved by changing the surface force constants on the order of 50 per cent. Further work is required, however, to establish whether such changes are meaningful. As mentioned in Sec. 2, Clark et al<sup>(32)</sup> have calculated changes of 25-30 per cent in the surface force constants for a model of iron (bcc lattice) with nearest and next-nearest neighbor Lennard-Jones interactions, so relatively large changes at the surface do seem possible.

Recently, Rovida, Torrini, and Zanazzi<sup>(178)</sup> have used a Morse interaction potential to investigate the (110) surface of nickel. They allow for surface relaxation and thus take into account force constant changes near the surface. Taking into account surface relaxation leads to significant improvement in the agreement between the calculated mean square displacements and the experimental results of MacRae.

At temperatures sufficiently small compared to the Debye temperature, the mean square displacement of an atom should exhibit quantum mechanical zero-point motion effects. This behavior has been revealed in calculations by Wallis et al<sup>(162)</sup> based on Eqs. (235) and (236) for the (110) surface of a face-centered cubic lattice with nearest-neighbor central forces. Additional

calculations of the temperature dependence of the mean square displacements for a face-centered cubic lattice have been carried out by Allen and DeWette<sup>(25)</sup> who treated the (100), (110), and (111) surfaces using a model involving Lennard-Jones interactions between all pairs of atoms. In a subsequent paper, these authors<sup>(173)</sup> point out that the ratio of surface to bulk mean square displacements is a nearly universal function of  $T/\Theta_D$ . Their results are shown in Fig. 14. The larger value of this ratio at the higher temperatures may be attributed to either the heavier weighting of surface modes at high temperatures than low temperatures or to the earlier onset of zero-point motion in the bulk than at the surface as the temperature is decreased.

In the work just mentioned, some account of anharmonic effects was included through the use of the quasiharmonic approximation. These effects tend to increase the surface-to-bulk ratio through decreases in the surface force constants. A more complete treatment of anharmonic effects is contained in the molecular dynamics calculation of Allen, DeWette, and Rahman<sup>(180)</sup> who solved the equations of motion on a computer for atoms interacting with a Lennard-Jones potential in a fcc lattice with (100), (110), or (111) surfaces. The surface mean square displacements at half the melting temperature were found to be 10-20 per cent larger than those calculated using lattice dynamics.

The calculations described so far have either been restricted to nearest-neighbor interactions (Rich<sup>(171)</sup>) or have involved central forces so that Cauchy's relation on the elastic constants  $C_{12} = C_{44}$  holds. A more general model consisting of nearest and

next-nearest neighbor central forces plus angle-bending interactions involving pairs of nearest neighbors has been employed by Wallis, Clark, and Herman<sup>(181)</sup> to the (001) surface of a fcc lattice in the high temperature limit. The force constants can be chosen to give an exact fit to the elastic constants for a given fcc material, and Cauchy's relation need not be obeyed. The results for the ratio of surface-to-bulk mean square displacements are remarkably independent of the material for the normal component, ranging only between 2.01 and 2.03 for Al, Pb, Pt, Pd, Ag, Au, Cu, and Ni. The ratio for the parallel component shows more variation, ranging from 1.21 for Au to 1.51 for Ni. The results for the normal component ratio are in reasonable agreement with experiment (cf. Table 1) for the (001) surface of Cu and Ni, but are only about one-half the experimental values for Pt and Pd. The latter discrepancy may indicate weak binding of the surface transformations can take place in Pt<sup>(149)</sup> and Pd<sup>(150)</sup>.

A model similar to that described above but including third neighbor central forces has been used by Wallis and Cheng<sup>(182)</sup> to calculate the temperature dependence of the mean square displacements of atoms on the (001) and (110) surfaces of chromium. The result for the surface-to-bulk ratio of the normal components at the (110) surface is in qualitative agreement with the experimental results of Kaplan and Somorjai<sup>(160)</sup>, but quantitative agreement will require inclusion of multiple scattering effects or temperature-dependent changes in the surface force constants. The result for the ratio at the (001) surface in the high temperature regime is significantly less than that found experimentally

by Tabor, Wilson, and Bastow.<sup>(159)</sup> More work is required, both experimentally and theoretically, on this problem.

An interesting approximate procedure for calculating mean square displacements has been proposed by Masri and Dobrzynski.<sup>(183)</sup> The dynamical matrix  $\underline{D}$  can be written as the sum of the diagonal part  $\underline{d}$  and the off-diagonal part  $\underline{R}$ :

$$\underline{D} = \underline{d} + \underline{R} \quad (239)$$

If Eq. (239) is substituted into Eq. (231) and the result expanded in a matrix power series in  $\underline{R}$ , the result for the first few terms in the expansion of the mean square displacement is

$$\begin{aligned} \langle u_{\alpha}^2(\underline{x}) \rangle = (\hbar/2m_{\alpha}) \left\{ \left[ \underline{d}^{-\frac{1}{2}} \coth \underline{a} \right]_{\underline{x}\alpha, \underline{x}\alpha} + \right. \\ \left. + \frac{1}{2}(\underline{R}^2)_{\underline{x}\alpha, \underline{x}\alpha} \left[ \frac{3}{4} \underline{d}^{-\frac{5}{2}} \coth \underline{a} + \frac{3}{8} (\hbar/k_B T) \underline{d}^{-2} \sinh^{-2} \underline{a} + \right. \right. \\ \left. \left. + \frac{1}{8} (\hbar/k_B T)^2 \underline{d}^{-\frac{3}{2}} \coth \underline{a} \sinh^{-2} \underline{a} \right]_{\underline{x}\alpha, \underline{x}\alpha} + \dots \right\} \quad (240) \end{aligned}$$

where  $\underline{a} = \hbar \underline{d}^{\frac{1}{2}} / 2k_B T$ . Since it is very easy to calculate the square root and other functions of a diagonal matrix and since only non-negative integer powers of the non-diagonal matrix  $\underline{R}$  are required, the right-hand side of Eq. (240) is readily evaluated. Masri and Dobrzynski treated the (001) surface of a simple cubic lattice using Rich's model<sup>(171)</sup> and obtained results accurate to about 20 per cent. In his thesis, Masri<sup>(184)</sup> has employed this procedure to calculate the mean square displacements as functions of temperature for atoms on various surfaces of a number of face-centered and

body-centered cubic metals. This work has recently appeared in papers by Masri and Dobrzynski<sup>(185)</sup> on the face-centered case and by Dobrzynski and Masri<sup>(186)</sup> on the body-centered case. The procedure has also been applied by Thesten and Dobrzynski<sup>(187)</sup> to the calculation of mean square displacements of atoms on the (100) and (111) surfaces of diamond, silicon, and germanium.

The effect of removing rotational invariance from the force-constant model has been studied by Musser<sup>(188)</sup> for the (001) surface of a fcc crystal. The non-rotationally invariant non-central forces were used. Rotational invariance was then imposed by modifying the surface force constants using the procedure of Ludwig and Lengeler.<sup>(42)</sup> Musser found that the non-rotationally invariant model gives larger mean square displacements than the rotationally invariant model. For the perpendicular component of Pd, the increase is rather sizeable, ~33%, while for Ni, it is much less, ~6%. Musser exploited matrix partitioning methods to reduce the size of the matrices to be inverted.

Theoretical studies of mean square displacements of adsorbed atoms have been carried out by several workers. Dlouha<sup>(189)</sup> has utilized the Rosenstock-Newell<sup>(41)</sup> model to study thin films on the (100) surface of a simple-cubic lattice. Allen, Alldredge, and De Wette<sup>(113)</sup> have employed the Lennard-Jones interaction to study the (100), (110), and (111) surfaces of a monatomic face-centered cubic crystal. Relaxation of the atoms near the surface was taken into account. They find that the mean square displacement of the adsorbate atom is enhanced or depressed according to whether the adsorbate atomic mass is smaller or larger than the substrate.

atomic mass, respectively. The effect increases as the temperature is lowered.

Recently, Theeten, Dobrzynski, and Domange<sup>(190)</sup> have studied the (001) surface of Ni with a (2x2) adsorbed layer where the adsorbed atoms are S, Na, Cs, or O. They calculated the mean square displacements parallel and perpendicular to the surface for the adsorbed atoms and compared the results with experimental data. They find that the adatom particularly affects the "extra spots"--e.g.,  $(\frac{1}{2}\frac{1}{2})$ --but not the ordinary spots. For S on Ni (001) Theeten et al. conclude that the Ni-S force constant is larger than the Ni-Ni nearest neighbor force constant.

The theoretical work discussed so far has been restricted to non-ionic crystals. Recently, Chen, Alldredge, De Wette, and Allen<sup>(191)</sup> have reported calculations for the (100) surface of NaCl using the rigid ion model. Interplanar relaxation near the surface was allowed, but was assumed to be the same for cations and anions. The dependences of the mean square displacements on distance from the surface and on temperature are qualitatively the same for cations and anions and also the same as for non-ionic crystals. However, the magnitudes of the surface-to-bulk mean square displacement ratios are about 20 per cent smaller than for non-ionic materials.

#### D. Mean Square Velocities of Surface Atoms

Closely related to mean square displacements are mean square velocities. The mean square velocity of an atom is in principle measurable through the second order Doppler shift<sup>(192)</sup> in the Mössbauer effect. The energy  $E$  of the emitted gamma ray is shifted by an amount  $\Delta E$  given by

$$\Delta E = E(\langle u^2 \rangle / 2c^2) \quad (241)$$

where  $\langle u^2 \rangle$  is the mean square velocity of the emitting nucleus. By experimentally measuring both  $E$  and  $\Delta E$ , one can obtain an experimental value for  $\langle u^2 \rangle$ . Such measurements can be used to obtain information about the coupling constants between the active atom and its neighbor.<sup>(193)</sup> The procedure has the significant limitation that it is restricted to suitable radioactive atoms such as  $^{57}\text{Fe}$  and  $^{119}\text{Sn}$ .

Theoretical expressions for the mean square velocity can be obtained in a fashion similar to that for the mean square displacement. In a normal mode of vibration of frequency  $\omega_p$ , the velocity and displacement components of atom  $i_k$  are related by the equation

$$\dot{u}_\alpha(i_k) = i\omega_p u_\alpha(i_k). \quad (242)$$

Consequently, the expression for  $\langle \dot{u}_\alpha^2(i_k) \rangle$  analogous to Eq. (230) taken the form

$$\langle \dot{u}_\alpha^2(i_k) \rangle = (1/m_k) \sum_p |\phi_{p\alpha}(i_k)|^2 \bar{E}(\omega_p) \quad (243)$$

Transforming this equation using the theory of matrices, we obtain

$$\langle v_{\alpha}^2(\underline{r}) \rangle = (\hbar/2m_{\alpha}) [D^{\frac{1}{2}} \coth(\hbar D^{\frac{1}{2}}/2k_B T)]_{\underline{r}\alpha, \underline{r}\alpha} \quad (244)$$

Equations analogous to Eqs. ( 233 ) and ( 236 ) follow from the same approach.

It is instructive to consider the expansion of Eq. ( 244 ) appropriate to high temperatures:

$$\langle v_{\alpha}^2(\underline{r}) \rangle \approx \frac{kT}{m_{\alpha}} + \frac{\hbar^2}{12m_{\alpha} kT} [D]_{\underline{r}\alpha, \underline{r}\alpha} + \dots \quad (245)$$

We note that in the extreme high temperature limit, the mean square velocity has the equipartition value  $kT/m_{\alpha}$  which is independent of the position of the atom relative to the surface. The correction term in  $1/T$  is proportional to the dynamical matrix  $D$ , so experimental measurement of this term will give the force constants at the surface directly. The primary obstacle is the extreme difficulty of making such experimental measurements for surface atoms. (166, 194) At low temperatures, the expansion of the mean square velocity starts as

$$\langle v_{\alpha}^2(\underline{r}) \rangle \approx (\hbar/2m_{\alpha}) [D^{\frac{1}{2}}]_{\underline{r}\alpha, \underline{r}\alpha} + \dots \quad (246)$$

The zero-point velocity consequently will depend on the proximity of the atom to the surface through the  $D^{\frac{1}{2}}$  factor in Eq. ( 246 ). The situation is illustrated in Fig. 15 for a one-dimensional monatomic lattice with free ends. (195) The mean square velocity is smaller for the end atoms than for the interior atoms as a consequence of the smaller number of interactions involving the end atoms compared to interior atoms.

Maradudin and Molngailis<sup>(175)</sup> have developed expressions for the mean square velocity of a surface atom in a Bravais lattice using a Green's function approach. The result is

$$\langle v^2(t) \rangle = (k_B T / Nm) \sum_{kj} \sum_{k'j'} e(kj) \cdot e(k'j') \times \\ \omega(kj) \omega(k'j') e^{i(k+k') \cdot x(t)} \sum_{n=-\infty}^{\infty} u(kj, j'; -\omega_n^2) \quad (247)$$

where  $u(kj, k'j'; -\omega_n^2)$  is given by Eq. (206) with  $\omega_n = (2\pi n k_B T / h)$  and  $n$  an integer. High temperature expansions such as Eq. (245) can be derived from Eq. (247).

Detailed calculations of mean square velocities for atoms on a {110} surface of a fcc crystal have been carried out by Wallis et al<sup>(162)</sup> using a nearest neighbor central force model. Anisotropy shows up only at low temperatures, since each component has the equipartition value  $kT/m$  at high temperatures. The smaller number of bonds which connect a surface atom to its neighbors than connect a bulk atom with its neighbors leads to a smaller mean square velocity for the surface atom at low temperatures.

Very few experimental investigations of the second-order Doppler shift for surface atoms have been made. Allen<sup>(165)</sup> studied the temperature dependence of this shift for  $^{57}\text{Fe}$  nuclei both in the bulk and on the (100) and (111) surfaces of silicon and found that a surface mean square velocity roughly five per cent less than in the bulk. Similar qualitative results have been obtained by Burton<sup>(186)</sup> for  $^{57}\text{Fe}$  on tungsten and by Godwin<sup>(194)</sup> for  $^{57}\text{Fe}$  on silver.

## 8. INELASTIC SCATTERING FROM CRYSTAL SURFACES

### A. Introduction

A very attractive method for determining surface phonon energies is the inelastic scattering of particles such as electrons or helium atoms from crystal surfaces. Helium atoms would be particularly suitable, since they are strongly scattered by the surface and since their energy is on the order of millivolts - i.e., in the range of phonon energies - when their DeBroglie wave length is on the order of a typical lattice spacing. Unfortunately, the experimental difficulties are rather severe. Neutrons are of little use because they penetrate deeply into the crystal. Electrons do not have the favorable energy - DeBroglie wave length relationship of helium atoms but are experimentally more tractable, and some success has been achieved by their use.

### B. Theoretical Development

Formal treatments of the inelastic scattering of particles from crystal surfaces have been given by Cabrera, Celli, and Manson, (197) Cabrera, Celli, Goodman, and Manson, (198), Goodman, (199) Roundy and Mills (200) Lucas and Sunjic, (201), and Evans and Mills. (202) Cabrom et al (197) employed the T-matrix formalism to derive an expression for the one-phonon reflection coefficient which was then evaluated (198) using a Morse interaction potential. Specific calculations were made for the cases of helium incident normally on silicon (203) and on LiF (204) with the aid of a Debye continuum model for the lattice vibrations. The differential reflection coefficient as a function of emission angle exhibits a continuous variation up to a cut-off angle and then a delta-function peak split

off by a finite gap. The continuous part is associated with the creation of bulk and mixed phonons, while the delta-function is associated with the creation of surface phonons (Rayleigh waves).

These calculations have been extended by Goodman<sup>(205)</sup> to the case of He atoms incident on silver. The results are found to be in reasonable agreement with experimental data of Subbarao and Miller.<sup>(206)</sup> One-phonon inelastic scattering has been observed by Fishor and Blodsoe<sup>(207)</sup> for the He atoms incident on the (001) surface of LiF. It should be mentioned that there is an extensive literature on the scattering of atoms from solid surfaces which has been reviewed recently by Goodman.<sup>(208)</sup> Additional references include the work of Chambers and Kinzer<sup>(209)</sup> and of Trilling<sup>(210)</sup> who treat the solid as a semi-infinite elastic continuum. The discrete atomic character of the solid has been taken into account by Armand<sup>(211)</sup> and by Beeby and Dobrzynski.<sup>(212)</sup>

Roundy and Mills<sup>(200)</sup> have developed a Green's function theory of one-phonon inelastic scattering of low-energy electrons from crystal surfaces where the electron interacts with the atoms of the crystal through short range forces. The interaction potential energy of the electron with the atom at the position  $\underline{R}(\underline{l})$  may be expanded in the form

$$v_{l_z}(\underline{r} - \underline{R}(\underline{l})) = (1/\Omega) \sum_{\underline{q}} v_{l_z}(\underline{q}) e^{i\underline{q} \cdot (\underline{r} - \underline{R}(\underline{l}))} \quad (248)$$

where it is assumed that the surface is in the xy plane, the subscript  $l_z$  takes into account that the potential for an atom near the surface may be different than for an atom in the bulk, and  $\Omega$  is a quantization volume. The incident and scattered electrons have energies  $\mathcal{E}_0$  and  $\mathcal{E}_s$  and wave functions  $\psi_0$  and  $\psi_s$  which can be written in the forms

$$\psi_0(\underline{r}_\parallel, z) = e^{ik_\parallel^{(0)} \cdot \underline{r}_\parallel} U^{(0)}(\underline{k}_\parallel^{(0)}, \epsilon_0; \underline{r}_\parallel, z) \quad (248a)$$

$$\psi_s(\underline{r}_\parallel, z) = e^{ik_\parallel^{(s)} \cdot \underline{r}_\parallel} U^{(s)}(\underline{k}_\parallel^{(s)}, \epsilon_s; \underline{r}_\parallel, z) \quad (248b)$$

where  $\underline{r}_\parallel$  is the two-dimensional position vector parallel to the surface,  $\underline{k}_\parallel^{(0)}$  and  $\underline{k}_\parallel^{(s)}$  are two-dimensional wave vectors parallel to the surface for the incident and scattered electron, and the functions  $U^{(1)}(\underline{k}_\parallel^{(1)}, \epsilon_1; \underline{r}_\parallel, z)$  are periodic in  $\underline{r}_\parallel$ . Outside the crystal, Roundy and Mills write  $\psi_s(\underline{r}_\parallel, z)$  in the form

$$\psi_s(\underline{r}_\parallel, z) = \Omega^{-1/2} \sum_{\underline{g}_\parallel} e^{i(\underline{k}_\parallel^{(s)} + \underline{g}_\parallel) \cdot \underline{r}_\parallel} e^{ik_z(\underline{g}_\parallel)z} a(\underline{k}_\parallel^{(s)}, \underline{g}_\parallel) \quad (249)$$

where  $a(\underline{k}_\parallel^{(s)}, \underline{g}_\parallel)$  is a Fourier amplitude,  $k_z(\underline{g}_\parallel) = [2m\epsilon_s - (\underline{k}_\parallel^{(s)} + \underline{g}_\parallel)^2]^{1/2}$ , and  $\underline{g}_\parallel$  is a two-dimensional reciprocal lattice vector associated with the surface.

In order to describe the phonons emitted or absorbed in the scattering process, it is convenient to introduce the normal coordinate transformation

$$\underline{u}(\underline{l}) = \sum_p (\hbar/2M\omega_p)^{1/2} \underline{\xi}_p(\underline{l}) (a_p + a_p^\dagger) \quad (250)$$

where  $\underline{u}(\underline{l})$  is the displacement of the atom at site  $\underline{l}$  from equilibrium,  $\omega_p$  and  $\underline{\xi}_p(\underline{l})$  are the frequency and eigenvector for the  $p^{\text{th}}$  normal mode of the crystal with the free surface,  $a_p$  and  $a_p^\dagger$  are the phonon annihilation and creation operators, and  $M$  is the atomic mass. The translational periodicity parallel to the surface can be exploited by writing

$$\xi_p(\underline{t}) = (1/N_s)^{1/2} \xi_j(\underline{k}_s, t_z) e^{-i\underline{k}_s \cdot \underline{r}_s} \quad (251)$$

and

$$\omega_p = \omega_j(\underline{k}_s) \quad (252)$$

where  $N_s$  is the number of atoms in the surface layer and  $j$  specifies the normal modes for given value of the wave vector  $\underline{k}_s$  parallel to the surface. The sum over  $p$  in Eq. (250) now becomes a sum over  $\underline{k}_s$  and  $j$ . One effect of the thermal vibrations is to renormalize the interaction potential through a Debye-Waller factor

$$\tilde{v}_{\underline{t}_z}(\underline{q}) = v_{\underline{t}_z}(\underline{q}) \exp[-\frac{1}{2} \langle (\underline{q} \cdot \underline{u}(\underline{t}))^2 \rangle_T] \quad (253)$$

where  $\langle \dots \rangle_T$  denotes a thermal average over a canonical ensemble.

The scattering cross section involves an electronic matrix element. A convenient measure of this matrix element is provided by the quantity

$$\begin{aligned} m_{\underline{t}_z}(\underline{k}_s^{(s)}, \underline{e}_s; \underline{k}_s^{(o)}, \underline{e}_o) &= (1N_s/\Omega) \sum_{\underline{q}_z} \tilde{v}_{\underline{t}_z}(\underline{K}) e^{-i\underline{q}_z \cdot \underline{r}_s} \times \\ &\times \int_{\text{cell}} d\underline{r}_s \int_{-\infty}^0 dz U^{(s)}(\underline{k}_s^{(s)}, \underline{e}_s; \underline{r}_s, z) \times \\ &\times e^{i\underline{q}_z \cdot \underline{r}_s + i\underline{G}_z \cdot \underline{r}_s} U^{(o)}(\underline{k}_s^{(o)}, \underline{e}_o; \underline{r}_s, z) \end{aligned} \quad (254)$$

where  $\underline{G}_z$  is a two-dimensional reciprocal lattice vector that places  $\underline{k}_s^{(o)} = \underline{q}_s + \underline{G}_z$  in the first Brillouin zone,  $\underline{K}$  is defined by its components  $\underline{K}_s = \underline{k}_s^{(o)} - \underline{k}_s^{(s)} + \underline{G}_s$ ,  $K_z = q_z$ , and the range of integration over  $z$  signifies that the crystal lies in the region  $z < 0$ .

Let us restrict our attention to phonon emission. The equations of conservation of energy and of wave vector component parallel to the surface take the forms

$$\epsilon_s = \epsilon_0 - \hbar\omega_j(k_{\parallel}) \quad (255)$$

and

$$k_{\parallel}^{(s)} = k_{\parallel}^{(o)} - k_{\parallel} + g_{\parallel} \quad (256)$$

The specification of the directions of the incident and scattered electron is completed by the equations

$$k_z^{(o)} = - [2m\epsilon_0 - (k_{\parallel}^{(o)})^2]^{1/2} \quad (257)$$

and

$$k_z^{(s)}(g_{\parallel}) = [2m\epsilon_s - (k_{\parallel}^{(s)} + g_{\parallel})^2]^{1/2} \quad (258)$$

A significant simplification of the analysis occurs if one neglects the energy of the phonon created relative to the energies of the incident or scattered electron. Then a Rayleigh wave and a bulk phonon with the same value of  $k_{\parallel}$  will scatter an electron into the same differential element of solid angle  $d\Omega$ .

The differential cross section for one-phonon emission can be expressed in the form

$$\frac{d^2\sigma}{d\Omega d\epsilon} = \frac{N_A \hbar k^{(s)}}{8\pi^2 m} |a(k_{\parallel}^{(s)}, g_{\parallel})|^2 [1+n(\omega)] \times \sum_{l_z, l_z'} \Gamma_{l_z, l_z'}(k_{\parallel}^{(s)}, \epsilon_s; k_{\parallel}^{(o)}, \epsilon_0) \sum_{\alpha\beta} Q_{\alpha} Q_{\beta}^* A_{\alpha\beta}(k_{\parallel}; l_z, l_z'; \omega) \quad (259)$$

where  $k^{(s)}$  is the magnitude of the scattered wave vector,  $\omega = \epsilon_0 - \epsilon_s$ ,  $n(\omega)$  is the Bose-Einstein occupation probability,  $A_{\alpha\beta}(k_{\parallel}; l_z, l_z'; \omega)$  is the phonon spectral density function,

$$T_{l_z l_z'}(\dots) = m_{l_z}(\dots) m_{l_z'}^*(\dots), \quad (260)$$

and  $Q = k_z + \hat{z} Q_z(l_z)$  with  $Q_z(l_z)$  specified by

$$Q_z(l_z) = i \frac{\partial}{\partial l_z} \log m_{l_z}(\dots) \quad (261)$$

The phonon spectral density function is related to the phonon Green's function  $U_{\alpha\beta}(k_1; l_z, l_z'; \omega)$  by

$$\begin{aligned} \lambda_{\alpha\beta}(k_1; l_z, l_z'; \omega) = (1/i\pi) [U_{\alpha\beta}(k_1; l_z, l_z'; \omega - i\eta) \\ - U_{\alpha\beta}(k_1; l_z, l_z'; \omega + i\eta)] \end{aligned} \quad (262)$$

where

$$U_{\alpha\beta}(k_1; l_z, l_z'; \omega) = \sum_j \frac{\xi_{\alpha j}(k_1, l_z) \xi_{\beta j}^*(k_1, l_z')}{\omega^2 - \omega_j^2(k_1)} \quad (263)$$

For a particular direction of the scattered electron ( $k_1$  fixed) and scattering only from the surface layer of atoms, one can write to a good approximation

$$\frac{d^2\sigma}{d\Omega d\omega} = K[1 + n(\omega)] \sum_{\alpha\beta} Q_{\alpha} Q_{\beta}^* \lambda_{\alpha\beta}(k_1; 0, 0; \omega) \quad (264)$$

where  $K$  is independent of the energy loss  $\omega$ . Roundy and Mills have evaluated the dependence of the cross section for a (100) surface of a fcc crystal with nearest neighbor central forces. They made very simple approximations for the periodic parts of the electron wave functions and the Fourier-transformed potential  $v(q)$ . The results are shown in Fig. 16. The delta function peak is associated with the excitation of Rayleigh waves, while the broad band at higher energy loss is associated with excitation of bulk modes. Thus, the surface mode dispersion curve can in principle be determined from energy loss measurements for various  $k_1$ . To date, however,

no one has succeeded in carrying out such measurements for Rayleigh waves.

We now turn to the case where the scattered electron interacts with the crystal through a macroscopic electric field. This case concerns ionic crystals or covalent crystals with surface-induced effective charges and is directly comparable to experiment.

A classical macroscopic theory of energy loss by electrons due to excitation of optical phonons has been given by Fujiwara and Ohtaka<sup>(213)</sup> who adapted the treatment of Ritchie<sup>(214)</sup> for plasmons. Consider a slab of an ionic crystal between the planes  $z = 0$  and  $z = a$  and an electron with velocity  $v$  incident on the slab. The energy loss per unit path length is simply given by

$$\frac{dW}{dx} = - \frac{e}{v} \underline{v} \cdot \underline{E}_m \quad (265)$$

where  $\underline{E}_m$  is the electric field due to the medium alone. The total field  $\underline{E}$  is given by  $\underline{E} = - \nabla \phi$  where the potential  $\phi$  satisfies the equations

$$\epsilon(\omega) \nabla^2 \phi = 4\pi e \delta(\underline{r} - \underline{v}t), \quad 0 \leq z \leq a \quad (266a)$$

$$\nabla^2 \phi = 4\pi e \delta(\underline{r} - \underline{v}t) \quad \text{elsewhere,} \quad (266b)$$

and  $\epsilon(\omega)$  is the frequency dependent dielectric constant given by Eq. (84). Equations (266) are to be supplemented by the conditions of continuity of the normal component of the electric displacement and the tangential components of the electric field at the boundaries of the slab.

It is convenient to introduce the Fourier transform

$$\phi(\underline{r}_1, \underline{r}_1, t) = (1/2\pi)^3 \int d\underline{k}_1 \int d\omega \phi(\underline{r}_1, \underline{k}_1, \omega) e^{i(\underline{k}_1 \cdot \underline{r}_1 + \omega t)} \quad (267)$$

where  $r_{\parallel}$  and  $r_{\perp}$  are coordinates parallel and perpendicular to  $\underline{v}$ , respectively, and  $\underline{k}_{\perp}$  is a two-dimensional wave vector perpendicular to  $\underline{v}$ . Equations (266) can now be solved together with the boundary conditions and the energy loss computed using Eq. (265). For normally incident electrons, the probability of loss of energy  $\hbar\omega$  can be written as

$$P(\underline{k}_{\perp}, \omega) = - (1/\hbar\omega) \int_{-\infty}^{\infty} dr_{\parallel} (e/v) \underline{v} \cdot \underline{E}_{\text{em}}|_{r_{\parallel}=vt} \quad (268)$$

$$= (e^2/\pi^2\hbar v^2) \left\{ \frac{a}{k_{\perp}^2 + \omega^2/v^2} \text{Im}\left(\frac{1}{\epsilon}\right) + \frac{2k_{\perp}}{(k_{\perp}^2 + \omega^2/v^2)^2} \text{Im}\left[\frac{1-\epsilon}{\epsilon}\right] \times \right. \\ \left. \times \frac{2(\epsilon-1)\cos(\omega a/v) + (\epsilon-1)^2 \exp(-k_{\perp} a) + (1-\epsilon^2) \exp(k_{\perp} a)}{(\epsilon-1)^2 \exp(-k_{\perp} a) - (\epsilon+1)^2 \exp(k_{\perp} a)} \right\} \quad (269)$$

The first term on the right hand side of Eq. (269) corresponds to excitation of bulk LO phonons and the second term to excitation of surface optical phonons. Setting the denominator of the second term to zero gives exactly the dispersion relation for the Fuchs-Kliwer surface optical phonons, Eq. (83), in the unretarded limit.

Lucas and Šunjić<sup>(201)</sup> have given a semiclassical treatment of the problem for polar crystals. The electron is treated as a classical point particle which moves on a fixed trajectory at constant speed. We have seen in Section 2 that the Fuchs-Kliwer type surface optical mode has an electric field which penetrates outside the crystal. The electron couples to this electric field and drives the lattice. The interaction energy between the electron and the surface mode in the

non-retarded limit is simply  $e\phi(\underline{r})$  where  $\phi(\underline{r})$  is the electrostatic potential set up by the surface mode. The probability of excitation of one or more surface optical phonons is then calculated quantum mechanically. For a slab of thickness  $2a$ , Lucas and Šunjić find that the probability of the electron losing an energy  $\hbar\omega$  is

$$P(\omega) = (P_0/2\pi) \int_{-\infty}^{\infty} dt e^{i\omega t} \exp\left[\int d\underline{k}_\parallel (Q_+ e^{-i\omega_+ t} + Q_- e^{-i\omega_- t})\right] \quad (270)$$

where  $P_0$  is the no-loss probability,  $\omega_\pm$  are solutions of the Fuchs-Kliwer dispersion relation for surface optical phonons,

$$\sinh(2ka) = \pm 2\epsilon(\omega)/[\epsilon^2(\omega) - 1], \quad (271)$$

$k = |\underline{k}_\parallel|$ , and  $\epsilon(\omega)$  is the dielectric constant given by Eq. (84).

The quantities  $Q_\pm$  are specified by

$$Q_\pm(\underline{k}_\parallel) = \frac{e^2 \Omega_p^2}{4\pi\hbar} \frac{\sinh(2ka)}{\omega_\pm} e^{-2ka} \left| \frac{1}{k|\underline{v}_\perp| + i(\omega_\pm - \underline{k}_\parallel \cdot \underline{v}_\parallel)} + \frac{1}{k|\underline{v}'_\perp| - i(\omega_\pm - \underline{k}_\parallel \cdot \underline{v}'_\parallel)} \right|^2 \quad (272)$$

where  $\Omega_p$  is the ion plasma frequency and the vectors  $\underline{v} = (\underline{v}_\perp, v_\parallel)$  and  $\underline{v}' = (\underline{v}'_\perp, v'_\parallel)$  are the velocities (resolved into components parallel and perpendicular to the surface) of the incident and scattered electron.

In general, Eqs. (270) and (272) describe a Poisson distribution for the excitation of  $n$  phonons. For the case of specular reflection from a very thick slab, the probability for the excitation of one phonon becomes

$$P(\omega) = \frac{\omega^2 \Omega^2}{2\hbar \omega_B^2 v_\perp} G(|\underline{v}_\parallel|, v_\perp) \delta(\omega - \omega_B) \quad (273)$$

where  $G(|\underline{v}_\parallel|, v_\perp)$  is a relatively slowly varying function of its arguments. From Eq. (273) we see that the probability varies with energy  $E$  of the incident electron as  $E^{-1/2}$  to a good approximation. This dependence is in agreement with the experimental results of Ibach<sup>(215)</sup> on ZnO. For a review of this topic, see the recent article by Lucas and Šunjić<sup>(216)</sup> in this journal.

A quantum mechanical treatment of inelastic electron scattering from surfaces of polar crystals and covalent crystals with surface-induced charges has been given by Evans and Mills<sup>(202)</sup>. For polar crystals, their results reduce to those of Lucas and Šunjić in the specular case. For covalent crystals, the surface optical modes are always localized within a few atomic layers of the surface. Evans and Mills find that the angular dependence of the one-phonon scattering cross section is less for the covalent crystals than for the ionic crystals. Furthermore, the energy dependence of the cross section for the covalent case is more complicated than the  $E^{-1/2}$  dependence for the ionic case. These differences can in principle be used to identify the type of surface mode involved in the scattering. Recently, Evans and Mills<sup>(217)</sup> have extended their work to multiphonon processes.

### C. Experimental Results

Among the earliest observations of surface vibrational modes by inelastic electron scattering is that of Boerach, Geiger, and

Stickel<sup>(218)</sup> on LiF. These workers used relatively high energy electrons (25 KeV), but were able to achieve sufficient resolution to identify loss peaks due to excitation of phonons. They found a peak in the energy loss spectrum in the region between the long wavelength TO and LO phonon frequencies and identified this peak as due to excitation of Fuchs-Kliever type surface optical phonons. This identification has been confirmed by Fujiwara and Ohtaka.<sup>(213)</sup>

Surface modes of a different type have been observed by Propst and Piper<sup>(219)</sup> who studied hydrogen and other molecular species adsorbed on tungsten using low-energy electrons. Loss peaks were observed corresponding to the excitation of vibrational modes localized in the vicinity of the adsorbed species.

Further extensions of the inelastic scattering technique have been achieved by Ibach<sup>(215)</sup> who observed surface optical modes in ZnO using electrons in the range 1 - 100 eV and resolution ~ 10 - 20 meV. For the (1100) surface, Ibach observed loss peaks associated with the excitation of 0, 1, 2, 3, and 4 surface optical phonons. The intensities  $S(0-n)$  of the peaks are consistent with the Poisson distribution predicted by quantum mechanics for an oscillator driven by a time-dependent force  $K(t)$ :

$$S(0-n) = \frac{1}{n!} |G|^{2n} e^{-|G|^2} \quad (274)$$

$$G = i/(2\pi\hbar\omega)^{1/2} \int_0^\infty dt e^{i\omega t} K(t) dt \quad (275)$$

This result is also in agreement with the more elaborate theory of Lucas and Šunjić.<sup>(201)</sup>

In a subsequent paper, Ibach<sup>( 220 )</sup> studied the inelastic scattering of low-energy electrons from the (111) surface of silicon and found a peak at 55 meV, which is to be compared to the Raman frequency of 65 meV. The intensity of the loss peak is relatively small compared to the case of ZnO, but is larger than one would expect for scattering from localized atomic potentials. Ibach concludes that his scattering is due to a macroscopic electric field derived from a polarizing surface-induced effective charges and estimates the charge to be on the order of 0.1 e.

As mentioned earlier, inelastic neutron scattering is not particularly favorable for surface studies of lattice dynamics. However, mention should be made of the work by Rieder and Hurl<sup>( 221 )</sup> who studied fine powders of MgO. Using the incoherent approximation, they find deviations of the frequency distribution from that of bulk crystals which suggest the presence of both acoustical surface modes and optical surface modes (both Lifshitz and Fuchs-Kliwer types).

## 7. THERMAL DIFFUSE SCATTERING

### A. Introduction.

Thermal diffuse scattering is a form of inelastic scattering which is quite familiar from x-ray diffraction. Not only do the thermal vibrations of the atoms lead to a gain or loss of energy by the incident beam, but also they lead to a broadening or diffuseness to the diffraction spots. Ordinarily, in discussing thermal diffuse scattering, one ignores the change in energy of the incident beam. This is satisfactory, even for low-energy electrons, if one focuses on the diffuseness of the diffraction spots and not on energy loss or gain, since phonon energies are  $\sim 0.01$  eV and therefore small compared to typical incident electron energies.

### B. Theoretical Development

A theoretical expression for the intensity of first-order thermal diffuse scattering has already been exhibited in Eq. (217) for a Bravais crystal. In terms of the correlation function defined by

$$C_T(\underline{r}, \underline{r}') = \langle [\underline{Q} \cdot \underline{u}(\underline{r})][\underline{Q} \cdot \underline{u}(\underline{r}')] \rangle \quad (276)$$

we can rewrite  $I_2$  as

$$I_2 = I_0 \sigma_0 f_0^2 \sum_{\underline{r}} \sum_{\underline{r}'} \alpha(\underline{r}) \alpha(\underline{r}') e^{i\mathbf{Q} \cdot [\underline{R}(\underline{r}) - \underline{R}(\underline{r}')] } \times \\ \times e^{-\frac{1}{2}M(\underline{r}) - \frac{1}{2}M(\underline{r}')} C_T(\underline{r}, \underline{r}') \quad (277)$$

If we utilize the normal coordinate transformation given by Eq. (225), then the correlation function can be rewritten as

$$C_T(\underline{r}, \underline{r}') = (1/N) \sum_p [\underline{Q} \cdot \underline{e}_p(\underline{r})][\underline{Q} \cdot \underline{e}_p(\underline{r}')] \tilde{c}(p) / m_p^2 \quad (278)$$

where  $\bar{\epsilon}(p)$  is the mean energy of mode  $p$ . Taking the crystal surface to be parallel to the 1- and 2-directions, we use Eq. (233) and obtain after some manipulation

$$I_2 = N_s I_0 \sigma_0^2 \sum_{l_3, l'_3} \alpha(l_3) \alpha(l'_3) e^{-\mu(l_3) - \mu(l'_3)} \times \\ \times e^{iQ_3(l_3 - l'_3)} \sum_q \Delta(Q_1 - q) B_T(l_3, l'_3, q) \quad (279)$$

where we have replaced  $k_1^{(p)}$  by  $q$ ,  $q = (q_1, q_2)$ ,  $Q = (Q_1, Q_2)$ ;  $\Delta(x)$  is unity if its argument is a two-dimensional reciprocal lattice vector  $Q_1$  and zero otherwise, and

$$B_T(l_3, l'_3, q) = (1/N) \sum_j [Q \cdot e^*(q, j, l_3)] [Q \cdot e(q, j, l'_3)] [\bar{\epsilon}(qj)/\omega^2(qj)]. \quad (280)$$

Applying the previously mentioned theorem of matrices, we can rewrite  $B_T(l_3, l'_3, q)$  as

$$B_T(l_3, l'_3, q) = (\hbar/2M) \sum_{\alpha\beta} Q_\alpha Q_\beta \left[ D^{-\frac{1}{2}}(q) \coth \frac{\hbar D^{\frac{1}{2}}(q)}{2k_B T} \right]_{l_3\alpha, l'_3\beta} \quad (281)$$

where  $D(q)$  is defined in Eq. (234). Both Eqs. (280) and (281) can be conveniently used for numerical calculations. We note a rather general result that integration of  $I_2$  over  $Q_1$  and  $Q_2$  yields a quantity which is a linear combination of mean square displacements [cf. Eq. (235)]. If the scattering is entirely from the surface layer, the integrated  $I_2$  is simply proportional to the surface atom mean square displacement.

The thermal diffuse scattering intensity can be expressed in terms of Green's functions by using the relations

$$\bar{\epsilon}(p) = \hbar \omega_p (n_p + \frac{1}{2}), \quad (282)$$

$$n_p = \left[ e^{\hbar \omega_p / k_B T} - 1 \right]^{-1}, \quad (263)$$

$$n_{p+\frac{1}{2}} = (\omega_p k_B T / \hbar) \sum_{n=-\infty}^{\infty} (\omega_p^2 + \omega_n^2)^{-1}, \quad (284)$$

where  $\omega_n = 2\pi n k_B T / \hbar$  with  $n$  an integer. Then  $C_T(\underline{r}, \underline{r}')$  can be re-written as

$$C_T(\underline{r}, \underline{r}') = -k_B T \sum_{\alpha\beta} Q_\alpha Q_\beta \sum_{n=-\infty}^{\infty} U_{\alpha\beta}(\underline{r}, \underline{r}'; -\omega_n^2) \quad (285)$$

$$= -k_B T \sum_{\alpha\beta} Q_\alpha Q_\beta U_{\alpha\beta}(\underline{r}, \underline{r}'; 0) \text{ as } T \rightarrow \infty \quad (286)$$

where

$$U_{\alpha\beta}(\underline{r}, \underline{r}'; \omega^2) = (1/M) \sum_p \frac{e_{\alpha p}^*(\underline{r}) e_{\beta p}(\underline{r}')}{\omega^2 - \omega_p^2} \quad (267)$$

The surface can be treated as a perturbation on an otherwise perfect crystal. If the perfect crystal eigenfrequencies and eigenvectors are  $\omega(\underline{k}j)$  and  $\underline{e}(\underline{k}j)$ , then

$$U_{\alpha\beta}(\underline{r}, \underline{r}'; \omega^2) = (1/M) \sum_{\underline{k}j} \sum_{\underline{k}'j'} e_{\alpha}^*(\underline{k}j) e_{\beta}(\underline{k}'j') \times \\ \times e^{i\underline{k} \cdot \underline{R}(\underline{r}) + i\underline{k}' \cdot \underline{R}'(\underline{r}')} u(\underline{k}j, \underline{k}'j', \omega^2) \quad (288)$$

where  $u(\underline{k}j, \underline{k}'j', \omega^2)$  is given by Eq. (206).

Wallis and Maradudin<sup>(222)</sup> have evaluated  $I_2$  with the aid of Eqs. (277) and (285) for the Maradudin-Melngailis isotropic model<sup>(175)</sup> of a sc crystal. Both high temperatures and long wavelengths were assumed. For scattering only from the surface layer of atoms, the result is

$$I_2 = (ab/2) \Delta(Q_1 - Q_1) \Delta(Q_2 - Q_2) \sum_{\alpha\beta} Q_\alpha Q_\beta (1/q) \times \\ \times [t_{\alpha\beta} - \frac{1}{2} t_{\alpha 3} t_{\beta 3} - \frac{1}{2} (1 - t_{\alpha 3})(1 - t_{\beta 3}) q_\alpha q_\beta / q^2] \quad (289)$$

where  $q^2 = q_1^2 + q_2^2$ ,  $a$  is the lattice constant,

$$b = I_0 N_s (k_B T / M c_2^2) \sigma_0 f_0^2 \sigma^2(0) e^{-2M(0)}, \quad (290)$$

and  $c_2$  is the speed of long wavelength transverse acoustic waves. Note that the intensity is proportional to the number of surface atoms and to the absolute temperature. An interesting feature is the inverse proportionality of intensity to the distance  $q$  of the scattering vector from the nearest reciprocal lattice rod. Bulk scattering, in contrast, varies as  $1/q^2$ . Wallis and Maradudin also found that the iso-intensity curves for the surface and bulk cases are frequently different. This is illustrated in Fig. 17.

Another calculation based on the isotropic model is that of Huber<sup>(223)</sup> who considered a slab of a general isotropic material following the approach of Stratton.<sup>(98)</sup> Huber's result for the intensity of thermal diffuse scattering can be written as

$$I_2 = J \sum_{\underline{G}_s}' (|\underline{Q}_s - \underline{G}_s|)^{-1} [U \underline{Q}_s^2 \cos^2 \varphi + V \underline{Q}_s^2 \sin^2 \varphi + W \underline{Q}_s^2] \quad (291)$$

where the scattering vector  $\underline{Q} = \underline{K}' - \underline{K} = (\underline{Q}_s, Q_z)$ ,  $U$ ,  $V$ , and  $W$  are functions of the speeds of transverse, longitudinal, and surface waves,  $\varphi$  is the angle between  $\underline{Q}_s$  and  $\underline{Q}_s - \underline{G}_s$ ,  $J = N_s (k_B T / M c_2^2) \times a \sigma_0 f_0^2 \exp[-2M(0)]$  and the prime on the sum indicates that only the minimum value of  $|\underline{S}_s - \underline{G}_s|$  is to be counted. Qualitatively, Huber's result is similar to that of Wallis and Maradudin, but quantitatively it is larger by about a factor of 2. The origin of this discrepancy has not been pinned down.

A numerical calculation of the thermal diffuse scattering from the (100), (110), and (111) surfaces of argon has been carried

out by DeWette and Allen<sup>(224)</sup> using a Lennard-Jones potential. The eigenfrequencies and eigenvectors for a slab 11 atomic layers thick were calculated and then used in Eq. ( 280 ) to obtain  $I_2$ . The results are not valid in the immediate vicinity of the reciprocal lattice rods, but give a better picture of the situation far from the reciprocal lattice rods than does the continuum approximation. These calculations have recently been extended by Kesmodel, DeWette, and Allen<sup>(225)</sup> who have treated in detail the (100), (110), and (111) surfaces of Xe. They included contributions to the scattering from the first five layers of the nine-layer slabs employed and assumed a geometrical decrease in the transmission factor with distance from the surface. Kesmodel et al. found significant interference effects between layers leading to different intensity distributions around different reciprocal lattice rods. They also found an "extra" spot near the (04) rod for the (100) surface.

### C. Experimental Results

Early observations of surface thermal diffuse scattering were made by Aldag and Stern<sup>(155)</sup> who studied the (110) surface of tungsten with electrons in the 230 - 700 eV range. They observed an anisotropy in the scattering which they attributed to anisotropic surface modes.

A detailed study of thermal diffuse scattering from the (111) surface of silver has been reported by McKinney, Jones, and Wobb<sup>(226)</sup>. Those authors verified a number of the theoretical predictions for surface thermal diffuse scattering. Thus, they found the predicted inverse dependence of intensity on distance from the nearest reciprocal lattice rod. Furthermore, the ratio of diffuse intensity

to peak intensity is proportional to the absolute temperature and to the square of the magnitude of the scattering vector. Finally, the ratio of integrated diffuse and peak intensities is approximately proportional to the exponent in the Debye-Waller factor.

In a subsequent paper, Barnes, Lagally, and Webb<sup>(227)</sup> discussed experiments using the (111) surface of nickel. They observed, in addition to the one-phonon scattering, a uniform background which is a function of energy and temperature. Barnes et al present arguments that this background is due to multiphonon scattering - i.e., to higher order terms in the expansion in Eq. (213). In the case of the (111) surface of silver, the multiphonon scattering is relatively small. Lagally, Ngoc, and Webb<sup>(228)</sup> have extended this work and have shown that kinematic intensities can be recovered from LEED data by averaging the LEED intensities at constant momentum transfer. This procedure could prove useful in determinations of surface structures and surface Debye-Waller factors.

## 8. SURFACE EFFECTS ON OPTICAL PROPERTIES

In this section we shall discuss the effect of free surfaces on optical properties associated with lattice vibrations. In particular, we shall discuss infrared absorption or reflection and Raman scattering.

### A. Infrared Absorption

#### (i). Theoretical Results

Since infrared wavelengths are large compared to lattice spacings in crystals one can treat the wave vector of the infrared radiation as negligible. Under these circumstances, the infrared absorption coefficient of a crystal lattice is proportional to the quantity<sup>(229)</sup>

$$I(\omega) = \sum_i \sum_j v_i \left| \int \psi_i^*(\underline{R}) \underline{M}(\underline{R}) \psi_j(\underline{R}) d\underline{R} \right|^2 \times \\ \times \delta(E_f - E_i + \hbar\omega) \quad (292)$$

where  $\underline{R}$  stands for the set of nuclear coordinates,  $\psi_i$  and  $\psi_f$  are the vibrational wave functions for the initial and final states,  $E_i$  and  $E_f$  are the corresponding energy eigenvalues,  $v_i$  is the Boltzmann occupancy factor, and  $\underline{M}(\underline{R})$  is the electric dipole moment.

The dipole moment can be expanded in power series in the displacements of the ions from equilibrium  $\underline{u}(\underline{l}\underline{x})$ :

$$\underline{M}_\alpha(\underline{R}) = \underline{M}_{\alpha 0} + \sum_{\underline{l}\underline{x}\beta} \underline{M}_{\alpha\beta}(\underline{l}\underline{x}) u_\beta(\underline{l}\underline{x}) \\ + \sum_{\underline{l}\underline{x}\beta} \sum_{\underline{l}'\underline{x}'\gamma} \underline{M}_{\alpha\beta\gamma}(\underline{l}\underline{x}, \underline{l}'\underline{x}') u_\beta(\underline{l}\underline{x}) u_\gamma(\underline{l}'\underline{x}') + \dots \quad (293)$$

The constant term  $M_{00}$  is of no interest for infrared absorption. The terms linear and quadratic in the displacements are, respectively, the first order and second order terms. We shall restrict our discussion to the first order terms, which are important in ionic crystals and are subject to strict selection rules if the crystal is periodic.

The coefficients  $M_{\alpha\beta}(\underline{l}, x)$  play the role of effective ionic charges. Infinitesimal translational invariance imposes the condition

$$\sum_{\underline{l}, x} M_{\alpha\beta}(\underline{l}, x) = 0 \quad (294)$$

In a periodic crystal,  $M_{\alpha\beta}(\underline{l}, x)$  does not depend on  $\underline{l}$ , so

$$\sum_x M_{\alpha\beta}(x) = 0 \quad (295)$$

In many cases, the tensor  $M_{\alpha\beta}(x)$  can be taken to be diagonal

$$M_{\alpha\beta}(x) = e_x \delta_{\alpha\beta} \quad (296)$$

where  $e_x$  is a scalar effective charge for ions for type  $x$ . Again considering a periodic crystal, one can expand in terms of the normal coordinates  $Q(\underline{k}, j)$  instead of the displacements  $u(\underline{l}, x)$

$$M_{\alpha}(R) = M_{0\alpha} + \sum_{\underline{k}, j} M_{\alpha}(\underline{k}, j) Q(\underline{k}, j) + \dots \quad (297)$$

where

$$M_{\alpha}(\underline{k}, j) = (4\pi N)^{-1} \sum_{\underline{l}, x, \beta} M_{\alpha\beta}(\underline{l}, x) e_{\beta}(x | \underline{k}, j) e^{i \underline{k} \cdot \underline{R}^{(0)}(\underline{l})} Q(\underline{k}, j) \quad (298)$$

and  $e_{\beta}(x | \underline{k}, j)$  is specified by Eq. (143). It can be shown<sup>(3)</sup> that the coefficient  $M_{\alpha}(\underline{k}, j)$  vanishes unless  $\underline{k} = 0$  and  $j$  refers to

the transverse optical branch. This result is a consequence of periodicity; when a free surface is present other modes can give a non-vanishing dipole moment and infrared absorption.

A theoretical investigation of the effect of free surfaces on the infrared absorption of an ionic crystal was carried out by Rosenstock<sup>(230)</sup> who simplified the calculations by retaining only short-range forces in the lattice dynamics. The first order dipole moment was evaluated with the aid of Eqs. (293), (295), and (296). The use of Eqs. (295) and (296) is not strictly correct, but should be all right for qualitative estimates. For a linear chain of  $N$  ions of alternating charge but equal mass and nearest neighbor interactions, Rosenstock found for the first-order dipole moment associated with normal mode  $s$ ,

$$M_s = eu_0/\cos(\varphi_s/2) \quad , \quad s \text{ odd} \quad (299)$$

$$= 0 \quad , \quad s \text{ even}$$

where  $\varphi_s = \pi s/N$ ,  $s = 0, 1, 2, 3, \dots, N-1$ , and  $u_0$  is an arbitrary amplitude. The dipole moment has a maximum for  $s = N-1$  (the mode which has the maximum frequency  $\omega_m$  and which would be the long-wave length optical mode if the lattice were made diatomic) and decreases in magnitude as  $s$  decreases. The important point is that the dipole moment, and hence the infrared absorption, are non-zero for  $s \neq N-1$ . Thus the free surfaces lead to absorption in frequency regions not allowed with periodic boundary conditions. Taking into account the frequency distribution, the absorption coefficient turns out to be proportional to  $(\omega_m - \omega)^{-3/2}$ .

In a second paper, Rosenstock<sup>(231)</sup> treated two- and three-dimensional crystals. The Coulomb interactions were ignored in the lattice dynamics by use of the Rosenstock-Nowell model<sup>(41)</sup>. The main difference from the one-dimensional case is the appearance of critical points in the frequency distribution. Since the free surfaces lead to a continuous distribution of infrared absorption over the normal modes, the critical points produce subsidiary peaks superposed on a continuous background absorption. This is in sharp contrast with the single delta-function absorption predicted by periodic boundary conditions.

Rosenstock has subsequently included the Coulomb interactions in his analysis. For the one-dimensional case,<sup>(232)</sup> he finds that the absorption coefficient varies as  $[-\log(\omega_m - \omega)]^{1/2} (\omega_m - \omega)^{-3/2}$  rather than as  $(\omega_m - \omega)^{-3/2}$  without Coulomb interactions. For three-dimensions,<sup>(233)</sup> he has calculated the frequencies of subsidiary peaks using a model of NaCl-type lattices involving Coulomb interactions and nearest-neighbor repulsive interactions. Rosenstock found that the experimental values of the fundamental lattice absorption frequency for many alkali halides are fitted better by a subsidiary frequency than by the classical limiting frequency. However, it is not clear that the model used is sufficiently precise to remove all doubt about such an identification.

Recently, Hass and Rosenstock<sup>(234,235)</sup> have taken into account the different masses which the ions of different charges generally have in an ionic crystal. They furthermore investigated the dependence of the infrared absorption in various frequency regions on the volume and surface area of the crystal. They found

that the absorption in a frequency interval containing the fundamental lattice frequency is proportional to the volume, but the absorption in other frequency regions is proportional to the surface area. Thus, to experimentally observe the absorption induced by the free surfaces away from the fundamental, one should do experiments on samples consisting of many thin layers to enhance the surface-to-volume ratio. The experiments should also be done at low temperatures to avoid complications due to anharmonic broadening of the fundamental absorption.

Since the fundamental absorption of infrared radiation by a crystal is primarily restricted to small wave vectors, it is reasonable to apply macroscopic theory in the frequency region near the fundamental. This has been done by Englman and Ruppin<sup>(70)</sup> who have discussed the optical properties of finite ionic crystals. These authors have recently published a review<sup>(71)</sup> of the situation. We shall take up only selected topics and refer the reader to the Ruppin-Englman review article for further details.

We now consider the optical properties of finite crystals. For spheres, one can utilize the Mie theory.<sup>(236)</sup> The absorption cross section (in units of  $\pi R^2$ ,  $R$  the radius) is given by

$$\sigma_a = \frac{2}{(k_0 R)^2} \sum_{l=1}^{\infty} (2l+1) (-\text{Re } a_l - |a_l|^2 - \text{Re } b_l - |b_l|^2) \quad (300)$$

where

$$a_l = - \frac{j_l(x_1)[x_0 j_l(x_0)]' - j_l(x_0)[x_1 j_l(x_1)]'}{j_l(x_1)[x_0 h_l(x_0)]' - h_l(x_0)[x_1 j_l(x_1)]'} \quad (301)$$

$$b_l = - \frac{\epsilon_M j_l(x_0) [x_1 j_l(x_1)]' - \epsilon j_l(x_1) [x_0 j_l(x_0)]'}{\epsilon_M h_l(x_0) [x_1 j_l(x_1)]' - \epsilon j_l(x_1) [x_0 h_l(x_0)]'} \quad (302)$$

$x_0 = k_0 R$ ,  $x_1 = k_1 R$ ,  $k_0 = \epsilon_M^{1/2} \omega/c$ ,  $k_1 = \epsilon^{1/2} \omega/c$ ,  $\epsilon_M$  is the dielectric constant of the medium surrounding the sphere,  $\epsilon$  is the dielectric constant of the sphere, and  $j_l$  and  $k_l$  are the spherical Bessel and Hankel functions, and the prime denotes differentiation with respect to the argument of the Bessel or Hankel function. The scattering cross section is given by

$$\sigma_s = \frac{2}{(k_0 R)^2} \sum_{l=1}^{\infty} (2l+1) (|a_l|^2 + |b_l|^2) \quad (303)$$

and the total (extinction) cross section is specified by

$$\sigma_t = \sigma_a + \sigma_s$$

$$= - \frac{2}{(k_0 R)^2} \sum_{l=1}^{\infty} (2l+1) \operatorname{Re}(a_l + b_l) \quad (304)$$

Ruppén and Engelman<sup>(71)</sup> have evaluated the extinction cross section for spheres of NaCl. Peaks in the cross section occur for excitation of the various radiative surface modes characterized by  $l = 1, 2, 3, \dots$  as given in Eq. (89). For very small spheres,  $R \rightarrow 0$ , only the  $l = 1$  mode causes appreciable absorption. This mode is in fact the mode discussed by Fröhlich<sup>(72)</sup> which has a frequency  $\omega_F$  given by

$$\frac{\omega_F^2}{\omega_T^2} = \frac{\epsilon_0 + 2\epsilon_M}{\epsilon_\infty + 2\epsilon_M} \quad (305)$$

For small but finite  $R$ , the  $l = 1$  mode frequency has corrections specified by the equations

$$\frac{\omega_{SO}^2(1)}{\omega_T^2} = \frac{\epsilon_0 + 2\epsilon_M(1+\Delta)}{\epsilon_\infty + 2\epsilon_M(1+\Delta)} \quad (306)$$

$$\Delta = \frac{6}{5} \left( \frac{\epsilon_0 + 2\epsilon_M}{\epsilon_\infty + 2\epsilon_M} \right) \epsilon_M \left( \frac{\omega_T R}{c} \right)^2 \quad (307)$$

In Fig. 18, the extinction cross section calculated for a  $1 \mu\text{m}$  radius sphere of NaCl is plotted as a function of frequency. The peak due to the  $l = 1$  mode is clearly evident between the long wavelength transverse and longitudinal optical mode frequencies. As the size of the sphere increases, additional peaks appear at the  $l = 2, 3, \dots$  surface mode frequencies and at bulk mode frequencies lying just below  $\omega_T$ .

Englman and Ruppin have also considered absorption by cylinders. For very narrow cylinders (radius  $\sim 1 \mu\text{m}$ ) and electric vector perpendicular to the axis of the cylinder, there is a peak in extinction at a surface mode with frequency specified by

$$\omega_{SO}^2 = \omega_T^2 (\epsilon_0 + \epsilon_M) / (\epsilon_\infty + \epsilon_M) \quad (308)$$

For parallel polarization, the extinction peaks at  $\omega_T$ . A related problem, the absorption by needle-shaped crystals, has been discussed by Rosenstock. (237)

A particularly interesting case is the thin slab. We have seen in Section 2 that a slab exhibits surface modes of the Fuchs-Kliwer type with frequency specified by Eq. (83). These modes,

however, are nonradiative and do not interact directly with electromagnetic radiation, although coupling can be achieved by special means to be described later. The optical properties of a slab of an alkali halide have been discussed by Berreman.<sup>(238)</sup> For radiation incident normally on the slab, there is the usual absorption peak at  $\omega_T$ . For non-normal incidence, Berreman observed an additional absorption peak at  $\omega_L$  if P-polarization is used (electric vector parallel to the plane of incidence). That coupling should occur in this situation is clear, since the electric vector has a component normal to the surface and therefore parallel to the macroscopic electric field of the longitudinal optical phonon. A detailed theoretical analysis of the optical properties of an ionic slab has been given by Fuchs, Kliever, and Pardee<sup>(239)</sup> using a macroscopic approach and by Jones and Fuchs<sup>(85)</sup> using a microscopic approach.

In a second paper, Berreman<sup>(240)</sup> analyzed the effects of microscopic pits and domes on the infrared reflectance. He found that these defects introduce structure into the reflectivity just below  $\omega_L$ .

In the foregoing discussion, the boundary conditions have been handled satisfactorily either for the short-range forces (Rosenstock) or the long-range forces but not for both. Tong and Maradudin<sup>(30)</sup> and Grimm, Maradudin, and Tong<sup>(241)</sup> have tackled the problem of handling the boundary conditions with both types of forces. The imaginary part of the dielectric response tensor (which relates the polarization to the external electric field) can be written as

$$\epsilon_{\mu\nu}^{(2)}(\omega) = (2\pi/\hbar\Omega)(e^{\beta\hbar\omega}-1) \int_0^\infty dt e^{-i\omega t} \langle M_\nu(t) M_\mu(0) \rangle \quad (309)$$

where  $\Omega$  is the volume of the crystal,  $\beta = 1/k_B T$ ,  $M_\mu(t)$  is given by Eq. (293) with the displacements  $u_\mu(t, \mathbf{x})$  taken to be time dependent, and the angular brackets denote an average over a canonical ensemble. By generalizing the normal coordinate transformation specified by Eqs. (250) and (251) to two atoms per unit cell and writing the time dependence of the creation and annihilation operators as

$$a_j(\mathbf{k}_j, t) = a_j(\mathbf{k}_j, 0) \exp[-i\omega_j(\mathbf{k}_j)t] \quad (310)$$

and

$$a_j^\dagger(-\mathbf{k}_j, t) = a_j^\dagger(-\mathbf{k}_j, 0) \exp[i\omega_j(\mathbf{k}_j)t], \quad (311)$$

one can reduce the expression for  $\epsilon_{\mu\nu}^{(2)}(\omega)$  to the form

$$\epsilon_{\mu\nu}^{(2)}(\omega) = \frac{\pi^2 e^2}{N(2r_0^3)} \sum_{j=1}^{6N} \frac{\delta[\omega - \omega_j(0)]}{\omega_j(0)} f_{\mu j} f_{\nu j}^* \quad (312)$$

where

$$f_{\mu j} = \sum_{\mathbf{l}_z} \sum_{\mathbf{x}=\pm} M_{\mathbf{x}}^{-\frac{1}{2}} x_{\mu j}^z(0, \mathbf{x}, t_z). \quad (313)$$

We see that only  $k_z=0$  modes contribute to  $\epsilon_{\mu\nu}^{(2)}(\omega)$  and hence to the absorption. The tetragonal symmetry of the slab is reflected in  $\epsilon_{\mu\nu}^{(2)}(\omega)$  by the fact that  $\epsilon_{xx}^{(2)}(\omega) \neq \epsilon_{zz}^{(2)}(\omega)$ .

These calculations have been extended by Grimm, Maradudin, and Tong<sup>(241)</sup> who included the real part of  $\epsilon_{\mu\nu}(\omega)$ . For a 100-layer slab of NaCl, they find that the diagonal components can be represented by

$$\epsilon_{xx}(\omega) = 1 + \frac{1.229\omega_0^2}{(2.418\omega_0)^2 - \omega^2 - i\gamma\omega} + \frac{26.65\omega_0^2}{(2.491\omega_0)^2 - \omega^2 - i\gamma\omega}, \quad (314)$$

$$\epsilon_{zz}(\omega) = 1 + \frac{28.79\omega_0^2}{(2.238\omega_0)^2 - \omega^2 - i\gamma\omega}, \quad (315)$$

where  $\omega_0 = 10^{13} \text{ sec}^{-1}$  and  $\gamma$  is the damping constant ( $\sim 0.02\omega_0$  at room temperature). The poles of  $\epsilon_{xx}(\omega)$  in the limit  $\gamma \rightarrow 0$  are at  $\omega_T = 2.491\omega_0$  and at a transverse surface mode  $\omega_{TSM} = 2.418\omega_0$ . This surface mode is localized within a few atomic layers of the surface and is distinct from the Fuchs-Kliwer mode. The zero of  $\epsilon_{zz}(\omega)$  in the limit  $\gamma \rightarrow 0$  is at  $\omega_L = 5.837\omega_0$ . For an angle of incidence of  $30^\circ$ , the absorption coefficient is plotted against frequency in Fig. 19. Peaks are clearly evident at  $\omega_{TSM}$ ,  $\omega_T$ , and  $\omega_L$ . As mentioned previously, there is no direct coupling of the radiation to the Fuchs-Kliwer mode and hence no peak in absorption at its frequency.

#### (11) Experimental Results

A great many workers have made infrared absorption measurements of very fine powders of various materials. We consider only a few examples and refer the reader to the review article of Ruppin and Englman<sup>(71)</sup> for further references. Typically, the powders are suspended in mineral oil, polystyrene, or KBr disks and are found to give peak absorption at a frequency higher than  $\omega_T$ . Assuming that the particles can be approximated by spheres, these results are entirely consistent with the Englman-Ruppin result that the peak absorption of very small spheres occurs at the surface mode frequency given by Eq. (89) rather than at  $\omega_T$ . Thus, for  $\text{CaO}$ ; McDevitt and Braun<sup>(242)</sup> observed peaks at  $400 \text{ cm}^{-1}$  and  $290 \text{ cm}^{-1}$ . These are close to the calculated surface mode frequency of  $402 \text{ cm}^{-1}$  and the bulk

transverse frequency of  $289 \text{ cm}^{-1}$ . Similar results have been obtained for NiO, MgO, and a variety of more complicated crystals.

Martin has studied fine powders of KCl<sup>(243)</sup> and NaCl<sup>(244)</sup> and observed absorption in the region between  $\omega_T$  and  $\omega_L$ . The peak in absorption occurs at a somewhat lower frequency than  $\omega_F$ . This may be due to absorption by  $\ell > 1$  modes or to the non-spherical shape of the crystals. Genzel and Martin<sup>(245)</sup> have recently made infrared measurements on finely powdered CdO containing free carriers. One may therefore expect coupled surface optical phonon-surface plasmon modes. The experiments indeed reveal two resonances in the absorption coefficient as well as an antiresonance which is also predicted by theory.

Systems of particles which can be approximated by cylinders rather than spheres have also been investigated experimentally. Pultz and Hertl<sup>(246)</sup> studied very thin fibres of  $\beta$ -SiC and observed peaks at  $\omega_T$  and at the surface mode as predicted by the Engelman-Ruppin theory. Hass<sup>(247)</sup> carried out an interesting study of the transmittance of thin films of NaCl and of LiF deposited on diffraction gratings. For radiation with electric vector polarized parallel to the grooves the transmittance had a minimum at  $\omega_T$  whereas with polarization perpendicular to the grooves, the minimum moved to a higher frequency whose value corresponds to the surface mode in an elliptic cylinder with axial ratio of 30.

We have alluded to Berreman's work on the effect of pits and domes on the optical properties of a crystal. Another type of surface defect which must be considered is an impurity atom adsorbed on the surface. Some years ago Pliskin and Eischens<sup>(248)</sup> studied the infrared absorption associated with hydrogen adsorbed

on platinum. They observed two absorption peaks which they attributed to two different types of bonding. The vibrational origin of the peaks was confirmed by the isotopic shift when hydrogen was replaced by deuterium. In another paper, Eischens and Pliskin<sup>(249)</sup> investigated carbon monoxide adsorbed on platinum and found two absorption bands at  $476\text{ cm}^{-1}$  and  $2000\text{ cm}^{-1}$ . If it is assumed that the CO molecule is bound to a surface Pt atom by at C-Pt bond, then the force constants for the C-Pt and C-O bonds can be determined using the theoretical analyses of Grimley<sup>(58)</sup> and of Masri and Armand.<sup>(38)</sup>

It has been pointed out that radiation does not interact directly with the Fuchs-Kliwer surface modes of an isolated ionic slab with perfectly planar surfaces. This is a result of the dispersion curve for the Fuchs-Kliwer modes lying to the right of the light line  $\omega = kc$ . However, by suitable experimental tricks, it is possible to make these modes accessible to experimental study.

One procedure is to study the infrared reflectance from a sample upon which a grating has been ruled. If the spacing of the grooves is  $d$ , then the wave vector component of the radiation parallel to the surface is augmented by  $2\pi n/d$  where  $n$  is an integer. Thus,

$$k_{\parallel} = (\omega/c) \sin \theta + 2\pi n/d \quad (316)$$

where  $\theta$  is the angle of incidence. The reflectance curve exhibits dips at frequencies specified by the surface polariton dispersion curve and Eq. (316). From the observed reflectance dips, an experimental dispersion curve can be deduced. This technique has been employed by Marschall, Fischer and Queisser<sup>(250)</sup> to determine

the dispersion curve for surface plasmons in n-InSb and by Anderson, Alexander, and Bell<sup>(251)</sup> to investigate the interaction of surface plasmons with optical phonons, also in n-InSb.

An alternative and perhaps more convenient procedure is attenuated total reflection.<sup>(252)</sup> Ruppin<sup>(253)</sup> suggested that this technique would be useful in the experimental investigation of nonradiative surface polaritons. The incrementation of the wave vector is achieved by placing a prism adjacent to the sample of interest and separated from the sample by a few microns. In the absence of the sample, the radiation is totally internally reflected in the prism. In the presence of the sample, the exponential tail of radiation penetrating outside the sample couples with the surface polaritons in the sample. Coupling is possible because the effective wave vector of the radiation parallel to the surface is given by

$$k_1 = (\omega/c) n \sin \alpha \quad (317)$$

where  $n$  is the refractive index of the prism and  $\alpha$  is the angle of incidence in the prism. Since  $n > 1$ , wave vectors to the right of the light line in vacuum can be achieved. This technique has recently been exploited by Marschall and Fischer<sup>(254)</sup> who determined the dispersion curve for surface optical phonons in GaP. An independent investigation along the same lines is that of Bryksin, Gerbshtein, and Mirlin<sup>(255)</sup> on NaCl and  $\text{CaF}_2$ .

#### B. Raman Scattering

In Raman scattering, the frequency of the scattered radiation is down-shifted (Stokes) or up-shifted (anti-Stokes) from the

frequency of the incident radiation. The advent of high intensity lasers has stimulated an enormous upsurge of experimental investigations of the Raman effect in bulk crystals. However, the use of the Raman effect to study surface phonons is in a very rudimentary state.

Raman scattering can be ascribed to the modulation of the electronic polarizability by the vibrations of the ions. The intensity of Raman scattering at frequency  $\omega$  is proportional to the quantity<sup>(3)</sup>

$$I_{\alpha\gamma, \beta\lambda}(\omega) = \sum_{v, v'} \{ \langle v' | P_{\alpha\gamma}^* | v \rangle \langle v | P_{\beta\lambda} | v' \rangle \} \delta(\omega - \omega_0 - \omega_{vv'}) \quad (318)$$

where  $v, v'$  designate the vibrational quantum numbers of the crystal,  $\omega_0$  is the incident frequency,  $\hbar\omega_{vv'}$  is the change in vibrational energy of the crystal and  $P_{\alpha\gamma}$  is the electronic polarizability tensor. The polarizability can be expanded in power series in the ionic displacements. When one transforms to normal coordinates  $Q(\underline{k}j)$ , one finds for a bulk (periodic) crystal that only optical modes with  $\underline{k} \approx 0$  are active in the Raman effect. The polarizability expansions can then be written as

$$P_{\alpha\beta} = P_{\alpha\beta}^{(0)} + \sum_j P_{\alpha\beta}(j) Q(0j) + \dots \quad (319)$$

where  $j$  runs over the optical branches. It turns out from symmetry considerations that crystals such as NaCl with every atom at a center of inversion do not exhibit a first-order Raman effect. However, crystals such as diamond which have centers of inversion midway between pairs of atoms do show a first-order Raman effect.

The creation of a free surface can result in the elimination of centers of inversion symmetry and lead to surface-induced Raman

scattering. A theoretical discussion has been given by Ruppin and Englman<sup>(256)</sup> who treated the case of the incident beam perpendicular to a thin slab and the scattered beam at an angle  $\theta$  to the normal. Conservation of energy and momentum components parallel to the surface yield the conditions for Stokes scattering

$$\omega_1 = \omega_2 + \omega \quad (320)$$

$$q_2 = k_{12} = |k_2| \sin \theta \quad (321)$$

where the subscripts 1 and 2 refer to the incident and scattered radiation and the unsubscripted quantities refer to the phonon.

From Eqs. (320) and (321), one finds

$$\sin \theta = \frac{cq_2}{\omega_1 - \omega(q_2)} \quad (322)$$

This relation between  $q_2$  and  $\theta$  can be used in principle to determine the dispersion curve  $\omega(q_2)$ .

According to Ruppin and Englman, the Fuchs-Kliwer modes of a slab of NaCl-type crystal will not exhibit first-order Raman scattering, since the displacement patterns of these surface modes are similar to those of the bulk longitudinal and transverse optical modes which are Raman inactive. For crystals which are Raman active in the bulk, however, the Fuchs-Kliwer surface modes should be Raman active.

A calculation which emphasizes the effect of the surface on the short-range interactions is that of Litzman and Cely<sup>(257)</sup> who analyzed the Rosenstock-Newell model of a NaCl-type crystal with a (001) surface. Following the approach of Loudon,<sup>(258)</sup> Litzman and Cely show that the transition probability of first order Raman scattering into unit solid angle can be expressed as

$$\begin{aligned}
W = & \frac{2h^2 e^4 \omega_s}{\pi v_m^4 c^3} \frac{n_o(n_s+1)}{\omega_o} \sum_{\beta\gamma\mu\nu} e_{\beta o} e_{\mu o} e_{\gamma s} e_{\nu s} \times \\
& \times \sum_{\underline{l}\alpha} \sum_{\underline{l}'\lambda} A_{\alpha\beta\gamma}(\underline{l}\alpha) A_{\lambda\mu\nu}^*(\underline{l}'\lambda) \left\{ \frac{n(\Omega)}{n(\Omega)+1} \right\} \times \\
& \times \lim_{\epsilon \rightarrow 0^+} \text{Im } U_{\alpha\lambda}(\underline{l}\alpha, \underline{l}'\lambda; \Omega^2 + i\epsilon)
\end{aligned} \quad (323)$$

where the subscripts o and s refer to the incident and scattered radiation,  $\underline{e}$  is the polarization vector of the radiation,  $A_{\alpha\beta\gamma}(\underline{l}\alpha)$  is a third-order electronic matrix element,  $n$  is a Bose-Einstein factor, the lower and upper lines refer to Stokes and antiStokes scattering, and  $U_{\alpha\lambda}(\underline{l}\alpha, \underline{l}'\lambda; \omega^2)$  is the Green's function specified by Eq. (138). After evaluating the Green's function for a monatomic Rosenstock-Newell model, Litzman and Cely find a continuous band of scattering which peaks at a frequency below the maximum frequency of the lattice. Unfortunately, no surface modes exist for the model considered. In a recent publication, Kawabata<sup>(259)</sup> has given a theoretical treatment of light scattering by surface phonons (Rayleigh waves) in metals.

### C. Brillouin Scattering

The inelastic scattering of light associated with the emission or absorption of acoustic phonons is termed Brillouin scattering and can be viewed as arising from the Doppler effect. The frequency shift is  $\pm\omega_a$  where  $\omega_a$  is the acoustic mode frequency. Experimentally, one can drive a surface acoustic wave with an external power source. The acoustic wave then serves as a diffraction grating so that diffracted beams appear in the scattered radiation. For the  $m^{\text{th}}$  order,

$$\sin \theta_m = \sin \theta_o + (m\lambda/\Lambda) \quad (324)$$

where  $\theta_0$  and  $\theta_m$  are the angles of incidence and scattering and  $\lambda$  and  $\Lambda$  are the wavelengths of the radiation and the acoustic phonon, to the acoustic power  $P(\omega)$  at frequency  $\omega$  by

$$I_m = (I_0/m!) [AP(\omega)]^m \quad (325)$$

where  $I_0$  is the incident intensity and  $A$  is a constant.

Using these techniques, Lean, Tseng, and Powell<sup>(128)</sup> have studied the harmonic generation of Rayleigh waves on y-cut, z-oriented  $\text{LiNbO}_3$  with the aid of a He-Ne laser. Cambon, Rouzeyre, and Simon<sup>(128)</sup> have used the same type of laser to measure the velocity of Rayleigh waves on y-cut quartz.

### 9. SURFACE THERMAL EXPANSION

We have seen in Section 2 that the equilibrium spacings of the atomic layers close to a free surface are in general different from the bulk value. One may also anticipate that the change in equilibrium spacing with temperature--i.e., the thermal expansion--will also be different near a surface from that in the bulk.

Experimental information concerning surface thermal expansion can be obtained in principle from the temperature shifts of Bragg peaks in low energy electron diffraction if the kinematic approximation is valid. Multiple scattering effects will tend to obscure the extraction of surface thermal expansion values from the experimental data.

A discussion of experimental and theoretical aspects of surface thermal expansion has been given by Wilson and Bastow.<sup>(260)</sup> The positions of normal incidence diffraction peaks are given in the kinematic approximation by

$$|Q| = \frac{4\pi}{\lambda} = n \frac{\pi}{a_{\perp}} \quad (326)$$

where  $Q$  is the scattering vector,  $\lambda$  is the electron wavelength,  $n$  is an integer, and  $a_{\perp}$  is the spacing between equivalent layers in the direction normal to the surface. The electron accelerating potential  $E_p$  and the inner potential  $V_1$  are related to  $\lambda$  by

$$\lambda(\text{\AA}) = [150.4/E'_p(\text{eV})]^{1/2} \quad (327)$$

where  $E'_p = E_p + V_1$ . The thermal expansion is then given

$$\alpha_s = \frac{1}{a_{\perp}} \frac{da_{\perp}}{dT} = -\frac{1}{2} \frac{1}{E'_p} \frac{dE'_p}{dT} \quad (328)$$

For low values of  $E_p$ , the scattering will be mainly from the surface and the surface thermal expansion will be obtained.

Experimental results have been reported by various workers. Gelatt, Lagally, and Webb<sup>(261)</sup> found values of  $\alpha_s/\alpha_b$  ( $\alpha_b$  is the bulk value) on the order of one to two for Ag and Ni. However, temperature-dependent asymmetries of the Bragg peaks due to absorption and the variation of the Debye-Waller factor with distance from the surface complicate the interpretation of the data. Wilson and Bastow<sup>(260)</sup> have studied the (100) surfaces of Cr and Mo. They find values of  $\alpha_s/\alpha_b$  in the range between two and three. Ignatjevs<sup>(262)</sup> has investigated the (111) surface of Xe and found  $\alpha_s/\alpha_b$  values of about four or five.

A simple theoretical treatment of surface thermal expansion has been given by Wilson and Bastow<sup>(260)</sup> based on the Grüneisen expression for thermal expansion. They find

$$\alpha = (k_B \gamma / a_0 M) (\hbar / k_B \theta_D)^2 \quad (329)$$

where  $\gamma$  is the Grüneisen constant,  $M$  is the atomic mass,  $a_0$  is the lattice spacing, and  $\theta_D$  is the Debye temperature. If  $\gamma$  is the same for surface layers as for bulk layers, then

$$\frac{\alpha_s}{\alpha_b} = \left( \frac{\theta_{Db}}{\theta_{Ds}} \right)^2 = \frac{\langle u_s^2 \rangle}{\langle u_b^2 \rangle} \quad (330)$$

This relation seems to be in rough agreement with the available experimental data.

In a more complete theory, one would minimize the Helmholtz free energy with respect to variations in the various layer spacings. This has been done by Allen<sup>(263)</sup> and by Kenner and Allen.<sup>(264)</sup> For the change in thermal expansion relative to the bulk value, they obtain the expression for the  $i^{\text{th}}$  layer

$$\Delta\alpha_i = k_B \sum_j a_{oi}^{-1} (\ddagger^{-1})_{ij} a_{oj}^{-1} \times \sum_p \gamma_j(\omega_p) \left( \frac{\hbar \omega_p}{2k_B T} \right)^2 \operatorname{csch}^2 \left( \frac{\hbar \omega_p}{2k_B T} \right) \quad (331)$$

where  $\ddagger$  is the potential energy matrix,  $\omega_p$  is the  $p^{\text{th}}$  normal mode frequency,  $\gamma_j(\omega_p)$  is the Grüneisen parameter given by

$$\gamma_i(\omega) = - a_i \frac{\partial \ln \omega}{\partial a_i}, \quad (332)$$

$a_i$  is the  $i^{\text{th}}$  lattice spacing, and  $a_{oi}$  is a reference lattice spacing. Kenner and Allen have carried out detailed calculations for the (100) and (111) surfaces of Ar, Kr, and Xe using Lennard-Jones interactions. They find a peak in  $\alpha_s/\alpha_b$  at low temperatures associated with the dispersion of the surface modes. Their results for Xe are significantly lower than the experimental results of Ignatjevs.

An alternative formulation of surface thermal expansion has recently been given by Dobrzynski and Maradudin.<sup>(265)</sup> They evaluate the Helmholtz free energy including anharmonic terms with the aid of many-body theoretic techniques. Specific calculations of the surface thermal expansion for the (100) surface of  $\alpha$ -iron were made using the model of Clark et al.<sup>(32)</sup> They found that  $\alpha_s/\alpha_b$  is somewhat greater than unity at high temperatures, but increases rapidly at temperatures below 50°K.

References

1. A. A. Maradudin, E. W. Montroll, G. H. Weiss, and I. P. Ipatova, Lattice Dynamics in the Harmonic Approximation, Second Edition, Academic Press, New York, 1972.
2. Lord Rayleigh, Proc. London Math. Soc. 17, 4 (1887).
3. M. Born and K. Huang, Dynamical Theory of Crystal Lattices, Oxford University Press, Oxford, 1954.
4. R. Stonoley, Proc. Roy. Soc. (London) A232, 447 (1955).
5. D. C. Gazis, R. Herman, and R. F. Wallis, Phys. Rev. 119, 533 (1960).
6. T. C. Lim and G. W. Farnell, J. Appl. Phys. 39, 4319 (1968); J. Acoust. Soc. Am. 45, 845 (1969); see also R. G. Pratt and T. C. Lim, Appl. Phys. Ltrs. 15, 403 (1969).
7. F. R. Rollins, T. C. Lim, and G. W. Farnell, Appl. Phys. Ltrs. 12, 236 (1968).
8. G. W. Farnell, Physical Acoustics, Vol. 6, edited by W. R. Mason and R. N. Thurston, Academic Press, New York, 1970, p. 109.
9. K. A. Ingebrigtsen and A. Tonning, Phys. Rev. 184, 942 (1969).
10. H. Deresiewicz and R. D. Mindlin, J. Appl. Phys. 28, 669 (1957).
11. H. Engan, K. A. Ingebrigtsen, and A. Tonning, Appl. Phys. Ltrs. 10, 311 (1967).
12. K. A. Ingebrigtsen and A. Tonning, Appl. Phys. Ltrs. 9, 16 (1966); G. A. Coquin and H. F. Tiersten, J. Acoust. Soc. Am. 41, 921 (1967).
13. C. C. Tseng and R. M. White, J. Appl. Phys. 38, 4274 (1967); C. C. Tseng, J. Appl. Phys. 38, 4281 (1967).

14. E. A. Kraut, Phys. Rev. 188, 1450 (1969).
15. J. L. Bleustein, Appl. Phys. Ltrs. 13, 412 (1968).
16. Yu. V. Gulyaev, Zh. Eksp. Teor. Fiz. Pis. v Red. 9, 63 (1969) [Soviet Physics JETP Ltrs. 9, 37 (1969)].
17. J. J. Campbell and W. R. Jones, IEEE Trans. Sonics Ultrasonics SU15, 209 (1968).
18. K. A. Ingebrigtsen, J. Appl. Phys. 40, 2681 (1969).
19. C. C. Tseng, Appl. Phys. Letters 16, 253 (1970); J. Appl. Phys. 41, 2270 (1970).
20. T. E. Feuchtwang, Phys. Rev. 155, 715, 731 (1967).
21. R. Shuttleworth, Proc. Phys. Soc. (London) A62, 167 (1949).
22. B. J. Aldor, J. R. Vaisnya, and G. Jura, J. Phys. Chem. Solids 11, 182 (1959).
23. H. H. Schmidt and G. Jura, J. Phys. Chem. Solids 16, 60 (1960).
24. G. C. Benson, and T. A. Claxton, J. Phys. Chem. Solids 25, 267 (1964).
25. R. E. Allen and F. W. de Wette, Phys. Rev. 179, 873 (1969).
26. K. S. Yun and G. G. Benson, J. Chem. Phys. 44, 2548 (1966).
27. J. Vail, Can. J. Phys. 45, 2661 (1967).
28. D. P. Jackson, Can. J. Phys. 49, 2093 (1971); see also P. Wynblatt and N. A. Gjostein, Surface Sci. 12, 109 (1968) for the (100), (110), and (111) surfaces of Cu.
29. G. C. Benson, P. Balk, and P. White, J. Chem. Phys. 31, 109 (1959); G. C. Benson, P. I. Freeman, and E. Dempsey, J. Chem. Phys. 38, 302 (1963); G. C. Benson and T. A. Claxton, J. Chem. Phys. 48, 1356 (1968).
30. S. Y. Tong and A. A. Nazadudin, Phys. Rev. 181, 1318 (1969).

31. D. C. Gazis and R. F. Wallis, *Surface Sci.* 3, 19 (1964); see also R. A. Toupin and D. C. Gazis, *Lattice Dynamics*, edited by R. F. Wallis, Pergamon Press, Oxford, 1965, p. 597.
32. B. C. Clark, R. Herman, D. C. Gazis, and R. F. Wallis, *Ferroelectricity*, edited by E. F. Weller, Elsevier Publishing Co., Amsterdam, 1967, p. 101.
33. M. Lax, *Lattice Dynamics*, edited by R. F. Wallis, Pergamon Press, Oxford, 1965, p. 583.
34. R. F. Wallis, *Surface Sci.* 2, 146 (1964); R. F. Wallis and D. C. Gazis, *Lattice Dynamics*, edited by R. F. Wallis, Pergamon Press, Oxford, 1965, p. 537.
35. H. Matsuda, *Prog. Theor. Phys. Suppl. No. 23*, 22 (1962).
36. T. Asahi and J. Hori, *Lattice Dynamics*, edited by R. F. Wallis, Pergamon Press, Oxford, 1965, p. 571; M. Fukushima, *Prog. Theor. Phys.* 33, 624 (1965).
37. J. Hori and T. Asahi, *Prog. Theor. Phys.* 31, 49 (1964).
38. P. Masri and G. Armand, *Surface Sci.* 19, 53 (1970).
39. I. M. Lifshitz and S. I. Pekar, *Uspekhi Fiz. Nauk* 56, 531 (1955); R. F. Wallis, *Phys. Rev.* 105, 540 (1957).
40. D. C. Gazis and R. F. Wallis, *J. Math. Phys.* 3, 190 (1962).
41. H. B. Rosenstock and G. F. Newell, *J. Chem. Phys.* 21, 1607 (1953).
42. W. Ludwig and B. Lengeler, *Solid State Comm.* 2, 83 (1965).
43. M. Fukushima, *Prog. Theor. Phys.* 33, 624 (1965).
44. D. C. Gazis and R. F. Wallis, *Surface Sci.* 5, 482 (1966).
45. H. Kaplan, *Phys. Rev.* 125, 1271 (1962).
46. R. E. Allen, G. P. Alldredge, and F. W. de Wette, *Phys. Rev. Lett.* 23, 1285 (1969).
47. R. E. Allen, G. P. Alldredge, and F. W. de Wette, *Phys. Rev. Lett.* 24, 361 (1970).

48. R. E. Allen, G. P. Alldredge, and F. W. de Wette, Phys. Rev. B6, 632 (1972).
49. R. E. Allen, G. P. Alldredge, and F. W. de Wette, Phys. Rev. B4, 1648 (1971).
50. R. E. Allen, G. P. Alldredge, and F. W. de Wette, Phys. Rev. B4, 1661 (1971).
51. G. P. Alldredge, R. E. Allen, and F. W. de Wette, J. Acoust. Soc. Am. 49, 1453 (1971).
52. G. P. Alldredge, Phys. Ltrs. 41A, 281 (1972).
53. J. M. Dickey and A. Paskin, Phys. Rev. B1, 851 (1970).
54. G. P. Alldredge, R. E. Allen, and F. W. de Wette, Phys. Rev. B4, 1662 (1971).
55. R. E. Allen, G. P. Alldredge, and F. W. de Wette, Phys. Rev. B2, 2570 (1970).
56. L. Dobrzynski and D. L. Mills, J. Phys. Chem. Solids 30, 1043 (1969); for a thin film on a substrate, see O. Litzman and V. Janka, Surface Sci. 18, 357 (1969); O. Litzman, Czech. J. Phys. B18, 1587 (1968).
57. S. W. Yasser and K. H. Rieder, Phys. Rev. B2, 3034 (1970).
58. T. B. Grisley, Proc. Phys. Soc. (London) 79, 1203 (1962).
59. E. W. Montroll and R. B. Potts, Phys. Rev. 100, 525 (1955).
60. S. L. Cunningham, L. Dobrzynski, and A. A. Maradudin, to be published.
61. M. Ashkin, Phys. Rev. 136, A821 (1964).
62. L. Dobrzynski, Surface Sci., 20, 99 (1970).
63. E. C. Clark, D. C. Gazis, and R. F. Wallis, Phys. Rev. 134, A1486 (1964).

64. A. A. Maradudin, R. F. Wallis, D. L. Mills, and R. L. Ballard, Phys. Rev. B5, 1106 (1972).
65. I. M. Lifshitz and L. M. Rosenzweig, Zh. Eksp. Teor. Fiz. 18, 1012 (1948); I. M. Lifshitz, Nuovo Cimento Suppl. 3, 732 (1956).
66. R. F. Wallis, Phys. Rev. 116, 302 (1959).
67. R. F. Wallis, D. L. Mills, and A. A. Maradudin, Localized Excitations in Solids, edited by R. F. Wallis, Plenum Publishing Co., New York, 1968, p. 403.
68. R. Fuchs and K. L. Kliever, Phys. Rev. 140, A2076 (1965).
69. K. L. Kliever and R. Fuchs, Phys. Rev. 144, 495 (1966); 150, 573 (1966).
70. R. Engman and R. Ruppin, Phys. Rev. Lett. 16, 898 (1966); Localized Excitations in Solids, edited by R. F. Wallis, Plenum Publishing Co., New York, 1968, p. 411; J. Phys. C1, 614, 1515 (1968); R. Ruppin and R. Engman, J. Phys. C1, 630 (1968).
71. R. Ruppin and R. Engman, Repts. on Prog. Phys. 33, 149 (1970).
72. H. Fröhlich, Theory of Dielectrics, Oxford University Press, Oxford, 1949.
73. M. I. Kheifets, Fiz. Tverd. Tela 7, 3485 (1965). [Sov. Phys. Solid State 7, 2816 (1966)].
74. R. Ruppin, J. Phys. Chem. Solids 30, 2349 (1969); also, Conference on Surface Properties and Surface States of Electronic Materials, Rolla, Missouri, 1972; Surface Sci. 34, 20 (1973).
75. K. W. Chiu and J. J. Quinn, Phys. Lett. 35A, 469 (1971).
76. R. F. Wallis and J. J. Brion, Solid State Comm. 9, 2099 (1971).

77. I. J. Roshina, Yu. M. Gorbshstein, and D. N. Mirlin, *Fiz. Tverd. Tela* 14, 1280 (1972). [*Sov. Phys. Solid State* 14, 1104 (1972)].
78. J. J. Brion, R. F. Wallis, A. Hartstein, and E. Burstein, Conference on Surface Properties and Surface States of Electronic Materials, Rolla, Missouri, 1972; *Surface Sci.* 34, 73 (1973).
79. K. W. Chiu and J. J. Quinn, Eleventh International Conference on the Physics of Semiconductors, Warsaw, Poland, 1972.
80. G. D. Mahan, *Phys. Rev.* B5, 739 (1972).
81. N. G. Van Kampen, B. R. A. Nijboer, and Y. Schrama, *Phys. Ltrs.* 26A, 307 (1968).
82. E. Gerlach, *Phys. Rev.* B4, 393 (1971).
83. A. A. Lucas, *J. Chem. Phys.* 48, 3156 (1968).
84. F. W. de Wette and G. E. Schacher, *Phys. Rev.* 137, 73 (1965).
85. W. E. Jones and E. Fuchs, *Phys. Rev.* B4, 3563 (1971).
86. T. S. Chen, R. E. Allen, G. P. Alldredge, and F. W. de Wette, *Solid State Comm.* 8, 2105 (1970).
87. T. S. Chen, G. P. Alldredge, F. W. de Wette, and R. E. Allen, *Phys. Rev. Ltrs.* 26, 1543 (1971); *Phys. Rev.* B6, 627 (1972).
88. T. S. Chen, G. P. Alldredge, and F. W. de Wette, *Solid State Comm.* 10, 941 (1972).
89. T. S. Chen, G. P. Alldredge, and F. W. de Wette, *Phys. Ltrs.* 42A, 401 (1972).
90. B. N. N. Achar and G. R. Barsch, *Phys. Rev.* 198, 1381 (1969).
91. R. E. Allen, *Phys. Rev.* B3, 3586 (1971).

92. V. V. Bryksin and Yu. A. Firsov, *Fiz. Tverd. Tela* 11, 2167 (1969). [*Sov. Phys. Solid State* 11, 1751 (1970)].
93. C. C. Ackermann, B. Bortman, H. A. Fairbank, and R. A. Gayer, *Phys. Rev. Lett.* 16, 789 (1966).
94. T. F. McNelly, S. J. Rogers, D. J. Chaunin, R. J. Rollefson, W. M. Goubau, G. E. Schmidt, J. A. Krumhansl, and R. O. Pohl, *Phys. Rev. Lett.* 24, 100 (1970).
95. I. V. Ioffe, *Phys. Lett.* 28A, 632 (1969).
96. E. W. Montroll, *J. Chem. Phys.* 18, 183 (1950).
97. A. Brager and A. Schuckowitzky, *Acta Physicochim. U.R.S.S.* 21, 1001 (1946).
98. R. Stratton, *Phil. Mag.* 44, 519 (1953); *J. Chem. Phys.* 37, 2972 (1962).
99. M. Dupuis, R. Mazo, and L. Onsager, *J. Chem. Phys.* 33, 1432 (1960).
100. H. Lamb, *Proc. Roy. Soc. (London)* A93, 114 (1917).
101. D. Patterson, *Can. J. Phys.* 33, 1079 (1955).
102. A. A. Maradudin and R. F. Wallis, *Phys. Rev.* 148, 945 (1966).
103. W. H. Lien and H. E. Phillips, *J. Chem. Phys.* 29, 1415 (1958).
104. D. Patterson, J. A. Morrison, and F. W. Thompson, *Can. J. Chem.* 33, 246 (1955); J. A. Morrison and D. Patterson, *Trans. Faraday Soc.* 52, 764 (1956).
105. J. H. Barkman, R. L. Anderson, and T. E. Brackett, *J. Chem. Phys.* 42, 1112 (1965).
106. W. de Sorbo and G. E. Nichols, *J. Phys. Chem. Solids* 6, 353 (1959).

107. J. C. Bowman and J. A. Krumhansl, *J. Phys. Chem. Solids* 5, 367 (1958).
108. R. E. Allen and F. W. de Wette, *J. Chem. Phys.* 51, 4820 (1969).
109. T. S. Chen, G. P. Alldredge, F. W. de Wette, and R. E. Allen, *J. Chem. Phys.* 55, 3121 (1971); G. P. Alldredge, T. S. Chen, and F. W. de Wette, Thirteenth International Conference on Low-Temperature Physics, Boulder, Colorado, 1972.
110. L. Dobrzynski and G. Leman, *J. de Physique* 30, 116 (1969).
111. S. L. Cunningham, *Surface Sci.* 33, 139 (1972).
112. L. Dobrzynski and J. Friedel, *Surface Sci.* 5, 65 (1968).
113. R. E. Allen, G. P. Alldredge, and F. W. de Wette, *J. Chem. Phys.* 54, 2605 (1971).
114. P. Masri, G. Allan, and L. Dobrzynski, *J. de Physique* 33, 85 (1972).
115. P. Press and I. Healy, *J. Appl. Phys.* 28, 1323 (1957); see also I. A. Viktorov, Rayleigh and Lamb Waves, Plenum Publishing Co., New York, 1967, p. 25.
116. S. L. McBride, *Can. J. Phys.* 47, 1143 (1969).
117. H. J. Maris, *Phil. Mag.* 9, 901 (1964).
118. H. J. Maris, *Phys. Rev.* 188, 1308 (1969).
119. P. J. King and F. W. Sheard, *J. Appl. Phys.* 40, 5189 (1969).
120. P. J. King and F. W. Sheard, *Solid State Comm.* 8, 1099 (1970); *Proc. Roy. Soc. (London)* A320, 175 (1970).
121. E. Salzmann, T. Plieninger, and K. Dransfeld, *Appl. Phys. Ltrs.* 13, 14 (1968).
122. A. A. Maradudin and D. L. Mills, *Phys. Rev.* 173, 881 (1968).
123. L. Landau and C. Ruxer, *Physik. Z. Sowjetunion* 12, 18 (1937).

124. R. G. Steg and P. G. Klemons, *Phys. Rev. Lett.* 24, 381 (1970).
125. K. Dransfeld and E. Salzmänn, *Physical Acoustics*, Vol. 7, edited by W. R. Mason and R. N. Thurston, Academic Press, New York, 1970, p. 219.
126. I. A. Viktorov, *Rayleigh and Lamb Waves*, Plenum Publishing Co., New York, 1967.
127. G. A. Coquin and H. F. Tiersten, *J. Acoust. Soc. Am.* 41, 921 (1967); R. M. White and F. W. Voltmer, *Appl. Phys. Lett.* 7, 314 (1965).
128. E. G. H. Lean, C. C. Tseng, and C. G. Powell, *Appl. Phys. Lett.* 16, 32 (1970); G. Cambon, M. Rouzeyre, and G. Simon, *Appl. Phys. Lett.* 18, 295 (1971).
129. A. J. Budreau and P. E. Carr, *Appl. Phys. Lett.* 18, 239 (1971).
130. M. R. Daniel and J. de Klerk, *Appl. Phys. Lett.* 16, 30 (1970).
131. Yu. V. Gulyaev and V. I. Pustovoit, *Zh. Eksp. Teor. Fiz.* 47, 2251 (1964). [*Sov. Phys. JETP* 20, 1508 (1965)].
132. Yu. V. Gulyaev and P. E. Zil'berman, *Fiz. Tverd. Tela* 7, 2772 (1965) [*Sov. Phys. Solid State* 7, 2243 (1966)].
133. I. A. Viktorov, *Akust. Zh.* 14, 467 (1968) [*Sov. Phys. Acoustics* 14, 392 (1969)].
134. S. Kaliskí, *Proc. Vib. Problems (Warsaw)* 3, 221 (1968).
135. A. Bors and B. E. Burke, *Appl. Phys. Lett.* 16, 300 (1970).
136. R. M. White and F. W. Voltmer, *Appl. Phys. Lett.* 8, 40 (1966).
137. V. I. Vas'kova and I. A. Viktorov, *Akust. Zh.* 13, 292 (1967); 15, 529 (1969) [*Sov. Phys. Acoust.* 13, 249 (1967); 15, 460 (1969)]; see also I. A. Viktorov, *Akust. Zh.* 14, 467 (1968) [*Sov. Phys. Acoust.* 14, 392 (1969)].

138. J. H. Collins, K. M. Lakin, C. F. Quate, and H. J. Shaw, Appl. Phys. Ltrs. 13, 314 (1968).
139. S. Ludvik and C. F. Quate, J. Appl. Phys. 43, 3619 (1972).
140. M. Born, Repts. on Prog. Phys. 9, 294 (1942).
141. C. B. Duke and G. E. Laramore, Phys. Rev. B2, 4765, (1970); G. E. Laramore and C. B. Duke, Phys. Rev. B2, 4783 (1970); see also C. B. Duke, D. L. Smith, and E. W. Holland, Phys. Rev. B5, 3358 (1972); G. E. Laramore, Phys. Rev. B6, 1097 (1972).
142. D. W. Jepsen, P. M. Marcus, and F. Jona, to be published.
143. O. I. Zamsha and S. G. Kalashnikov, Zh. Eksp. Teor. Fiz. 9, 1408 (1939).
144. C. Menzel-Kopp and E. Menzel, Z. Phys. 142, 245 (1955).
145. A. U. MacRae and L. H. Germer, Phys. Rev. Ltrs. 8, 489 (1962).
146. A. U. MacRae, Surface Sci. 2, 522 (1964).
147. E. R. Jones, J. T. McKinney, and M. B. Webb, Phys. Rev. 151, 476 (1966).
148. C. Corcotte, P. Ducros, and A. Mascall, Compt. Rend (Paris) B267, 544 (1968); G. Rovida, M. Torrini, and E. Zanazzi, Il Nuovo Cimento 48, 97 (1971).
149. H. B. Lyon and G. A. Somorjai, J. Chem. Phys. 44, 3707 (1966).
150. R. H. Goodman, H. H. Farrell, and G. A. Somorjai, J. Chem. Phys. 48, 1046 (1968).
151. S. Andersson and B. Kasemo, Solid State Comm. 8, 1885 (1970).
152. D. P. Woodruff and M. P. Seah, Phys. Ltrs. 30A, 263 (1969); Phys. Status Solidi (a) 1, 429 (1970).
153. R. J. Reid, Phys. Status Solidi (a) 2, K109 (1970); Surface Sci. 29, 623 (1972).
154. R. H. Goodman, Ph.D. Thesis, Univ. of California, Berkeley, 1969.

155. J. Aldag and R. M. Stern, Phys. Rev. Lett. 14, 857 (1965); 172  
R. M. Stern, Trans. Am. Cryst. Assoc. 4, 14 (1968).
156. R. Baudoing, Thesis, Univ. of Grenoble, 1967.
157. P. J. Estrup, The Structure and Chemistry of Solid Surfaces,  
edited by G. A. Somorjai, John Wiley, New York, 1969, p. 19-1.
158. D. Tabor and J. Wilson, Surface Sci. 20, 203 (1970).
159. D. Tabor, J. M. Wilson, and T. J. Eastow, Surface Sci. 26,  
471 (1971).
160. R. Kaplan and G. A. Somorjai, Solid State Comm. 9, 505 (1971).
161. A. Ignatjevs, T. N. Rhodin, S. Y. Tong, B. I. Lundqvist, and  
J. P. Pendry, Solid State Comm. 9, 1851 (1971); International Conference on Solid Surfaces, Boston, 1971; Phys. Rev.,  
to be published.
162. R. F. Wallis, B. C. Clark, R. Herman, and D. C. Gazis,  
Phys. Rev. 80, 716 (1969).
163. B. A. Nesterenko, A. D. Borodkin, and O. V. Snitko, Surface  
Sci. 32, 576 (1972).
164. G. Albinet, J. P. Biberian, and M. Blenfait, Phys. Rev. B3,  
2015 (1971).
165. F. E. Allen, Bull. Am. Phys. Soc. [II] 9, 296 (1964).
166. J. W. Burton and R. P. Godwin, Phys. Rev. 158, 218 (1967).
167. P. A. Flinn, S. L. Ruby, and W. L. Kohl, Science 143,  
1434 (1964).
168. For a simple, semi-quantitative argument, see L. S. Kothari,  
Phys. Lett. 24A, 382 (1967).
169. S. G. Kalasnikov, Zh. Eksp. Teor. Fiz. 13, 295 (1943); see  
also F. R. L. Schoening, Acta Cryst. A24, 615 (1968).
170. R. L. Dennis and D. L. Huber, Phys. Rev. B5, 4717 (1972).
171. M. Rich, Phys. Lett. 4, 153 (1963).

172. A. Corciovei and A. Berinde, Rev. Phys. Acad. Rep. Populaire Roumaine 7, 107 (1962); J. Phys. Radium 24, 89 (1963); A. Corciovei and C. Motoc, Acta Phys. Acad. Sci. Hung. 15, 299 (1963); A. Corciovei and E. Radescu, Phys. Ltrs. 23, 32 (1966); A. Corciovei, D. Grecu, and E. Radescu, Z. Phys. 209, 134 (1968); A. Corciovei and D. Vamanu, J. Vac. Sci. Tech. 6, 680 (1969).
173. J. Cely, Phys. Status Solidi 4, 521 (1964).
174. L. S. Kothari and C. M. Singal, Phys. Rev. 168, 952 (1968).
175. A. Maradudin and J. Melngailis, Phys. Rev. 133, A1188 (1964).
176. B. C. Clark, R. Herman, and R. F. Wallis, Phys. Rev. 139, A860 (1965).
177. R. F. Wallis, B. C. Clark, and R. Herman, Phys. Rev. 167, 652 (1968).
178. G. Rovida, M. Torrini, and E. Zanazzi, Chem. Phys. Ltrs. 3, 201 (1969).
179. R. E. Allen and F. W. deWette, and A. Rahman, Phys. Rev. 198, 1220 (1969).
180. R. E. Allen, F. W. deWette, and A. Rahman, Phys. Rev. 179, 887 (1969).
181. R. F. Wallis, B. C. Clark, and R. Herman, The Structure and Chemistry of Solid Surfaces, edited by G. A. Somorjai, John Wiley, New York, 1969, p. 17-1.
182. R. F. Wallis and D. J. Cheng, Solid State Comm. 11, 221 (1972). See also P. Masri, J. Phys. Chem. Solids 34, 435 (1973).
183. P. Masri and L. Dobrzynski, J. de Physique 32, 939 (1971).
184. P. Masri, Thesis, University of Paris-South, 1971.

- 174
185. P. Masri and L. Dobrzynski, Surface Sci. 32, 623 (1972).
  186. L. Dobrzynski and P. Masri, J. Phys. Chem. Solids 33, 1603 (1972).
  187. J. B. Theeten and L. Dobrzynski, Phys. Rev. B5, 1529 (1972).
  188. S. W. Musser, J. Phys. Chem. Solids 32, 115 (1971).
  189. J. Dlouha, Czech. J. Phys. B16, 495 (1966).
  190. J. B. Theeten, L. Dobrzynski, and J. L. Domange, Surface Science 34, 145 (1973).
  191. T. S. Chen, G. P. Alldredge, F. W. deWette and R. E. Allen, Phys. Rev. B6, 623 (1972).
  192. R. V. Pound and G. A. Rabka, Phys. Rev. Ltrs. 4, 274 (1960);  
B. D. Josephson, Phys. Rev. Ltrs. 4, 341 (1960).
  193. A. A. Maradudin, P. A. Flinn, and S. Ruby, Phys. Rev. 126,  
9 (1962).
  194. R. P. Godwin, Thesis, University of Illinois, 1966.
  195. R. F. Wallis and D. C. Gazis, Phys. Rev. 128, 106 (1962);  
see also J. R. Clem and R. P. Godwin, Am. J. Phys. 34, 460  
(1966).
  196. J. W. Burton, Thesis, University of Illinois, 1964.
  197. N. Cabrera, V. Colli, and R. Manson, Phys. Rev. Ltrs. 22,  
346 (1969).
  198. N. Cabrera, V. Colli, F. O. Goodman, and R. Manson, Surface  
Sci. 19, 67 (1970).
  199. F. O. Goodman, Surface Sci. 19, 93 (1970).
  200. V. Roundy and D. L. Mills, Phys. Rev. B5, 1347 (1972).
  201. A. A. Lucas and M. Šunjić, Phys. Rev. Ltrs. 26, 229 (1971).
  202. E. Evans and D. L. Mills, Phys. Rev. B5, 4126 (1972).
  203. R. Manson and V. Colli, Surface Sci. 24, 495 (1971).
  204. F. O. Goodman, Surface Sci. 30, 1 (1972).

205. F. O. Goodman, J. Vac. Sci. Tech. 9, 812 (1972).
206. R. B. Subbarao and D. R. Miller, J. Vac. Sci. Tech. 9, 814 (1972).
207. S. S. Fisher and J. R. Bledsoe, J. Vac. Sci. Tech. 9, 814 (1972).
208. F. O. Goodman, Surface Sci. 24, 667 (1971).
209. C. M. Chambers and E. T. Kinzer, Surface Sci. 4, 33 (1966).
210. L. Trilling, Surface Sci. 21, 337 (1970).
211. G. Armand, Surface Sci. 9, 145 (1968).
212. J. L. Beeby and L. Dobrzynski, J. Phys. C 4, 1269 (1971).
213. T. Fujiwara and K. Ohtaka, J. Phys. Soc. Japan 24, 1328 (1968).
214. R. H. Ritchie, Phys. Rev. 106, 874 (1957).
215. H. Ibach, Phys. Rev. Ltrs. 24, 1416 (1970).
216. A. A. Lucas and M. Šunjić, Prog. Surf. Sci. 2, 75 (1972).
217. E. Evans and D. L. Mills, Phys. Rev. B7, 853 (1973).
218. H. Boersch, J. Geiger, and W. Stickel, Phys. Rev. Ltrs. 17, 379 (1966).
219. F. M. Probst and T. C. Piper, J. Vac. Sci. Tech. 4, 53 (1967).
220. H. Ibach, Phys. Rev. Ltrs. 27, 253 (1971); J. Vac. Sci. Tech. 9, 713 (1972).
221. K. H. Rieder and E. M. Hørl, Phys. Rev. Ltrs. 26, 239 (1968).
222. R. F. Wallis and A. A. Maradudin, Phys. Rev. 148, 962 (1966).
223. D. L. Huber, Phys. Rev. 153, 772 (1967).
224. F. W. deWette and R. E. Allen, The Structure and Chemistry of Solid Surfaces, edited by G. A. Somorjai, JONH alloy, New York, 1969, p. 18-1.

225. L. L. Kesmodel, F. W. deWette, and R. E. Allen, Solid State Comm. 11, 145 (1972); Phys. Rev. B7, 802 (1973).
226. J. T. McKinney, E. R. Jones, and M. B. Webb, Phys. Rev. 160, 523 (1967).
227. R. F. Barnes, M. G. Lagally, and M. B. Webb, Phys. Rev. 171, 627 (1968).
228. M. G. Lagally, T. C. Ngoc, and M. B. Webb, J. Vac. Sci. Tech. 9, 645 (1972); Phys. Rev. Ltrs. 26, 1557 (1971). See also C. B. Duke and D. L. Smith, Phys. Rev. B5, 4730 (1972).
229. M. Lax and E. Burstein, Phys. Rev. 97, 39 (1955).
230. H. B. Rosenstock, J. Chem. Phys. 23, 2415 (1955).
231. H. B. Rosenstock, J. Chem. Phys. 27, 1194 (1957).
232. H. B. Rosenstock, J. Phys. Chem. Solids 15, 50 (1960).
233. H. B. Rosenstock, J. Phys. Chem. Solids 4, 201 (1958).
234. M. Hass and H. B. Rosenstock, Phys. Rev. 153, 962 (1967).
235. M. Hass and H. B. Rosenstock, Appl. Optics 6, 2079 (1967).
236. G. Mie, Ann. Phys. 25, 377 (1908).
237. H. Rosenstock, Phys. Rev. 136, 1761 (1964).
238. D. W. Berreman, Phys. Rev. 130, 2193 (1963).
239. R. Fuchs, K. L. Kliewer, and W. J. Pardoe, Phys. Rev. 150, 589 (1966).
240. D. W. Berreman, Phys. Rev. 163, 855 (1967).
241. A. Grima, A. A. Maradudin, and S. Y. Tong, J. Phys. Coll. C1, suppl. to No. 4, 31, C1-9 (1970).
242. N. T. McDevitt and W. L. Baun, Spectrochim. Acta 20, 799 (1964).
243. T. P. Martin, Phys. Rev. 177, 1349 (1969).
244. T. P. Martin, Phys. Rev. B1, 3480 (1970). See also R. Ruppin, Phys. Rev. B3, 4422 (1971).

245. L. Gonzel and T. P. Martin, Conference on Surface Properties and Surface States of Electronic Materials, Rolla, Missouri 1972; Surface Sci. 34, 33 (1973).
246. W. W. Pultz and W. Hertl, Spectrochim. Acta 22, 573 (1966).
247. H. Nass, Phys. Rev. Ltrs. 13, 429 (1964).
248. W. A. Pliskin and R. P. Eischens, Z. Physik. Chem. 24, 11 (1960).
249. R. P. Eischens and W. A. Pliskin, Adv. Catalysis 10, 1 (1958).
250. N. Marschall, B. Fischer, and H. J. Queisser, Phys. Rev. Ltrs. 27, 95 (1971).
251. W. E. Anderson, R. W. Alexander, and R. J. Bell, Phys. Rev. Ltrs. 27, 1057 (1971).
252. A. Otto, Z. Physik 216, 298 (1968).
253. R. Ruppin, Solid State Comm. 8, 1129 (1970).
254. N. Marschall and B. Fischer, Phys. Rev. Ltrs. 28, 811 (1972); see also B. Fischer, N. Marschall, and H. J. Queisser, Surface Sci. 34, 50 (1973); A. S. Barker, Phys. Rev. Ltrs. 28, 892 (1972); Surface Sci. 34, 62 (1973).
255. V. V. Bryksin, Yu. M. Gorbzhtein, and D. N. Mirlin, Fiz. Tverd. Tela 14, 543, 3368 (1972) [Sov. Phys. Solid State 14, 453 (1972)]. Surface polaritons in  $\alpha$ -quartz have recently been studied by A. Hartstein, E. Burstein, J. J. Brion, and R. F. Wallis, Taormina Conference on Polaritons, Taormina, Italy, 1972 and by H. Falge and A. Otto, Phys. Status Solidi, to be published.
256. R. Ruppin and R. Englman, Light Scattering Spectra of Solids, edited by G. B. Wright, Springer-Verlag, New York, 1969, p. 157.
257. O. Litzman and J. Cely, Surface Sci. 21, 390 (1970).

- 258. R. London, Proc. Roy. Soc. (London) A275, 218 (1963).
- 259. A. Kawabata, Raman Memorial Volume, Vijnana Parishad  
Anusandhan Patrika 14, 157 (1971).
- 260. J. M. Wilson and T. J. Bastow, Surface Sci. 26, 461 (1971).
- 261. C. D. Gelatt, M. G. Lagally, and M. B. Webb, Bull. Am. Phys.  
Soc. 14, 793 (1969).
- 262. A. Ignatjevs, Thesis, Cornell University, 1972.
- 263. R. E. Allen, J. Vac. Sci. Tech. 9, 934 (1972).
- 264. V. E. Kenner and R. E. Allen, Phys. Ltrs. 39A, 245 (1972);  
Phys. Rev., to be published.
- 265. L. Dobrzynski and A. A. Maradudin, Phys. Rev. B7, 1207 (1973).

## FIGURE CAPTIONS

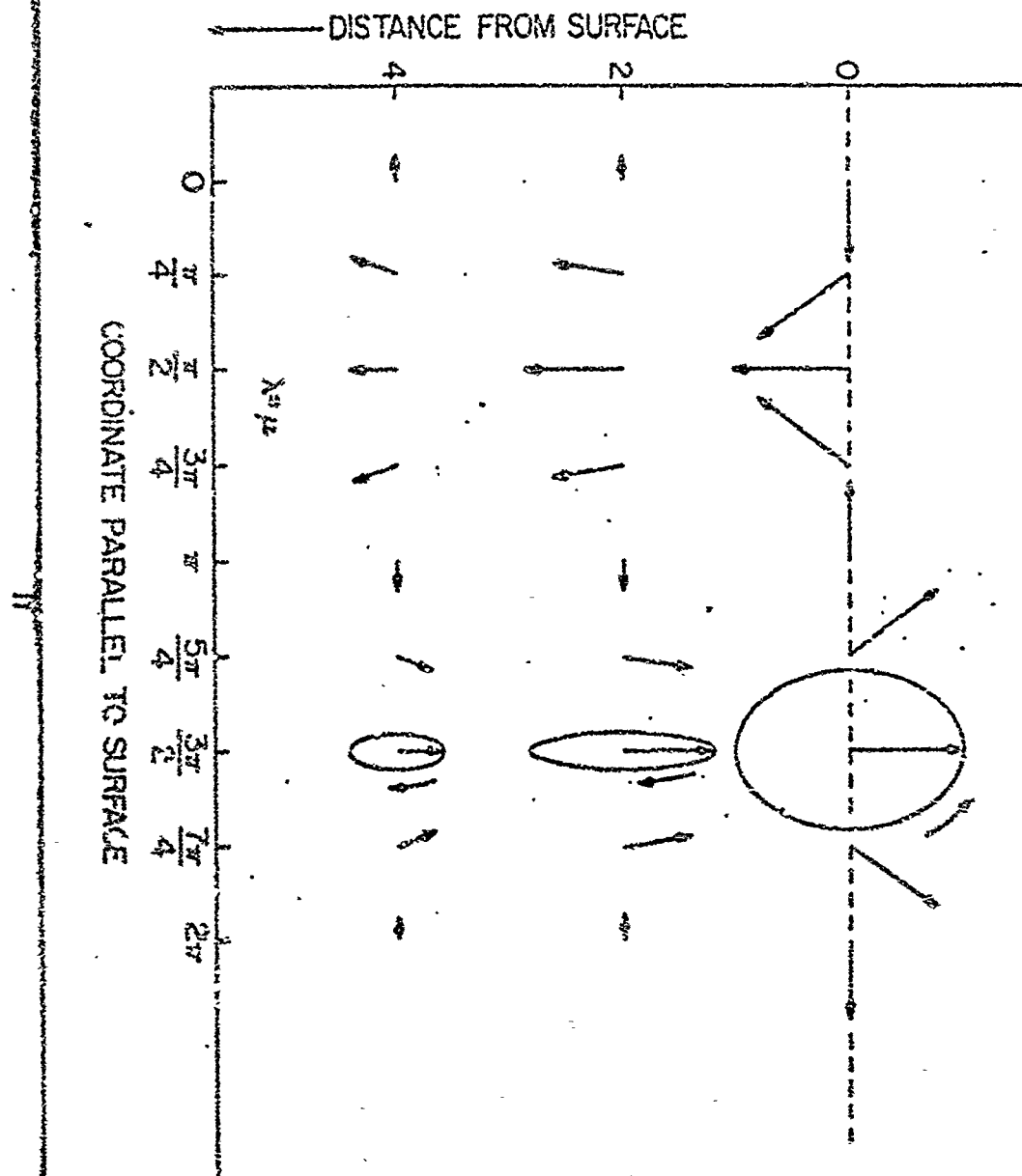
- Fig. 1. Particle displacements of a surface wave at a fixed instant of time. The ellipses show the time evolution of particle displacements at fixed positions.
- Fig. 2. Positions of various materials in the space of the elastic constant ratios  $c_{11}/c_{44}$  and  $c_{12}/c_{44}$ . The stable region lies to the right of the lines  $c_{11}-c_{12} = 0$  and  $c_{11}+2c_{12} = 0$ .
- Fig. 3. Reduced surface wave velocity versus angle between the direction of propagation and the [100] direction on a (001) surface.
- Fig. 4. Attenuation constants versus angle between the direction of propagation and the [100] direction on a (001) surface for Cu.
- Fig. 5. Theoretical and experimental wave velocities versus direction of propagation for the (001) surface of Cu. (After Rollins, Lin and Farnell, Ref. 7).
- Fig. 6. Atomic displacement amplitudes versus position in the lattice for the surface mode of a diatomic linear chain of 10 atoms.
- Fig. 7. Squared normal mode frequencies (in units of  $\alpha(m+M)/M\omega$ ) versus mode index  $n$  for a diatomic linear chain of 10 atoms.
- Fig. 8. Dispersion curve of reduced frequency versus reduced wave number for surface waves propagating in the [100] direction on the (001) surface of KCl. The surface wave is an ordinary surface wave to the left of the

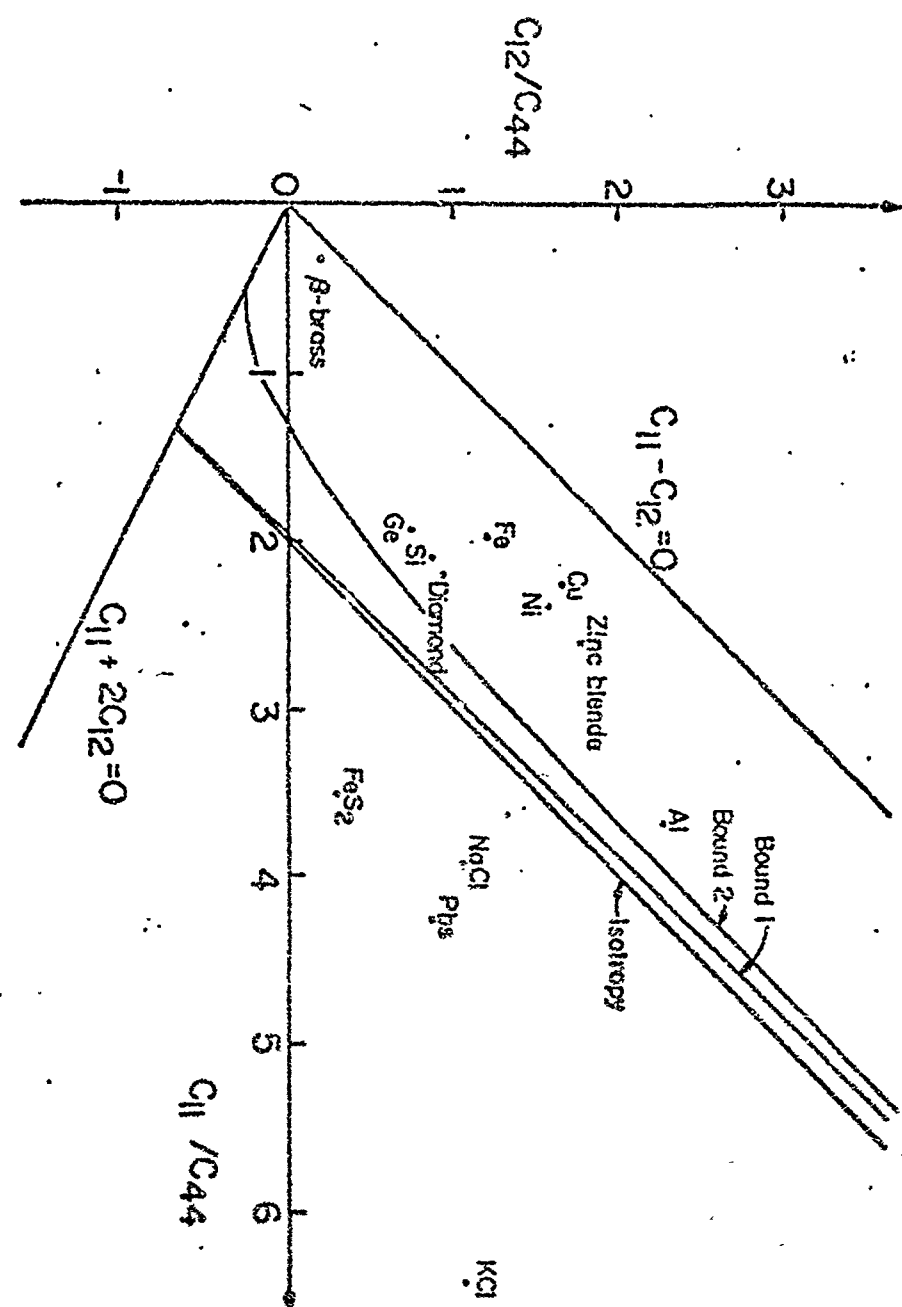
dashed line and a generalized surface wave to the right of this line.

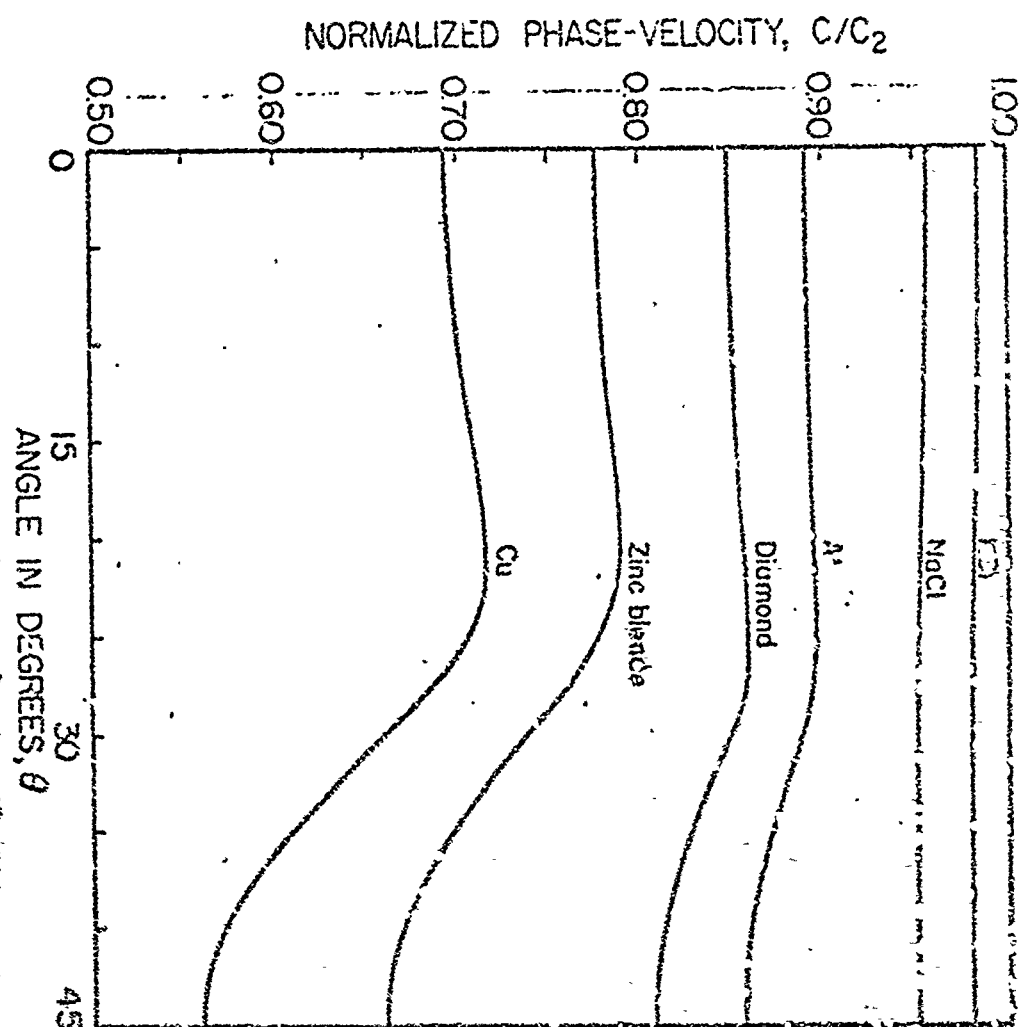
- Fig. 9. Frequency versus wave vector curves for a monatomic fcc crystal with two (111) surfaces. The surface waves are denoted by  $S_1$ . (a) 11-layer crystal; (b) Brillouin zone; (c) 21-layer crystal; (d) 21-layer crystal with outermost layers consisting of light adsorbed atoms, adatom-host atom mass ratio 1:5. (After Allen et al., Ref. 45).
- Fig. 10. Frequencies of transverse optical surface modes versus wave vector for a (001) surface of LiF. (a) high frequency modes; (b) low frequency modes. (After Kliever and Fuchs, Ref. 69.)
- Fig. 11. Frequencies versus wave vector for a 15-layer crystal of NaCl with two (001) surfaces. The surface modes are labeled by  $S_1$  and mixed modes by  $MS_1$ . (After Chen, et al., Ref. 87).
- Fig. 12. Intensity versus temperature for electrons scattered from the (110) surface of Ni. (a) close to the [001] direction; (b) close to the [110] direction. (After MacPae, Ref. 146.)
- Fig. 13. Mean square displacements versus atomic layer index for the (110) surface of Ni.  $\alpha$  is the nearest neighbor force constant.
- Fig. 14. Temperature dependence of the surface-to-bulk mean square displacement ratios for the (100), (110), and (111) surfaces of a monatomic fcc crystal. (After Allen and LeVette, Ref. 179).

- Fig. 15. Mean square velocity versus atomic position for a monatomic linear chain of 20 atoms at  $0^\circ\text{K}$ .
- Fig. 16. Energy-loss spectrum for a particular value of  $k_z$ . The line at  $\omega^2 = 1$  corresponds to the surface mode and the broad band to the bulk modes. (After Rounady and Mills, Ref. 200).
- Fig. 17. Iso-intensity curves in the  $q_1, q_2$  plane for surface scattering and for bulk scattering. In each case, the situations  $Q_3 \ll Q_1$  and  $Q_3 \gg Q_1$ , are presented.
- Fig. 18. Extinction cross-section in units of the geometrical cross-section versus frequency for a small spherical NaCl crystal of radius  $1\mu\text{m}$ . (After Ruppin and Englman, Ref. 71).
- Fig. 19. Absorption coefficient versus frequency for a crystal of NaCl 100 layers thick. (After Grim et al., Ref. (241)).

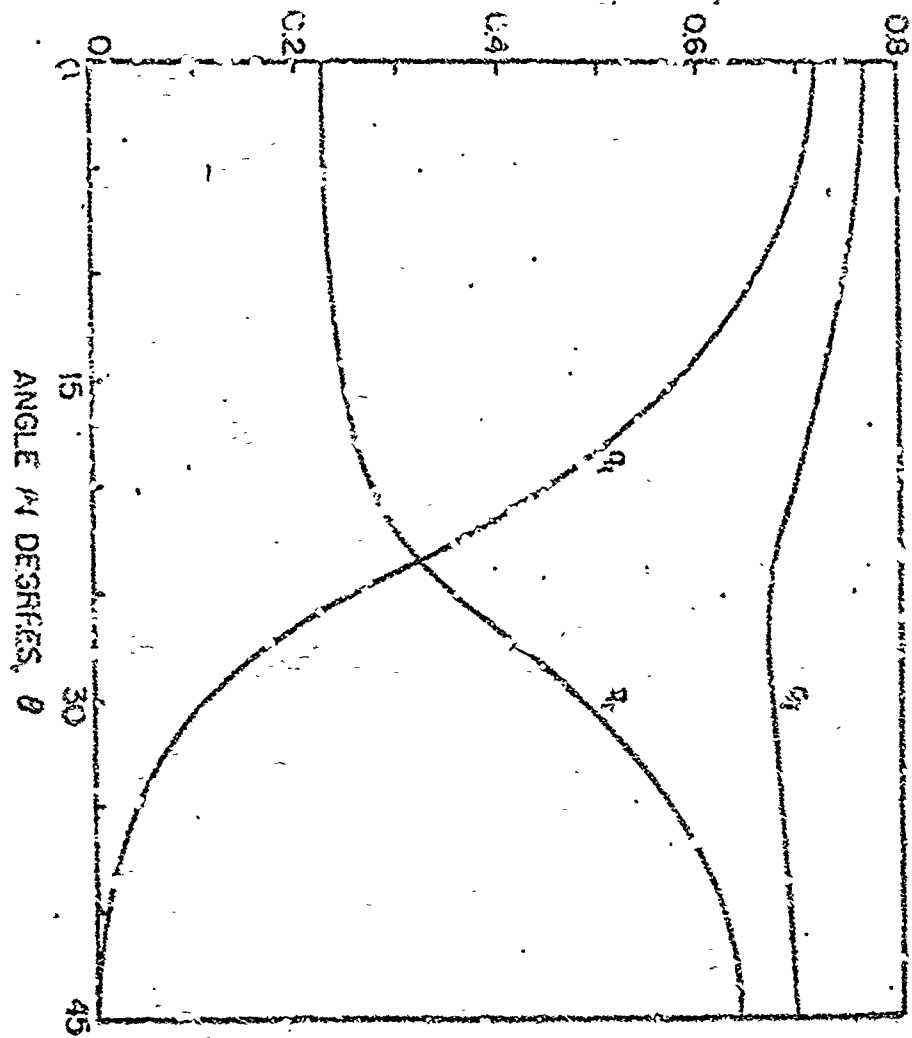
182

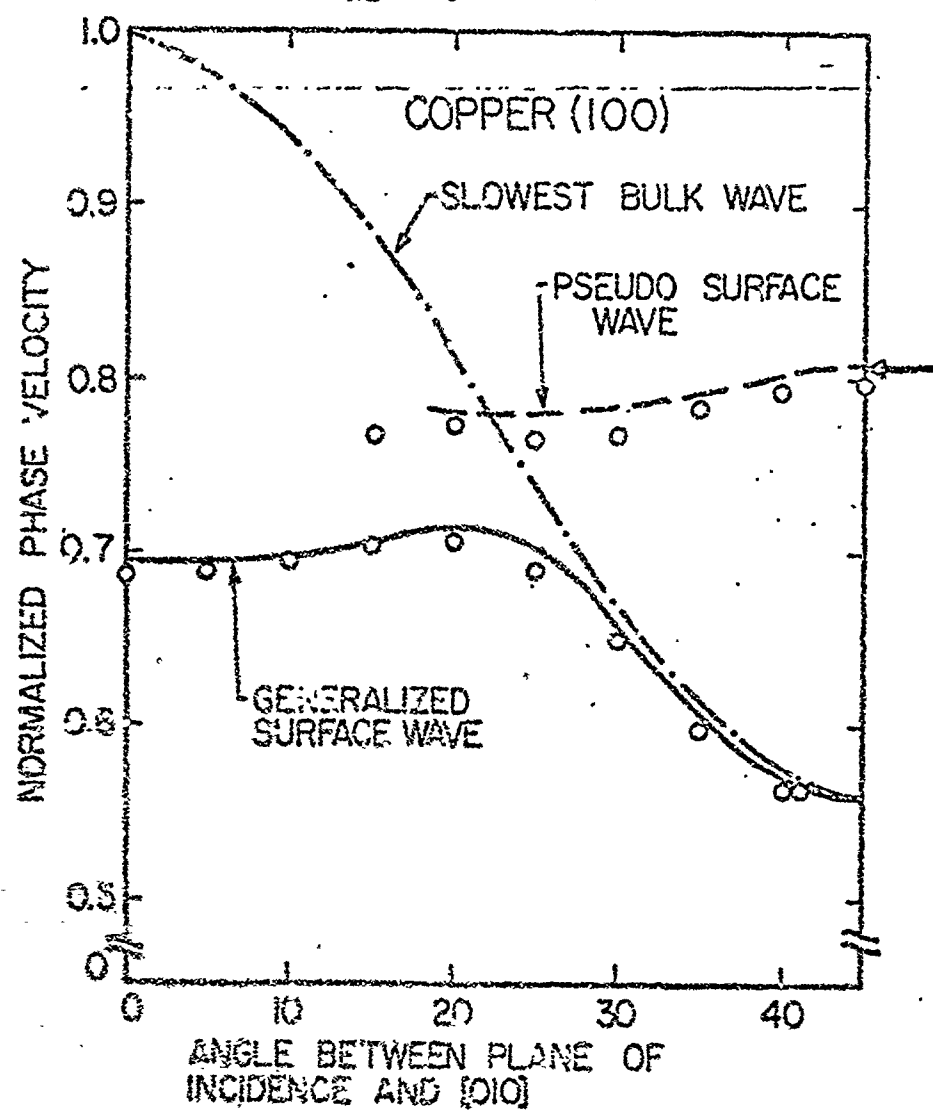


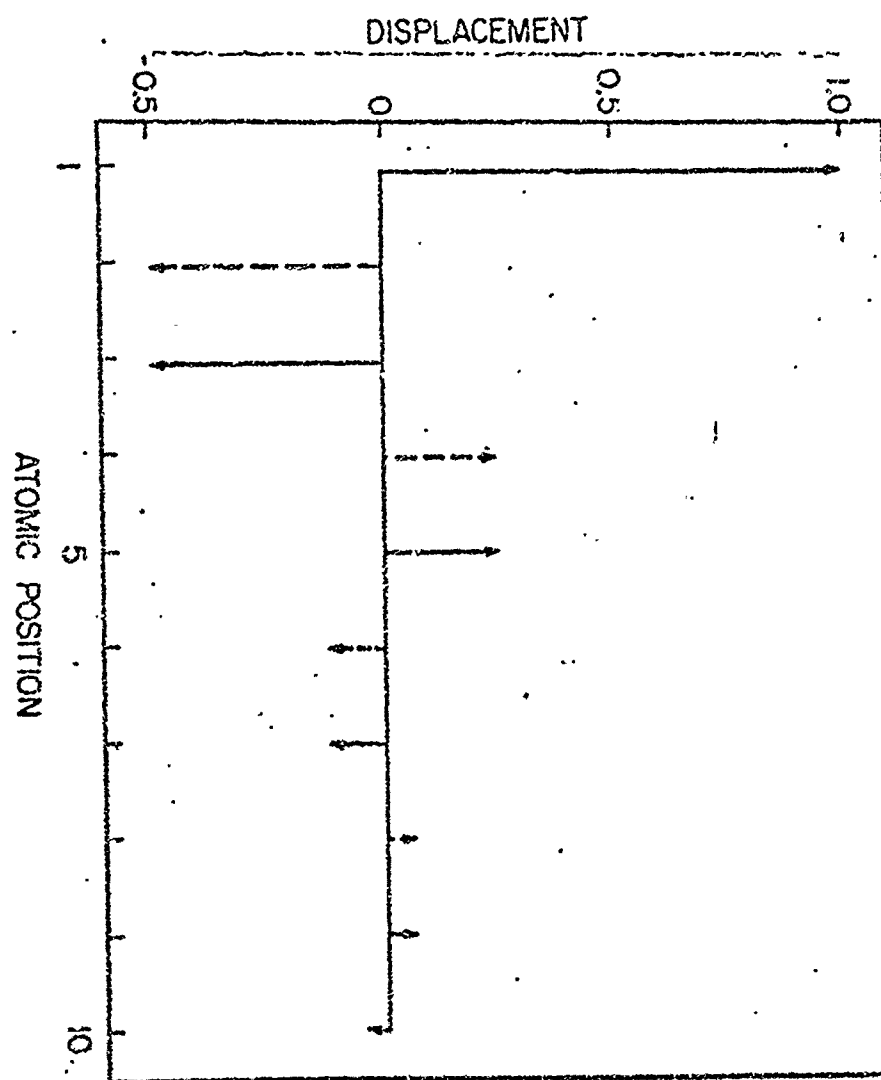




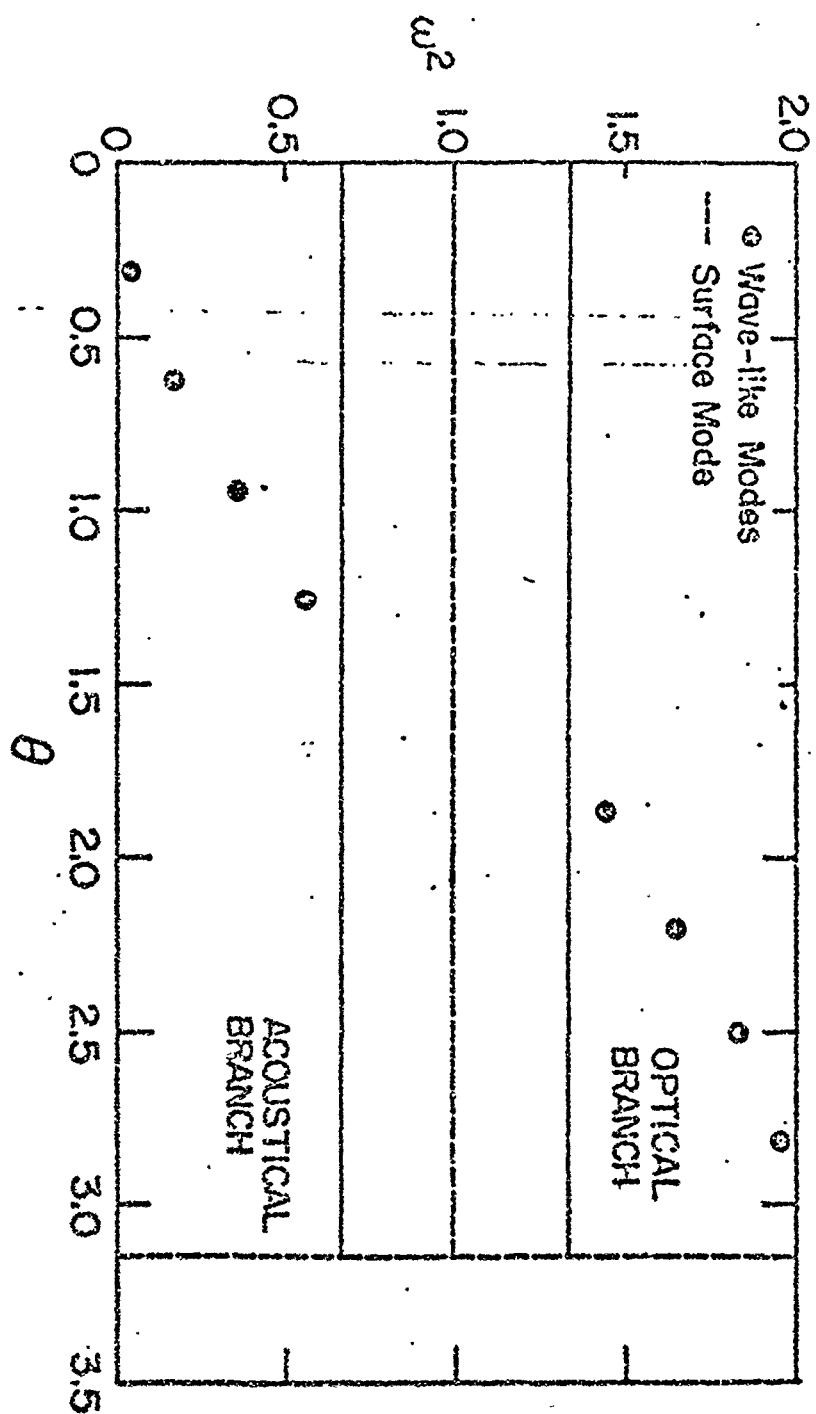
ATTENUATION CONSTANTS,  $q_i$ , FOR Cu

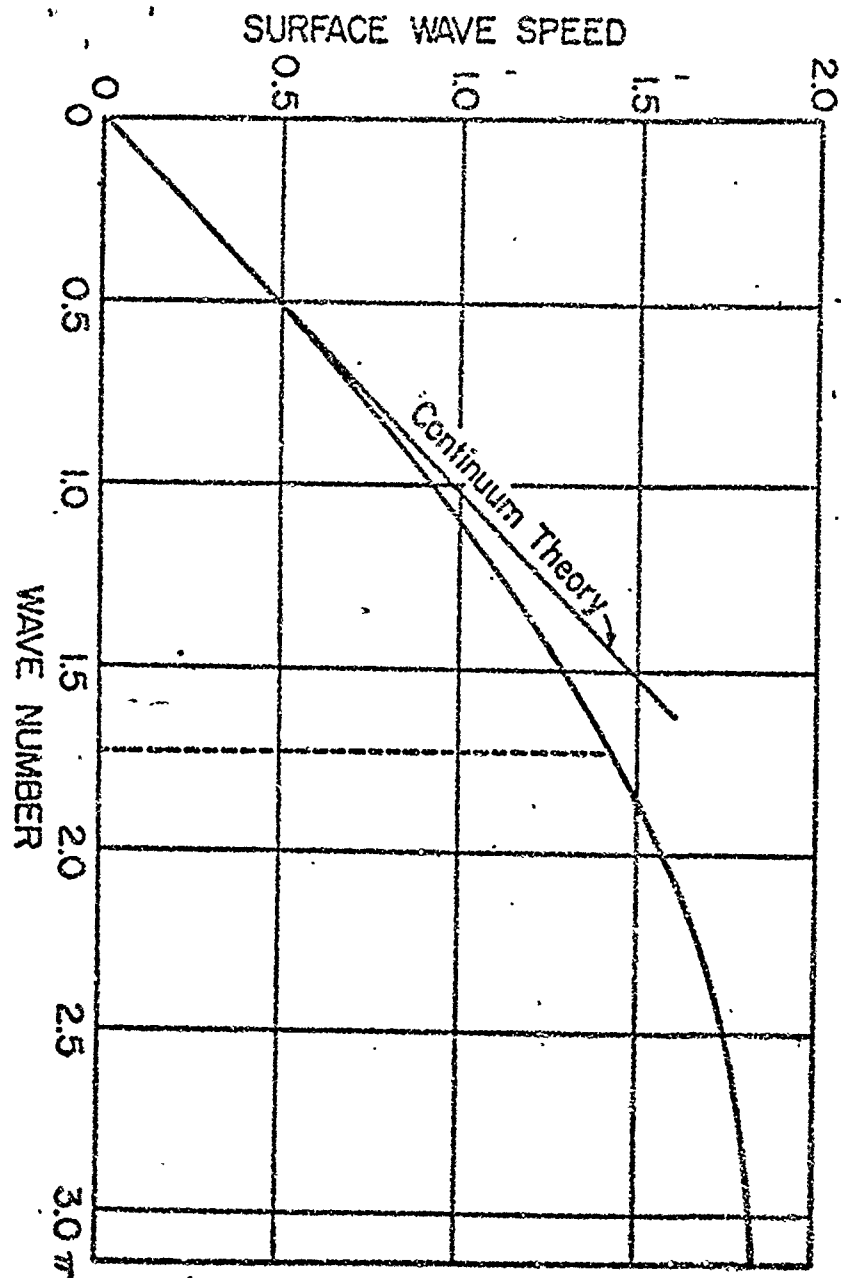


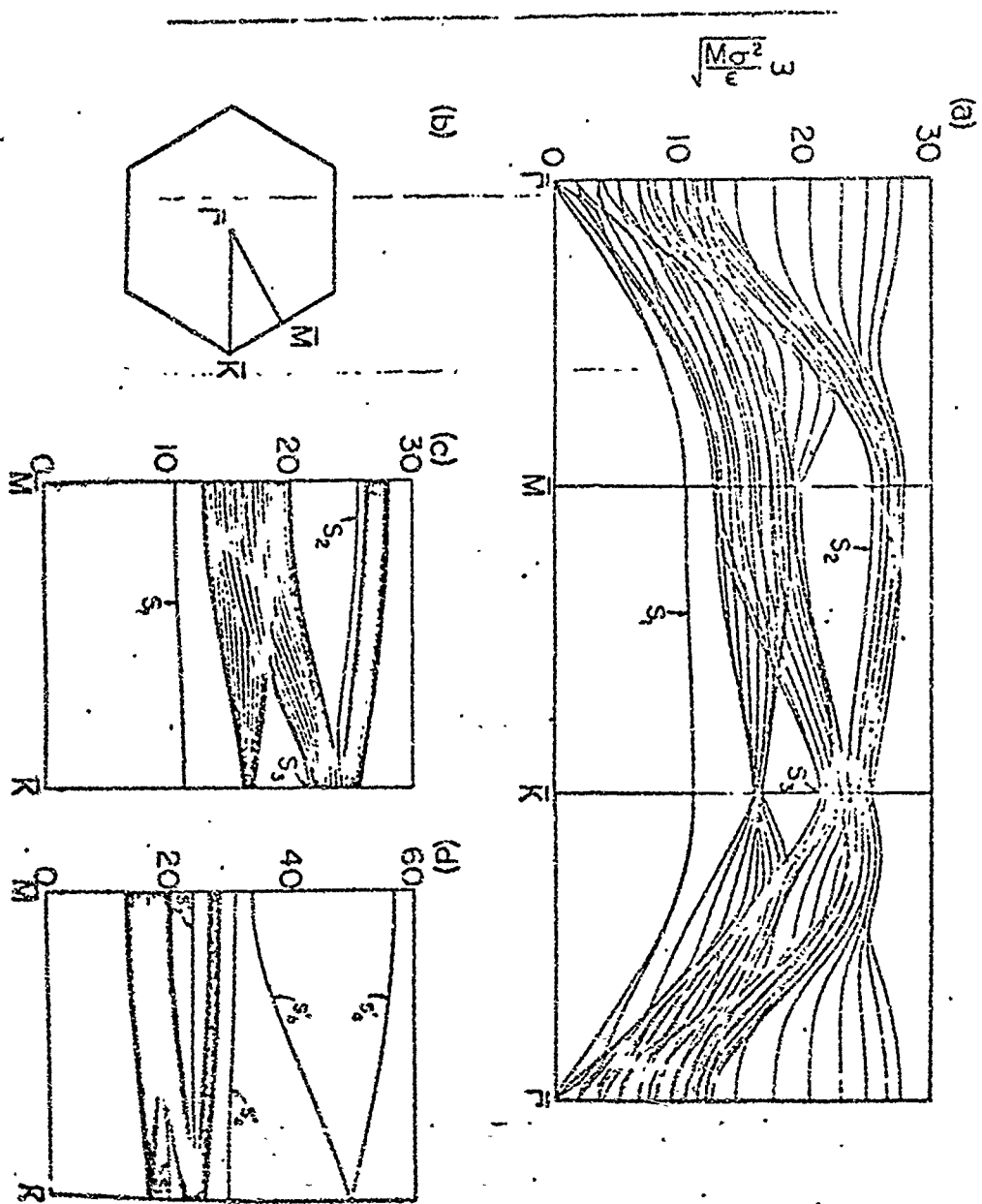


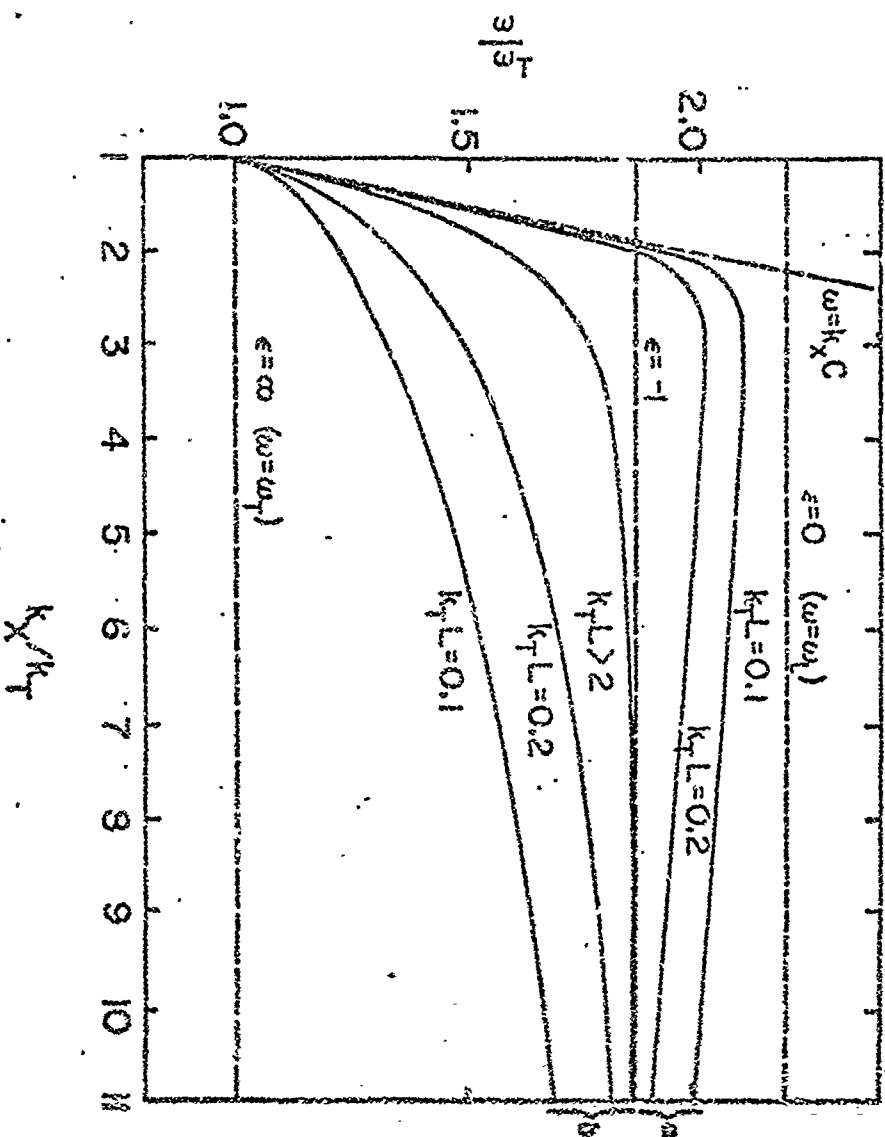


18.7

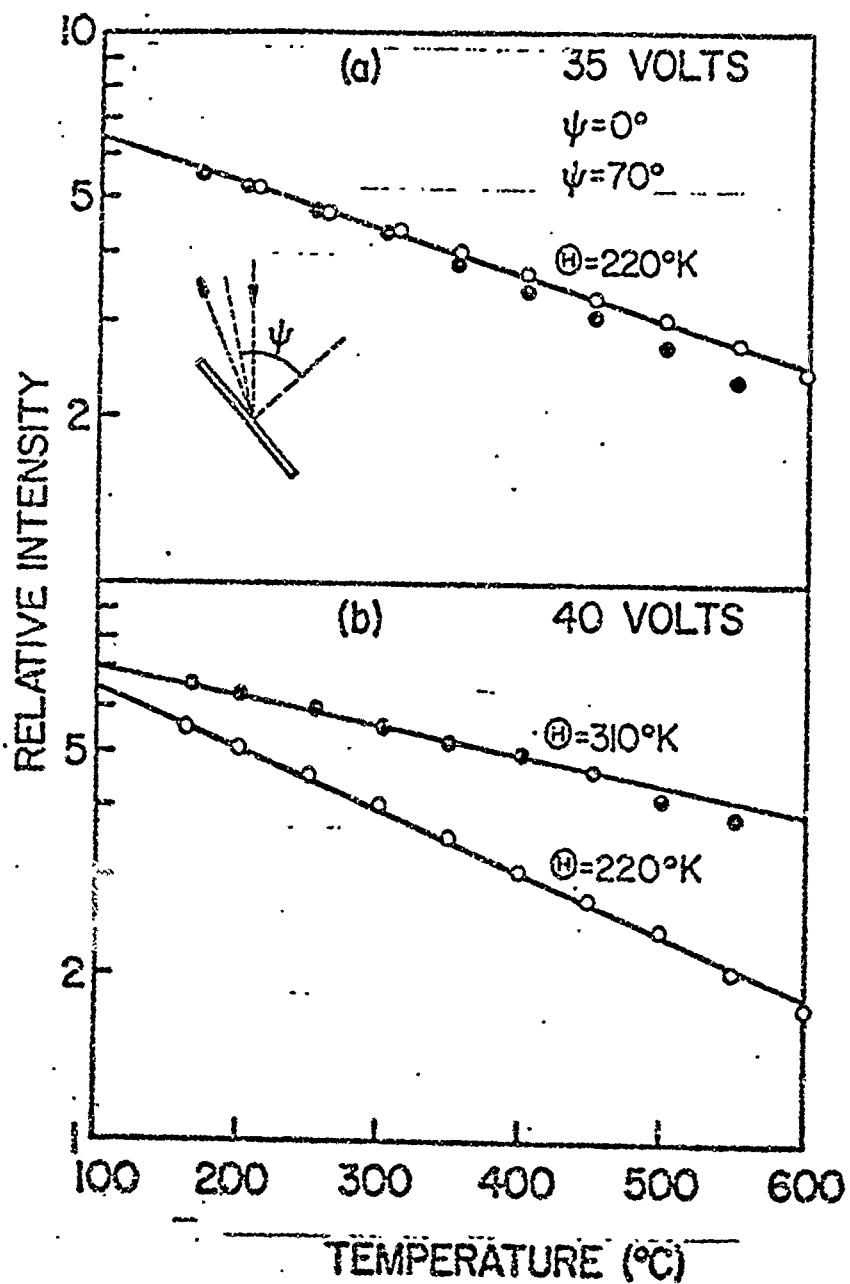


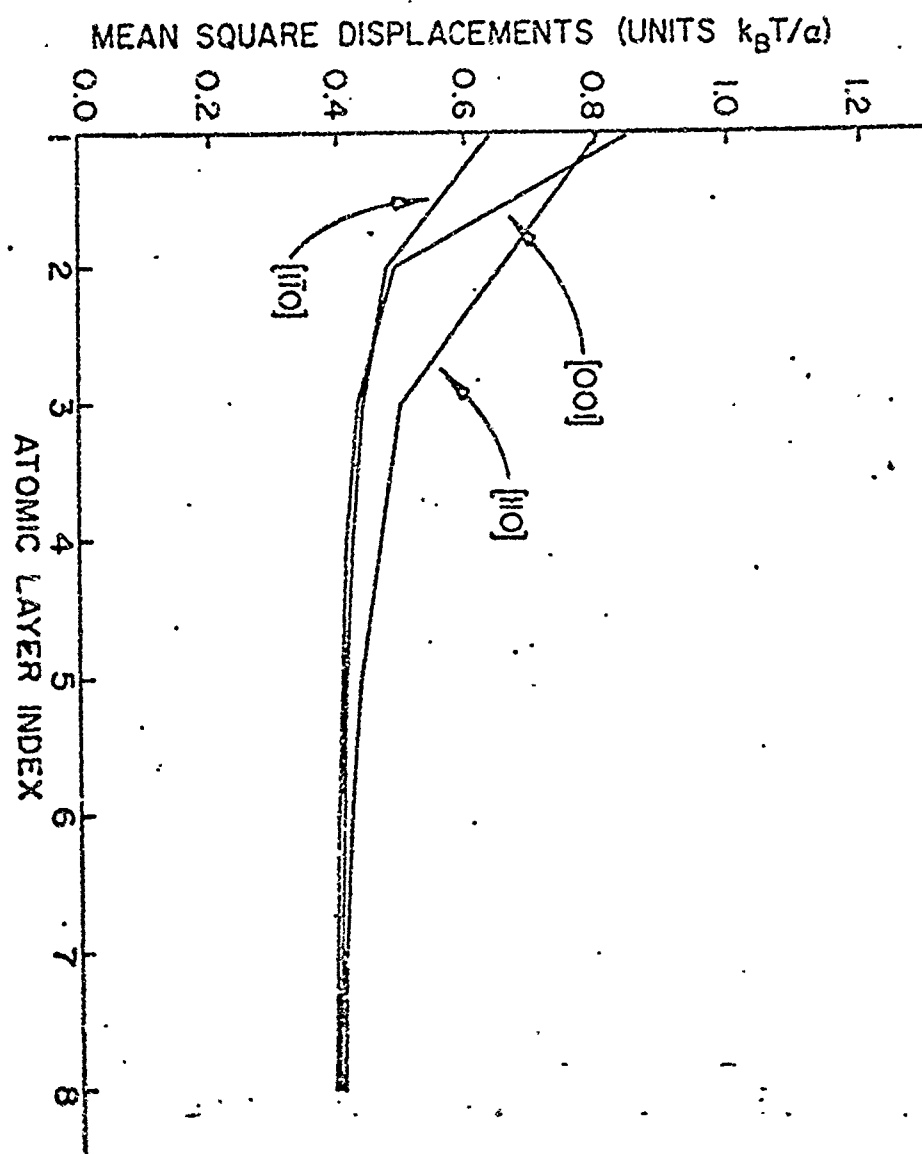


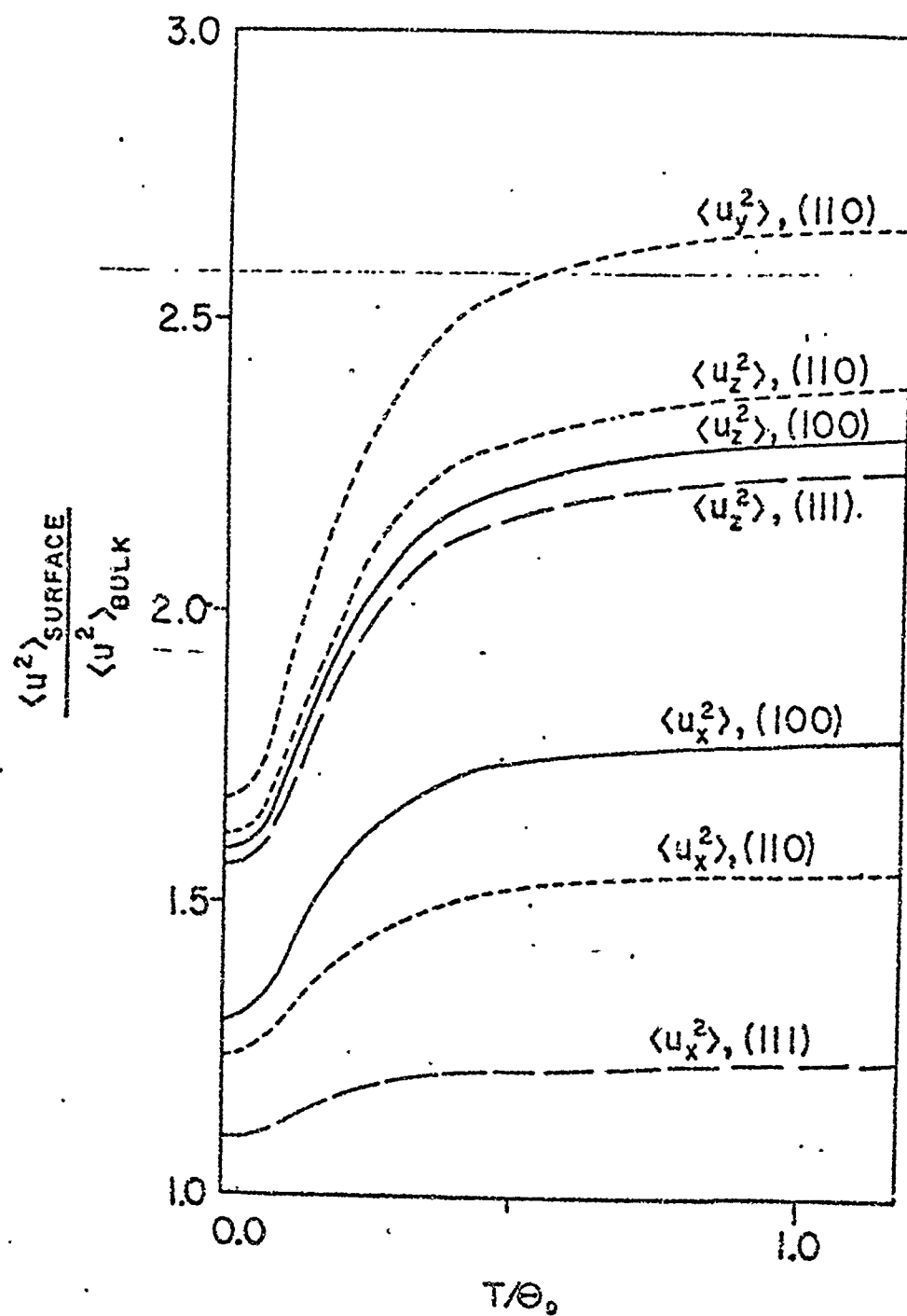


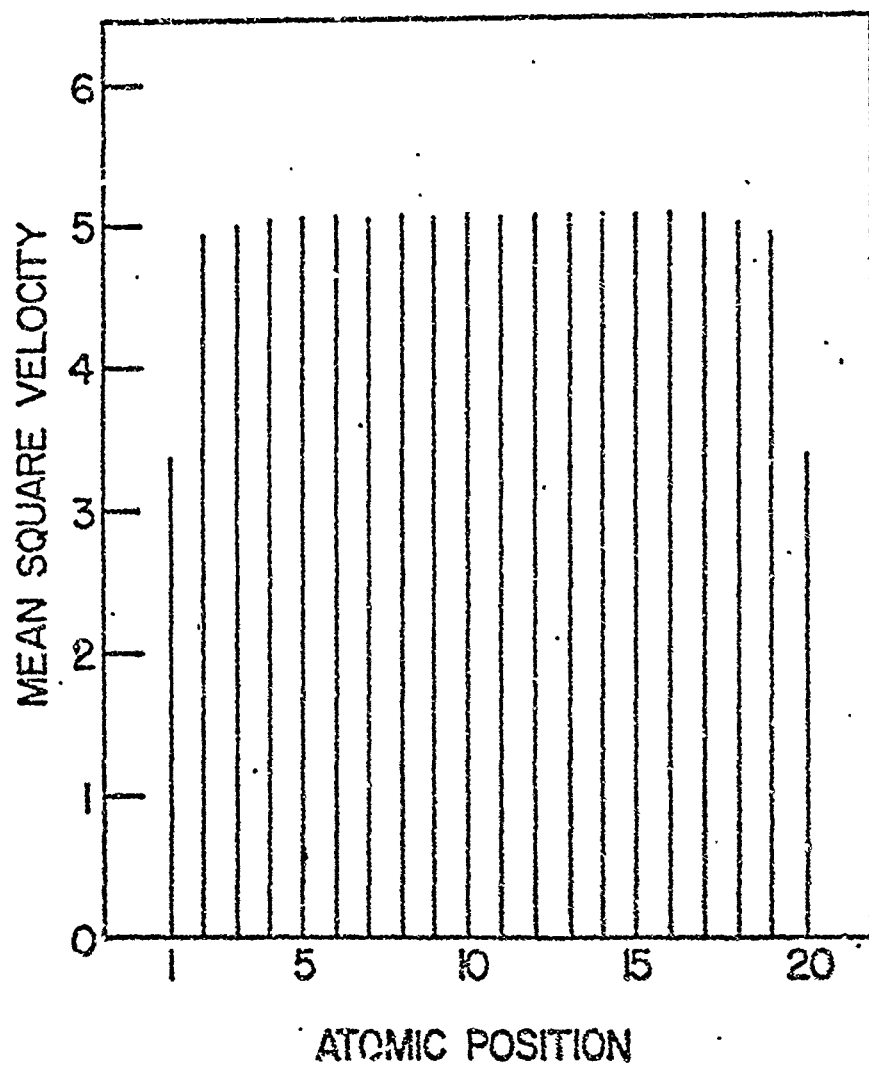










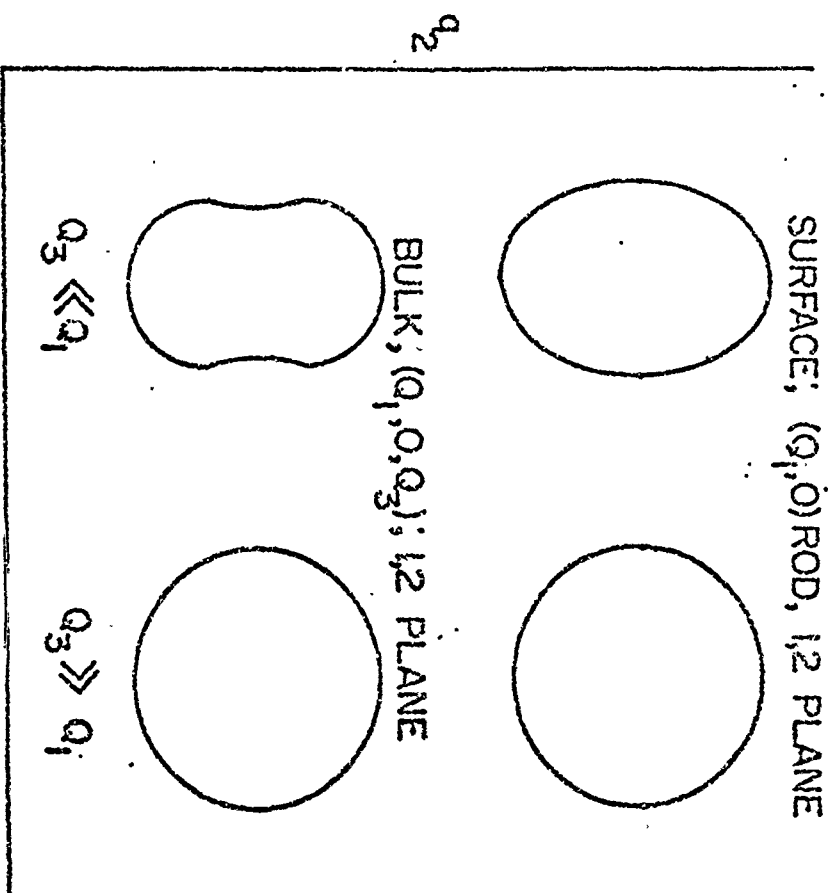


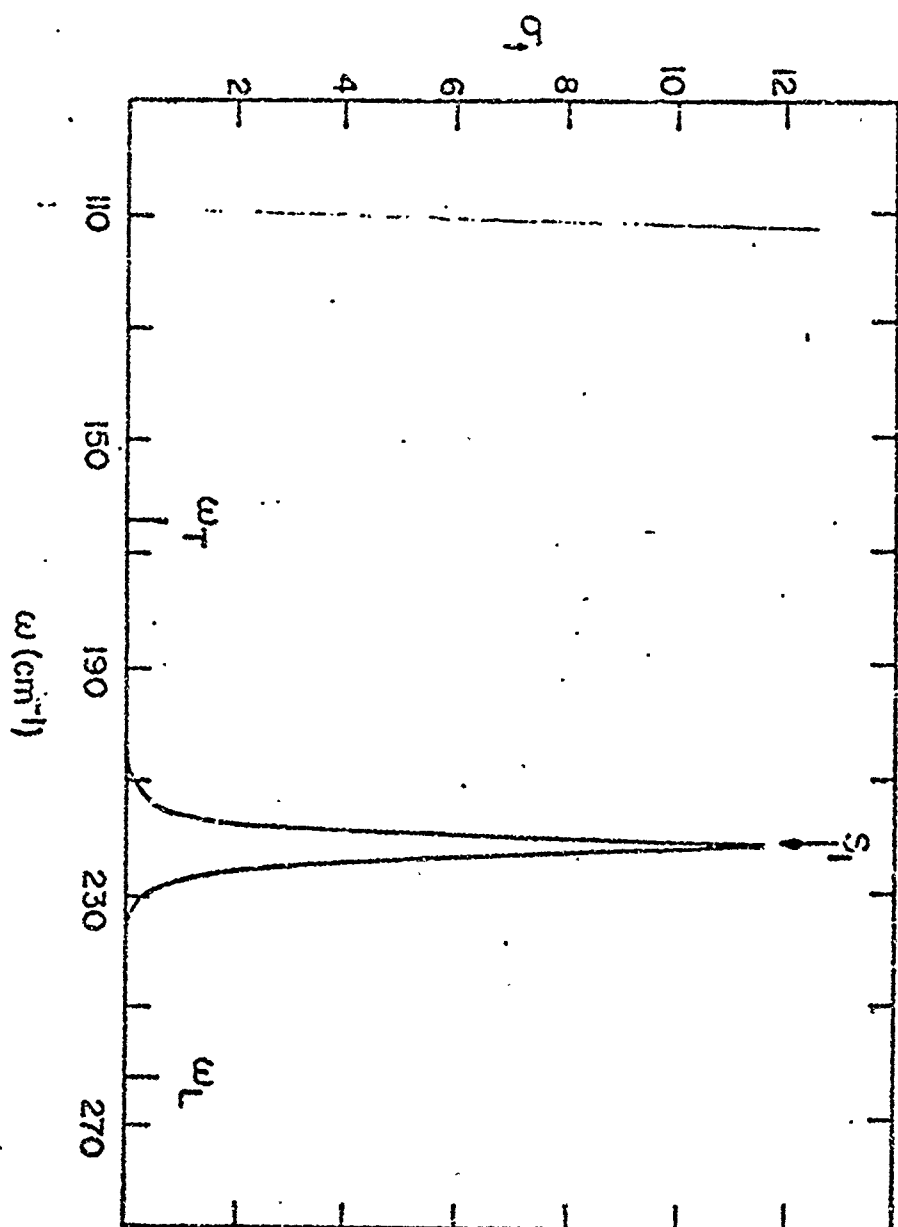
19 5

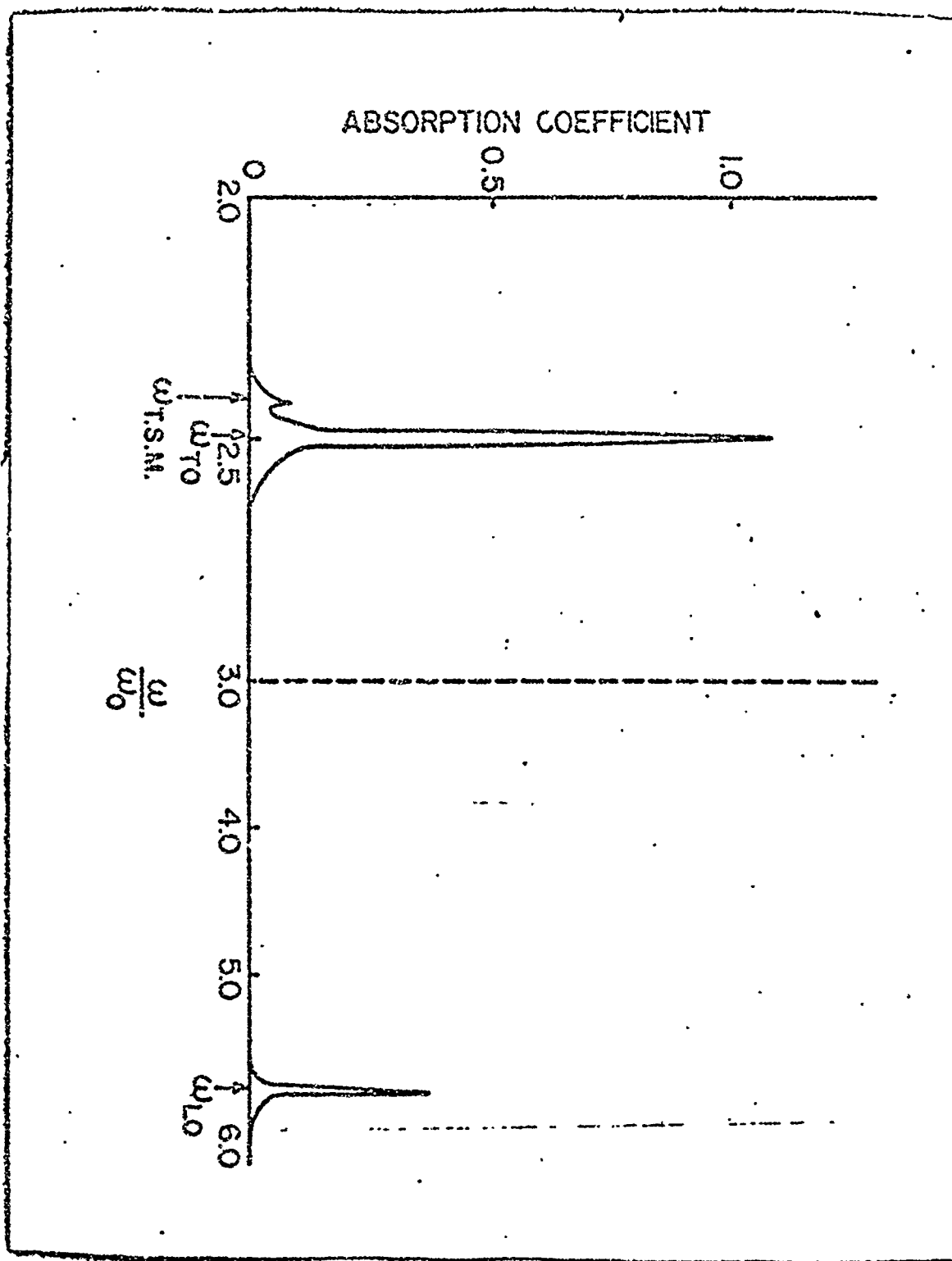
$$\frac{d^2\sigma}{d\Omega d\omega}$$

$$\omega^2$$

197







200